THE ORGANIZATION OF PROTEINS INVOLVED IN SYNAPTIC PLASTICITY

Amanda Louise Jacob

A dissertation submitted to the faculty of the University of North Carolina at Chapel Hill in partial fulfillment of the requirements for the degree of Doctor of Philosophy in the Curriculum of Neurobiology.

Chapel Hill
2011

Approved by:

Paul B Manis, PhD

Richard J Weinberg, PhD

Serena M Dudek, PhD

Thomas L Kash, PhD

Benjamin D Philpot, PhD

© 2012
Amanda Louise Jacob
ALL RIGHTS RESERVED

ABSTRACT

AMANDA LOUISE JACOB: The organization of proteins involved in synaptic plasticity
(Under the direction of Richard J Weinberg)

The role that PSD organization plays in synaptic function and plasticity is only beginning to be understood. AMPARs play a well-established role in LTP; up-regulation of AMPARs within the postsynaptic density (PSD) is generally accepted to be the primary mechanism of NMDAR-dependent LTP. The function that AIDA-1 (Amyloid-β protein precursor intracellular domain-associated protein-1), a recently discovered component of the PSD, plays within synapses is less clear; however, in cultured hippocampal neurons, a portion of AIDA-1 translocates to the nucleus and increases downstream protein translation in response to NMDAR activation, Thus, experimental evidence suggests a role for AIDA-1 in synapse-to-nucleus signaling during NMDAR activation. My project uses electron microscopy and other histological techniques to determine the basal organization of AMPARs and AIDA-1 within the PSD. These data may provide better understanding of the roles these proteins play.

DEDICATION

To my mother, Dona Louise Thompson Jacob, my first teacher and greatest inspiration. I never doubted my ability to complete a PhD because I have my mother as amazing example of a woman working in a technical field. Her intense curiosity about the natural world inspired me to be a scientist.

To my father, James Leland Jacob, always supportive.

To my maternal grandmother, Louise Heyfron Thompson. I wish you were here to see this day. I will miss you forever.

To my wonderful fiancé, Theo Christopher Alexander Walker. I don’t think any words could adequately express how much Theo’s love and support mean to me through my PhD. I feel privileged that someone so creative, sweet, insightful, and intelligent has chosen to spend his life with me.

I love you all.

ACKNOWLEDGEMENTS

I owe a great debt to my advisor Richard Weinberg. Richard is a gifted scholar and speaker, with an immense breadth and depth of knowledge. He has been extraordinarily generous with his time, pouring countless hours into teaching me to be the best scientist I can be. Choosing Richard as my advisor was one of the best decisions I have ever made.

Electron microscopy (EM) is an incredibly challenging technique, and I have been lucky to have two great teachers. Kristen Phend, an amazing research technician in the Weinberg lab, taught me EM tissue processing. Her extensive knowledge and attention to detail were a major reason for my success. Hal Mekeel, the phenomenal research technician who ran the EM core in the cell and developmental biology department, taught me to use the electron microscope and how to cut section on an ultramicrotome. Hal was forever patience and always ready with good advice. Susan Burette, another wonderful technician in the Weinberg lab, taught me immunohistochemistry. I'd also like to thank Dr. Alain Burette, Dr. Aldo Rustioni, Dr Juli Valtschanoff, Helen Willcockson, and Dr. Bence Racz for their feedback on projects and technical help.

I'm also grateful to my committee, composed of Dr. Paul Manis, Dr. Thomas Kash, Dr. Ben Philpot and Dr. Serena Dudek, for their feedback and support throughout my PhD. They

My acknowledgements would not be complete without thanking my friends and my colleagues in the UNC neuroscience center. When I struggled to make experiments work or just needed a shoulder to lean on, I had a wonderful, supportive community to count on. Particular thanks go out to Claire Moss, William Moss, Thomas Cowart, Anthony Ritz, Nick Chapman, Emily Riggan, Megan Goodwin, Jason Sullivan, Beth Knight, Liz Buttermore, Kevin Blauth, Luke Campagnola, Rose Campagnola , Miranda Steed, Srishti Garvey, Giselle Lopez, Sara Becker, Rebekah Corlew , and my beautiful dog Hazel. I couldn't have done it without you all!

TABLE OF CONTENTS

LIST OF FIGURES

LIST OF TABLES

LIST OF ABBREVIATIONS

Aβ	amyloid-β
AβPP	amyloid-β protein precursor
AIDA	Amyloid-β protein precursor intracellular domain-associated protein-1
AKAP	A kinase anchoring protein
AMPA	α-amino-3-hydroxyl-5-methyl-4-isoxazole-propionate acid
AMPAR	AMPA-type glutamate receptor
Arc	activity-regulated cytoskeletal-associated gene
BDNF	brain-derived neurotrophic factor
C	carboxyl; as in C terminal tail
CA1	Cornu Ammonis area 1
CA3	Cornu Ammonis area 3
CaMKII	calcium/calmodulin kinase II
cAMP	cyclic adeonosine 3',5' –monophoshate
CREB	cAMP response element binding
DAB	diaminobenzidine
DREAM	downstream regulatory element antagonist modulator
E-LTP	early phase long-term potentiation
EC	Enthorinal cortex
Egr-1	early growth response gene
EM	electron microscopy
ER	endoplasmic recticum
ERK	extracellular signal regulated kinase

GRIP	glutamate-receptor-interacting-protein
KO	knock-out
L-LTP	late phase long-term potentiation
LTD	long-term depression
LTP	long-term potentiation
MAGUK	membrane-associated guanylate kinase
MAPK	mitogen-activated-protein-kinase
mRNA	messenger ribonucleic acid
mGluR	metabotropic glutamate receptor
Narp	neuronal activity regulated pentraxin
NMDA	N-methyl-D-aspartate
NMDAR	NMDA-type receptor
nPIST	neuronal isoform of protein-interacting specifically with TC10
NSF	N-ethylmaleimide-sensitive factor
NTD	N-terminal domain
PB	phosphate buffer
PBS	phosphate buffered saline
PKA	cAMP dependant kinase
PKC	protein kinase C
PKMζ	protein kinase M ζ
PICK	protein interacting with C kinase
PSD	postsynaptic density
SAM	sterile α motif

SAP97	synapse associated protein 97
SAP102	synapse associated protein 102
SAPAP	synapse associated protein associated protein
SR	stratum radiatum
SynGAP	synaptic GTPase-activating protein
TARP	transmembrane AMPAR regulatory protein
TrkB	tropomyosin-related kinase B
WT	wild-type

CHAPTER 1

Understanding plasticity through synaptic structure

1.1. Introduction (Synaptic plasticity and structure)

Synapses serve as sites of information exchange between presynaptic neurons and their postsynaptic targets. Excitatory glutamatergic synapses form between axonal boutons and dendritic spines, femtoliter-sized membrane protrusions that compartmentalize postsynaptic signaling (Bourne et al., 2008). The postsynaptic density (PSD), a protein-rich region within spines that directly opposes sites of neurotransmitter release, serves as a general coordinator of postsynaptic neurotransmission (Okabe, 2007; Sheng et al., 2007). Organizing glutamate receptors is a primary function of the PSD. The number of glutamate receptors within the PSD controls the strength of synaptic transmission; synapses with more glutamate receptors produce larger postsynaptic signals, while fewer receptors result in smaller response (Takumi et al., 1999). PSDs also contain scaffolding proteins, which can arrange proteins into signaling complexes to facilitate downstream signal transduction. Knockout of scaffolding proteins alters synaptic currents, indicating the functional importance of PSD organization (Béïque et al., 2006; Weisenhaus et al., 2010). In addition, several diseases including autism spectrum disorders, schizophrenia, mental retardation, and early stage Alzheimer's disease have been linked to disruptions in synaptic function that might be due to abnormalities in PSD structure (Selkoe at al., 2002; Stephan et al., 2006; Knobloch

et al., 2008, Südhof, 2008; Schütt et al., 2009; Pfeiffer et al., 2009; van Spronsen et al., 2010).

Changes in the strength of synaptic responses, otherwise known as synaptic plasticity, are widely believed to underlie memory storage in the brain (Malenka et al., 1999; Malinow et al., 2003). Long-term potentiation (LTP), one of the most studied and best understood forms of synaptic plasticity, is a long-lasting increase in synaptic response. LTP was first discovered in dentate gyrus, an area of the hippocampus, known to play an important role in learning and memory (Bliss et al., 1973). The primary pathway through hippocampus has well-defined circuitry: input enters hippocampus from the enthorinal cortex (EC), passes from granule cells in dentate gyrus to pyramidal cells in region CA3 to pyramidal cells in CA1 to the subiculum, and then leaves the hippocampus to reenter the EC. Synapses formed by CA3 pyramidal cells onto CA1 pyramidal cells form in a subregion in hippocampus called stratum radium (SR); these synapses are arguably the most studied in the brain. Within CA1 SR synapses, NMDA (N-methyl-D-aspartate receptor) receptor-dependent LTP (NMDAR-LTP) is the primary mechanism of synaptic potentiation. During this form of LTP, high frequency activation of synapses leads to activation of NMDARs, leading to persistent increases in synaptic strength. Similar NMDAR-LTP occurs in other areas of the brain, including cerebral cortex (Kirkwood et al., 1995).

LTP is a complex multistep process, which can be divided into several temporal periods: short-term plasticity, early LTP (E-LTP) and late LTP (L-LTP). Short-term plasticity, which last a few second or less, is beyond the scope of this

review. E-LTP is transient, generally lasting less than 4 hours, mediated by changes in synaptic proteins. L-LTP is longer lasting and requires protein synthesis (Krug et al., 1984; Frey et al., 1989; Calixto et al., 2003). Protein synthesized during L-LTP can be translated from two different sources: preexisting mRNA and newly synthesized mRNA produced through nuclear communication. Translation of preexisting RNA plays an important role in the early phase of L-LTP expression (Sutton et al., 2005; Sutton et al., 2006). However, long term maintenance of L-LTP (>8 hours) requires transcription; application of the transcription inhibitor actinomycin-D can block late-phase LTP in synapses in hippocampus (Nguyen et al., 1994; Frey et al., 1996; Calixto et al., 2003). These studies indicate that gene expression and synapse-to-nucleus communication are required for long term maintenance of LTP.

Structural remodeling of the PSD helps to make LTP-induced changes in synaptic strength permanent. Multiple studies have correlated PSD size and morphology to synaptic plasticity; synapses that have undergone potentiation contain larger, perforated PSDs, while PSDs of synapses where plasticity has not occurred are smaller (Geinisman et al., 1991; Muller et al., 2000; Toni et al., 2001; Urakubo et al., 2006). In addition, changes in PSD composition accompany and, in some forms of LTP, account for LTP expression (Malenka et al., 2004; Malinow et al., 2002; Sheng et al., 2002). Increased numbers of glutamate receptors have been shown to be the major expression mechanism of NMDAR-LTP (Shi et al., 1999). However, the changes in PSD morphology and composition are just beginning to be understood.

1.2. Synapse organization and plasticity

A. PSD organization and biochemical composition

PSDs were first identified in electron microscopy studies of synapses; a subpopulation of synapses, later identified as excitatory, was found to have an electron-dense thickening at the postsynaptic membrane (Gray, 1959; Gray, 1961). PSDs are found throughout the nervous system, with particularly high densities in forebrain and cerebellum (Harris et al., 1988; Harris et al., 1989; Chicurel et al., 1992). PSD shape and size varies considerably across different areas of brain and even within specific brain regions. Within hippocampal CA1 stratum radiatum, PSDs typically have diameters between 200-500 nm, thicknesses between 30-60 nm, and areas between 0.008 to 0.54 μm^2 (Harris et al., 1992; Spacek et al., 1998; Harris et al., 1989). Smaller PSDs are typically circular discs, while larger PSD often have more complex and irregular shapes, and may contain perforations.

The PSD is estimated to contain up to a thousand different proteins (Jordan et al., 2004; Yoshimura et al., 2004; Peng et al., 2004). These PSD proteins carry out a variety of functions ranging from structural maintenance to signal transduction. Structural maintenance of synapses involves cytoskeletal elements, such as actin and actin binding proteins, which maintain synapse structure; and cell adhesions proteins, such as neuroligin, neurexin, and β-catenin, which stabilize the connection between presynaptic axon bouton and dendritic spine. Signal transduction proteins include glutamate receptors and other proteins that directly pass signals, receptor accessory proteins, and downstream signaling elements. Scaffolding proteins organize proteins within the PSD (Okabe, 2007; Sheng et al, 2007). Here, I focus on

describing proteins involved in signal transduction and the proteins that organize them within PSDs. Brain regions differ significantly in PSD protein composition; here, I focus on studies of CA1 SR synapses

I. Glutamate receptors and accessory proteins

PSDs within hippocampal CA1 stratum radium contain four types of glutamate receptors: AMPARs (α-amino-3-hydroxy-5-methyl-4-isoxazolepropionic acid), NMDARs, kainate receptors and mGluRs (metabotrophic glutamate receptors; Shinohara et al., 2011). AMPARs, NMDARs, and kainate receptors are ligand-gated ion channel that open to allow the flow of ions in response to glutamate (Traynelis et al., 2010). mGluR do not contain an ion channel; their activation initiates intracellular signaling cascades (Anwyl, 1999). Each receptor type plays a distinct role in synapse function. AMPARs pass the majority of synaptic current during basal synaptic transmission at excitatory synapses (Hollman et al. 1994). NMDARs play an important role in synaptic plasticity; under basal conditions, NMDARs are usually functionally silent due to a voltage-dependent Mg^{2+} block, and only open fully in plasticity-inducing conditions. Kainate receptors do not significantly contribute to current in CA1 SR; their role remains unknown (Huettner, 2003; Pinheiro et al., 2006). mGluRs play a modulatory role in synapse function, performing a variety of actions that alter synaptic transmission and neuroexciability (Mannaloni et al., 2001). Within a single PSD in CA1 SR, there are estimated to be an average of 15 AMPARs, 20 NMDARs, and 20 mGluRs (Sheng et al., 2007). mGluR expression levels have not been quantified; however an electron microscopy study indicates mGluRs are in a majority of synapse (Lujan et al., 1996). There is a close

correlation between AMPAR number and PSD size, while NMDAR number is not related to PSD size (Takumi et al., 1999; Racca et al., 2000). Virtually all excitatory CA1 synapses contain NMDARs, while AMPARs were undetectable within ~12% of synapses (Racca et al., 2000).

TARPs (transmembrane AMPA receptor regulatory proteins) are a family of auxiliary AMPAR subunits that modulate AMPAR trafficking and function (Tomita et al., 2003; Payne, 2008). There are 4 TARP isoforms: stargazin/ γ-2, γ-3, γ-4 and γ-8. Within hippocampus, stargazin and γ-8 are the most prevalent forms (Payne, 2008). Stargazin regulates synaptic retention; stargazin binds AMPARs to PSD-95, maintaining AMPARs in PSDs (Bats et al., 2007). The role of γ-8 is not as well understood; it has been shown to be important in synaptic transmission, but not in synaptic plasticity (Sumioka et al., 2011). TARPs alter electrophysiological properties of AMPARs; TARP overexpression increases AMPAR current, while TARP knock down decreases AMPAR current (Tomita et al., 2006). Cornichon, another auxiliary subunit, increases surface expression of AMPARs (Schwenk et al., 2009). Cornichon has also been found to affect the assembly of AMPAR auxiliary subunits by limiting the number of TARPs within AMPAR complexes (Gill et al., 2011). Both TARPs and cornichon modulate AMPAR gating dynamics (Kato et al., 2010).

II. **Downstream signaling proteins**

Several downstream signaling proteins have been found within the PSD. CaMKII (Calcium/calmodulin kinase II), a holoenzyme composed of 12-14 copies of α-CaMKII and β-CaMKII, plays an essential role in LTP, and will be discussed in

more detail later. SynGAP (synaptic GTPase-activating protein) plays multiple roles in the synapse: regulating enzymatic activity, playing a role in synaptic plasticity (knockdown mice have reduced LTP), and complexing with PSD-95 (Chen et al., 1998; Kim et al., 1998; Komiyama et al., 2002). Interestingly, α–CaMKII, β–CaMKII, and SynGAP are three of the most prevalent proteins in the PSD, representing ~ 7.4%, ~1.3% and ~1.0% mass of PSD respectively (Peng et al., 2004, Sheng et al., 2007). The reason that these downstream signaling proteins are so abundant in the PSD remains unknown.

III. Scaffolding proteins

Scaffolding proteins organize receptors and other signaling molecules (Okabe, 2007; Sheng et al., 2007). One major group of scaffold proteins within the PSD are members of the membrane-associated guanylate kinase (MAGUK) protein family. These proteins include PSD-95 (postsynaptic density protein-95), PSD-93 (postsynaptic density protein-93), SAP97 (synapse associated protein 97) and SAP102 (synapse associated protein 102). MAGUKS contain multiple binding domains that bind receptors, enzymes, and structural proteins, often creating signaling complexes. PSD-95, the most studied member of this protein family, is one of the most abundant PSD proteins; PSDs contain approximately 300 copies on average, which represents 2.3% of PSD mass (Peng et al., 2004.Chen et al., 2005). PSD-95 plays an essential role in organizing a variety of postsynaptic proteins. PSD-95 interacts directly with NMDARs, facilitating the formation of NMDAR signaling complex within the PSD (Valtschanoff et al., 2001). AMPARs lack a PSD-95 binding site; however, AMPARs bind TARPs, and other AMPAR binding proteins, which link

AMPARs to PSD-95. Interestingly, overexpression of PSD-95 has been found to mimic and occlude LTP, suggesting the importance of scaffolding proteins in expression of LTP (Stein et al, 2003).

Other scaffolding proteins not in the MAGUK family include Homer, Shank, SAPAP (synapse associated protein associated protein), and AKAP (A kinase anchoring protein). SAPAP directly binds PSD-95, but its function is not completely understood; however, a recent study of the SAPAP3 in striatum found that SAPAP3 KO decreases AMPAR synaptic transmission (Wan et al., 2011). Shank does not directly bind receptors; rather, Shank connects different scaffold protein-bound receptor complexes, suggesting that it is a “master scaffold” that holds together AMPAR, NMDAR, and mGluR signaling complexes (Kreienkamp, 2008). Mutations in Shank have been identified in autism disorders, and disrupting Shank3 in mice shows normal basal transmission but deficits in LTP (Wang et al., 2011). Homer binds mGluRs, plays a role in regulating synapse size and AMPAR current (Sala et al., 2003), and helps to maintain AMPAR synaptic density (Lu et al., 2007). These proteins act together to bind mGluRs to PSDs; forming a chain that link mGluRs to PSD-95 (mGluRs bind Homer that binds Shank that binds SAPAP that binds PSD-95) (Shinonara et al., 2011). AKAP is another scaffolding protein that, like Shank, has been suggested to be a “master scaffold.” AKAP binds an array of enzymatic proteins important in downstream signaling, including the protein kinases PKC and PKA and the phosphatase calcineurin, to NMDARs and AMPARs through interactions with PSD-95. This interaction facilitates downstream signaling during

LTP (Sanderson et al., 2011), and mutations in AKAP lead to electrophysiological and behavioral abnormalities in mice (Weisenhaus et al, 2010).

B. Basic properties of NMDAR-dependent LTP

Multiple mechanisms have been shown to play a role in the induction, expression and maintenance of NMDAR-LTP. Here, we do not provide an exhaustive review of all these mechanism; rather we focus on the best understood mechanisms of both early and late phase NMDAR-LTP.

I. Early phase LTP

Up-regulation of AMPARs is the primary mechanism of NMDAR-dependent E-LTP expression; AMPAR current increases after LTP-inducing stimulation, (Kauer et al., 1988; Muller at al., 1988), and optical assays show AMPAR up-regulation occurs in conjunction with E-LTP expression (Shi et al.1999). Induction of E- LTP begins when the concentration of postsynaptic Ca^{2+} increases pass a critical threshold. Under basal conditions, a voltage-sensitive Mg^{2+} block inhibits Ca^{2+} flow through NMDARs. LTP is initiated when repeated activation of AMPARs progressively depolarizes the postsynaptic apposition, removing the NMDAR Mg^{2+} block and allowing the influx of Ca^{2+} (Malenka et al., 1999). The magnitude and precise spatial targeting of Ca^{2+} required to induce NMDAR-dependent LTP remains unknown.

Increased Ca^{2+} affects multiple signaling cascades that play a role in LTP expression. Calcium/calmodulin kinase II (CaMKII), which is activated by increased Ca^{2+}, is both necessary and sufficient for NMDAR-LTP (Hayashi et al., 2000; Lisman et al., 2002). CaMKII plays several roles in NMDAR-LTP. Phosphorylation of

AMPARs at serine 831 by CaMKII increases single channel conductance (Roche et al., 1996; Barria et al., 1997; Mammen et al., 1997; Derkach et al., 1999); however, this conductance increase only occurs in a weakly expressed subpopulation of AMPARS, and does not appear to play a major role in NMDAR-LTP. CaMKII activation is involved in up-regulation of AMPAR into the synapse (Appleby et al., 2011). CaMKII-phosphylated AMPARs bind the adaptor protein Rab11, which attaches AMPARs to myosinVa, a transport protein that translocates vesicles containing AMPARs into the spine head (Correia et al., 2008). CaMKII also phosphorylates TARPs, leading to the interaction of PSD-95 and TARPs and binding AMPARs in the PSD (Opazo et al., 2010).

Several other enzyme and enzyme pathways have been shown to play a role in E-LTP. PKC (protein kinase C) phosphorylates serines 816 and 818 on AMPAR, facilitating the binding of AMPARs to 4.1N. 4.1N is an actin-binding protein that links the actin cytoskeleton, stabilizes AMPAR surface expression and plays a role in activity dependent surface expression (Shen et al., 2000, Lin et al., 2009). PKA (cyclic adeonosine 3',5' –monophoshate (cAMP) – dependent kinase) phosphorylates AMPARs at serine 845, which up-regulates AMPAR synaptic insertion.(Hayashi et al., 2000); however, the role of PKA in E-LTP is still not completely understood. ERK/MAPK (extracellular signal regulated kinase/mitogen-activated–protein-kinase), the pathway communicates membrane-bound receptor activation to the nucleus, and has been found to play a role in many cellular functions, including cell growth and apoptosis. RAS, a small GTPase that acts up stream of ERK/MAPK, increases AMPAR trafficking (Zhu et al., 2002; Patterson et

al., 2010). The tyrosine kinase Src has been suggested to phosphorylate NMDAR, enhancing NMDAR function during LTP induction (Salter al., 1998).

II. Late Phase LTP

Unlike E-LTP, the mechanisms underlying L- LTP are not well understood. L-LTP induction has been linked to activation of ERK/MAPK and calcium/calmodulin kinase IV, which have been linked to gene expression (Miyamoto, 2006), and PKA; however the connection between these induction signals and subsequent protein translation remains unknown. Initially L-LTP does not require gene expression; however, lasting LTP requires gene expression. Here, I focus on describing mechanisms of synapse-to-nucleus communication, genes that activate in response to L-LTP, and up-regulated proteins that have been shown to be important in L-LTP.

Many mechanisms have been shown to link synaptic activity to the nuclear response. Propagation of action potentials has been proposed to affect nuclear signaling by inducing transport of molecules found in the soma into the nucleus or by directly effecting gene transcription (Adams et al., 2005). Electrical activity is sufficient to activate MAPK/ERK (Dudek et al., 2002), and induces the transcription factor NF-ATc to enter the nucleus (Graef et al., 1999). In addition to action potentials, self-perpetuating waves of Ca^{2+} can travel down the dendrites and spread into the nucleus, directly activating transcription factors like DREAM (downstream regulatory element antagonist modulator, Osawa et al., 2001). Activity-induced upregulation of synaptic Ca^{2+} causes a variety of signals to translocate from the synapse to the nucleus (Deisseroth et al., 2003, West et al., 2002). Synaptic Ca^{2+} binding triggers nuclear translocation of calmodulin and other downstream signals

that activate CREB (cAMP response element binding; Deisseroth et al., 1996; Deisseroth et al., 1998; Dolmetch et al., 2001). Several transcription regulators, including cAMP-responsive element binding protein-2 (Lai et al., 2008), NF-κB (Kaltcshmidt et al.,1995), *Aplysia* cell adhesion molecule-associated protein (Mayford et al., 1992) and Abelson interacting protein-1 (Proepper et al., 2007), travel from the synapse to the nucleus, where they can modulate gene expression (Ch'ng et al., 2011).

Several genes activate in response to plasticity have been identified. These immediate early genes include *Arc* (activity-regulated cytoskeletal-associated gene), *Egr-1* (early growth response gene, also known as zif268), and *Narp* (neuronal activity regulated pentraxin). The protein product of *Arc* is a cytosolic protein that acts on multiple signaling pathways. Arc protein affects trafficking of AMPARs through interacting with the endocytic machinery involved in AMPAR removal; Arc overexpression down-regulates AMPAR and speeds up endocytosis, while Arc KO mice have synapses with high levels of AMPAR and slower AMPAR removal (Chowdhury et al., 2006; Shepherd et al., 2011). *Egr-1* encodes a zinc finger transcription factor that has been found to upregulate *Arc* transcription (Penke et al., 2011). *Narp* encodes a protein that has been found to cluster AMPAR at synapses and has been found to regulate homeostatic scaling (O'Brien et al., 1999; Chang et al., 2010).

Other proteins up-regulated during L-LTP include PKMζ (protein kinase M ζ) and BDNF (brain-derived neurotrophic factor). PKMζ is a brain-specific, autonomously active isoform of PKC that plays an important role in maintaining late-

LTP; inhibition of PKMζ *in vivo* prevents LTP maintenance, but not induction (Ling et al, 2002; Serreno et al, 2005). A recent study showed PKMζ acts though NSF (N-ethylmaleimide-sensitive factor), a protein involved in AMPAR trafficking (Yao et al., 2009; Migues et al, 2010). In addition, PKMζ has been suggested to be a synaptic tag, marking previously potentiated synapses (Sajikumar et al., 2005; Sacktor, 2011). BDNF (brain derived neurotrophic factor), a growth factor that acts on the tyrosine kinase receptor TrkB (tropomyosin-related kinase B), has also been implicated in L-LTP maintenance. BDNF translation is up-regulated in response to L-LTP, and BDNF gets released at synapses in response to Ca^{2+} increases after high frequency synapse activation (Aicardi et al., 2004). BDNF is critical for the maintenance of L-LTP, although its role is not completely understood (Lu et al., 2008).

1.3. AMPARs

A. AMPAR Properties

I. Subunit properties

AMPARs are composed of four subunits: GluA1-4 (Dingledine et al., 1999; Mansour et al., 2001). AMPAR subunits have high structural similarity; each is composed of ~900 amino acids, has a molecular weight of ~105 kDa, and contains an extracellular N-terminal domain (NTD), 4 hydrophobic domains (including the pore loop), and a carboxyl (C) terminal tail (Hollmann et al., 1994;Palmer et al., 2005). The extracellular and transmembrane regions are very similar between subunits. All four AMPAR subunits undergo alternative splicing in the NTD to produce the “flip” and “flop” variants. Flip desensitizes 4 times slower in respond to

glutamate than flop, and is more responsive to cyclothiazide, a drug used to block desensitization. Expression of flip and flop AMPAR variants vary throughout the central nervous system. Within hippocampal CA1 stratum radiatum, both flip and flop are expressed; however, flop is more abundant.(Sommer et al.1990).

Subunit C terminals, the most diverse region of each subunit, contain PDZ binding domains and determine the majority of AMPAR protein interactions (Reference). GluA1, GluA4, and an alternative splice form of GluA2 (GluA2L) have long C terminal tails with a type I PDZ domain, while GluA2, GluA3, and an alternative splice form of GluA4 (GluA4s) have short C terminal tails with a type II PDZ. GluA2L and GluA4s are less common than short-tailed GluA2 and long tailed GluA4 (Shepherd et al., 2007). Different PDZ domains bind different proteins, leading to different mechanisms of trafficking based on AMPAR subunit composition. Due to the importance of the C terminal in receptor trafficking, its structure will be further discussed in relation to AMPAR trafficking.

II. Receptor composition

AMPARs are tetramers composed of two pairs of four subunits. AMPAR subunit composition varies depending on brain region (Petralia et al., 1992). Within mature hippocampus, GluA1, GluA2 and GluA3 are the subunits expressed, and two AMPAR subunit combinations dominate: heteromers of GluA1 and GluA2 (GluA1/2) and GluA2 and GluA3 (GluA2/3) (Wenthold et al., 1996). These heteromers are also the dominant combinations in adult nucleus accumbens, dorsal striatum, and prefrontal cortex (Reimer et al., 2011), and are thought to be the dominant combination in cerebral cortex, olfactory bulb, lateral septum, basal ganglia, and

amygdala (Palmer et al., 2005). Heteromers of GluA1 and GluA3 have been shown to form in GluA2 KO mice; however, these heteromers rarely form *in vivo* synapse (Sans et al., 2003). GluA4 expression is generally low in the adult except in reticular thalamic nucleus, brain stem, and cerebellum.

Homomers, whose formation is less energetically favorable than heteromers, are receptors composed entirely of a single subunit (Greger et al., 2007b). Homomeric GluA2, GluA3, and GluA4 are uncommon *in vivo*; however, homomers made of GluA1 subunits are more common. The role GluA1 homomers play in synaptic transmission is not understood, although GluA1 homomers have been found to be stabilized adjacent to the PSD (He et al., 2009). In addition, GluA1 homomers potentially play an important role in induction of LTP (Plant et al., 2006), although this result is not universally accepted (Adenik et al., 2007).

Although GluA1/2 and GluA2/3 are known to be the predominant AMPAR subunit combination within the PSD, the proportion of GluA1/2 versus GluA2/3 within synapses has remained contentious. Within CA1 stratum radiatum, GluA2/3 was initially thought to be the predominant AMPAR subunit combination (Wenthold et al., 1996); however, GluA1/2 and GluA2/3 proportion were estimated by performing co-immunopurification, on a mixed population of cells that did not distinguish between receptors within in the PSD, receptors found on extrasynaptic sites, and receptors from intracellular pools. A recent study performed electrophysiology on cells with knocked out AMPAR subunit types suggests that ~80% AMPAR expressed in CA1 SR synapses are GluA1/2 heteromers and the remaining receptors are primarily GluA2/3 heteromers (Lu et al., 2009).

III. Receptor properties

AMPAR kinetic properties are highly dependent on subunit composition. The majority of AMPARs contain GluA2 (Greger et al., 2002; Wenthold et al., 1996; Lu et al., 2009), and the presence of GluA2 accounts for many of the defining properties of AMPARs (Isaac et al., 2007). A posttranslational modification within the GluA2 pore region (a glutamate-to-arginine edit) causes AMPARs to lack Ca^{2+} permeability, decreases channel conductance, and prevents polyamine blockage, leading to AMPARs being non-rectifying and having a linear relationship between membrane voltage and current (Verdoorn et al., 1998, Sommer et al., 1991; Hollmann et al., 1991). With the exception of receptors lacking GluA2, receptors generally have very similar responses. AMPARs lacking GluA2 are inwardly rectifying and permeable to Ca^{2+}, though much less Ca^{2+} permeable than NMDARs (Burnashev et al,.1992).

IV. AMPAR organization within PSD

The organization of receptors within the PSD plays an important role in synaptic function. During presynaptic vesicle release, glutamate concentration within the synaptic cleft peaks to 1-3 mM before rapidly decaying in 100 to 200 μs (Clements et al., 1992; Clements, 1996). Since AMPARs have a relatively low affinity for glutamate (Clements et al,. 1992) and multiple AMPAR sites must bind glutamate before the ion channel opens (Rosenmund et al., 1998), alignment between AMPAR and presynaptic sites of glutamate release is particularly important to ensure glutamate activates AMPARs. Indeed, modeling studies predict that precise alignment between presynaptic sites of glutamate release and postsynaptic

receptors increases synaptic efficiency (Xie et al., 1997; Raghavachari et al., 2002; Franks et al., 2003).

AMPARs were initially thought to display a uniform lateral distribution over the PSD (Baude et al., 1995). However, current data from multiple EM studies suggests that the average tangential position of AMPARs across the synapse is closer to the PSD edge. Using immunogold electron microscopy, higher labeling density was found towards the PSD edge rather than the PSD center in multiple brain regions, including organ of Corti (Matsubara et al., 1996; Ottersen et al., 1998), neostriatum (Bernard et al., 1997), cerebral cortex (Kharazia et al., 1997), and olfactory bulb (Sassoe-Poenetto et al., 2000). Similar results were found using electron tomography; structures whose extracellular domains matched the expected dimensions of AMPARs were found be arrayed around the PSD periphery (Chen et al., 2005). Imagining of AMPARs within main and accessory olfactory bulb PSD using the super-resolution light microscopy technique STORM (stochastic optical reconstruction microscopy) indicated a high level of variability in AMPAR distribution across PSDs (Dani et al., 2010). Other types of glutamate receptors organize within the PSD; NMDAR concentrate in the center of the PSD (Kharazia et al., 1997; Racca et al., 2000) and metabotropic glutamate receptors (mGluRs) lie at the PSD edge (Baude et al., 1993; Nusser et al., 1994); however, the functional consequences of this organization remain unknown.

The 2- dimensional distribution over the PSD has been studied using SDS-digested freeze fracture replica labeling, a technique that achieves higher immunogold labeling density than typical immunogold electron microscopy. AMPARs

are found to collect into microclusters on the PSDs in synapses between parallel fibers -Purkinje cell within cerebellum (Masugi-Tokita et al., 2007) and in synapses on relay cells from the retina (retinogeniculate) and visual cortex (corticogeniculate) in dorsal lateral geniculate nucleus (Tarusawa et al., 2009). Interestingly, the corticogeniculate synapses are twice as large as the retinogeniculate synapses, thus more area within the CG synapses lack AMPAR distribution. However, AMPAR microclustering has not been found to occur at all synapses; AMPAR distribution is homogenous over PSDs between synapses at climbing fiber- Purkinje cell synapses (Masugi-Tokita et al., 2007).

B. AMPAR synaptic insertion.

Synaptic insertion of AMPARs is multistep process that occurs in both an activity-dependent and constitutive manner. Activity-dependent trafficking changes the amplitude of synaptic response and occurs after LTP induction, while constitutive trafficking continuously replaces receptors and does not change the magnitude of synaptic response (Shi et al., 2001). Early research on AMPAR trafficking determined that different mechanisms exist for activity-dependent and constitutive insertion. These differences in AMPAR trafficking are subunit-dependent; in hippocampus, GluA1-containing receptors insert into the PSD in response to LTP, leading to NMDAR activation (Hayashi et al., 2000), while continued exchange of receptors at the synapse happens for receptors only containing GluA2 and GluA3 (Passafaro et al., 2001, Shi et al., 2001). These observations have led to a model where synaptic insertion of GluA1/2 is activity-dependent and GluA2/3 is constitutive.

I. Differences in C terminal tails

AMPAR trafficking routes depend on differences in AMPAR subunit C terminals. GluA1, GluA2, and GluA3 contain different phosphorylation sites, which affect properties such as channel kinetics and AMPAR trafficking, and protein binding sites, leading to activity-dependent trafficking of GluA1/2 and constitutive trafficking of GluA2/3; these differences account for the different trafficking routes (Malinow et al., 2003). Overexpression of the C tails of GluA1 and GluA2 has been shown to block or reduce both activity-dependent and constitutive trafficking (Passafaro et al., 2001; Shi et al., 2001).

Many of the regions in the C terminal of GluA1 are involved in AMPAR trafficking. Synapse-associated protein97 (SAP97), a member of the PSD-95-like membrane-associated guanylate kinase (PSD-MAGUK) protein family, is the only protein known to interact with the GluA1 C terminal PDZ domain, but its role in AMPAR trafficking and LTP remains unknown. Early studies indicated that SAP97 interacts with AMPARs contained in the ER (Sans et al., 2001; Klöcker et al., 2002). However, a recent study showed that overexpression of SAP97 in immature neurons increases synaptic AMPAR expression, and that mature neurons with increased levels of SAP97 through development have enhanced AMPAR currents (Howard et al., 2010). In addition, overexpression of SAP97 increases both size and complexity of PSDs (Poglia et al., 2011). Other important C terminal sites, such as phosphorylation sites serine 816, 818, 831, and 845 and binding site for 4.1N, have previously been discussed in reference to LTP.

The C termini of GluA2 and GluA3 are very similar, and contain many of the same phosphorylation and protein binding sites. Both GluA2 and GluA3 contain binding sites for GRIP1 (Glutamate-receptor-interacting-protein1), GRIP2 (also known as AMPA receptor-binding protein) and PICK (protein interacting with C-kinase). GRIP1 has been suggested to be important for intracellular transport of AMPAR; GRIP1 binds kinesin5, a microtubule-based motor protein that is important for the vesicular transport (Setou et al., 2002). In addition, both GRIP1 and GRIP2 have been suggested to play a role in activity-dependent AMPAR recycling (Mao et al., 2010). The role of PICK1 (protein interacting with C kinase) in AMPAR trafficking is less direct; PICK1 has been shown to maintain AMPAR internalization, which potentially provides a pool of AMPAR available to synaptic insertion (Perez et al., 2001; Citri et al., 2010). GluA2, but not GluA3, contains a binding site for NSF, an ATPase that plays an essential function in membrane fusion in intracellular trafficking and presynaptic vesicle fusion (Rothman, 1994; Nishimune et al., 1998; Araki et al., 2010) Expression of a peptide that interferes with NSF leads to a decrease in AMPAR surface density (Noel at al., 1999).

II. AMPAR trafficking pathways

AMPAR trafficking begins with subunit synthesis in the endoplasmic reticulum (ER) (Palmer et al., 2005, Greger et al., 2007a). After subunit translation, subunits first associate into dimers, and subsequently form tetramers (Ayalon et al., 2001; Mansour et al., 2001). The newly synthesized AMPAR undergoes several postranslation modifications, such as the previously discussed glutamine-to-arginine pore loop edit, and associate with TARPs before being trafficked to the Golgi

(Vandenberghe et al., 2005). Interestingly, GluA2 impedes trafficking out of the ER. This potentially maintains a large pool of GluA2 for binding with other subunits, and may partially explain why most AMPARs contain GluA2 (Greger et al., 2003).

Within the Golgi, AMPARs undergo several other modifications, such as modification of high-mannose sugar into more complex carbohydrates (Shepherd et al., 2007). nPIST (neuronal isoform of protein-interacting specifically with TC10), a Golgi apparatus resident protein, interacts with TARP, helping to target AMPARs to the synapse (Cuadra et al., 2004). After AMPARs are packaged on trafficking vesicles, these vesicles attach to motor proteins, such as myosin (Lisé et al., 2005; Correia et al., 2008), dynein and kinesin (Setou et al., 2002) and undergo active transport down actin or microtububles. There is evidence that intracellular transport of GluA1-containing AMPAR sis LTP-dependent, suggesting that different intracellular pathways may account for differences in AMPAR trafficking.

AMPAR synaptic delivery begins with exocytosis of AMPAR-containing vesicles. Although a few studies have indicated that AMPARs may be inserted directly into the PSD or at the soma (Gerges et al., 2006; Adenik et al., 2007), the majority of evidence suggests that AMPARs are inserted into the dendritic spine away from the synapse (Kopec et al., 2006; Park et al., 2006; Yang et al., 2008; Kennedy et al., 2010; Tao-Cheng et al., 2011), or on the dendritic shaft (Yudowski et al., 2007; Makino et al., 2009). After exocytosis, receptors inserted outside the PSD undergo lateral diffusion to enter synapses, and become trapped in PSDs (Borgdorff et al., 2002; Choquet et al., 2003, Choquet, 2010). It remains unknown if GluA1/2 and GluA2/3 are inserted at different location.

1.4. AIDA-1

A. AIDA-1 properties

AIDA-1 is a recently discovered protein whose function remains unclear. AIDA-1 was identified in a yeast-two hybrid screen using a cleavage product of amyloid-β protein precursor (AβPP) as bait (Ghersi et al., 2002; Ghersi et al., 2004). Two subsequent cleavages of AβPP, first by β-secretase and then γ-secretase, produces β–amyloid, a major component of the amyloid plaques often found in Alzheimer's disease (Duyckaerts et al., 2009). AβPP intracellular domain (AID, or AICD), the other AβPP product produced during the cleavage that produces Aβ and the yeast-2 hybrid bait, may play a role in apoptosis, calcium homeostasis, and transcriptional regulation (Hamid et al., 2007; Müller et al., 2008; Slomnicki et al., 2008); however, whether AID plays a role in Alzheimer disease remains controversial.

Alternative splicing of AIDA-1 produces several isoforms. Currently, four isoforms of AIDA-1 have been characterized, although many other isoforms are known to exist (Jordan, BA, unpublished data). All published AIDA-1 isoforms contain a phospho-tyrosine binding domain (PTB) and one or two sterile α motifs (SAM) domains; these domains mediate protein-protein interaction (Ghersi et al., 2002; Ghersi et al., 2004; Xu et al., 2005; Jordan et al., 2007). Interestingly, some AIDA-1 isoform, like AIDA-1b, are not capable of binding AβPP. AIDA-1 isoforms appear to have different functions. AIDA-1a has a modulatory effect on AβPP processing; binding of AIDA-1a to AβPP blocks the ability of γ-secretase to cleave AβPP, diminishing Aβ secretion. AIDA-1c, another AIDA-1 isoform, is a binding

partner of coilin, a marker protein of Cajal bodies. Cajal bodies are nuclear suborganelles that contain the highest nuclear proportion of small nuclear ribonucleoproteins (snRNPs), which play a role in pre-mRNA processing. Knock down of AIDA-1c with siRNA disrupts Cajal bodies and lead to increased cell death (Xu et al., 2005).

B. AIDA-1 and L-LTP

Recent evidence suggests that AIDA-1 may play a role in synapse-to nucleus signaling during NMDAR-dependent LTP. Using biochemical methods, AIDA-1d, a previously unrecognized isoform of AIDA-1, was identified and found to be a prevalent component of the PSD, having an estimated relative abundance of 50-190% that of PSD-95 (Jordan et al., 2004; Peng et al., 2004; Yoshimura et al., 2004). Intriguingly, AIDA-1d contains a nuclear localization sequence (Kurabi et al., 2009). AIDA-1 appears to have a unique synapse-to-nucleus signaling mechanism. After synaptic NMDAR activation, AIDA-1 is cleaved at the PSD and an AIDA-1 fragment translocates to the nucleus (Jordan et al., 2007). After entering the nucleus, AIDA-1 stabilizes the interaction between Cajal bodies and nucleoli, leading to downstream increases in protein translation (Jordan et al., 2007). Together, this evidence suggests that AIDA-1 might link synaptic activity to a nuclear response. However, AIDA-1 only has been studied in culture systems and little is known about its distribution *in vivo*.

1.5. Conclusion

Here, we study the basal organization of AMPAR and AIDA-1. For AMPARs, whose organization throughout the brain has been thoroughly studied, we

determined the lateral position of different subunit-containing AMPAR within the PSD. For AIDA-1, we determined the distribution throughout rat brain and determined the cellular and subcellular and PSD distribution. Together, these studies not only describe the position of AMPARs and AIDA-1, but also provide suggestions of potential functions based on their organization.

CHAPTER 2

The organization of AMPA-type glutamate receptors in rat hippocampus

2.1 Introduction

The postsynaptic density (PSD) serves as the primary postsynaptic site of signal transduction. A primary function of the PSD is to organize ionotropic glutamate receptors in the synapse, though it also contains downstream signaling molecules, scaffold proteins, and cytoskeletal elements (Okabe et al., 2007; Sheng et al., 2007); Computational studies suggest that the arrangement of receptors within the PSD influences the efficiency and specificity of synaptic transmission (Xie et al., 1997; Franks et al., 2003; Raghavachari et al., 2004).

The AMPA (α-amino-3-hydroxy-5-methyl-4-isoxazolepropionic acid) subtype of glutamate receptor (AMPAR) plays a major role in mediating fast excitatory neurotransmission within the CNS (Dingledine et al., 1999; Palmer et al., 2005). AMPARs are tetrameric heteromers comprising combinations of the four subunits, GluA1-4 (Hollmann et al., 1994; Rosenmund et al., 1998; Mansour et al., 2001). At synapses in adult hippocampus, the most common subunit combinations are GluA1 and GluA2 (GluA1/2 receptors) and GluA2 and GluA3 (GluA2/3 receptors; Wenthold et al., 1996; Lu et al., 2009). AMPARs appear to be highly mobile, at least in cultured neurons (Borgdorff et al., 2002; Groc et al., 2007), and can cycle into the postsynaptic membrane through both activity-dependent and constitutive insertion

(Shepherd et al., 2007). Synaptic insertion seems to be subunit-dependent: GluA1-containing AMPARs are thought to traffic into the synapse in response to synaptic activity (Shi et al., 1999; Hayashi et al., 2000), whereas GluA2/3 receptors undergo constitutive recycling (Passafaro et al., 2001; Malinow et al., 2003; Kessels et al., 2009).

Considerable evidence suggests that AMPARs are removed from the postsynaptic membrane at a specialized zone lateral to the PSD (Blanpied et al., 2002; Racz et al., 2004). However, the site(s) of AMPAR insertion remain more contentious. Work in reduced systems has demonstrated AMPAR insertion at a variety of locations including the postsynaptic soma (Adenik et al 2007; Tao-Cheng et al., 2011), dendritic shaft (Yudowski et al., 2007) and spine (Kopec et al., 2006; Yang et al., 2008; Makino et al., 2009; Kennedy et al., 2010; Tao-Cheng et al., 2011), as well as the postsynaptic membrane itself (Gerges et al., 2006). However, it remains unknown if GluA1/2 and GluA2/3 receptors are inserted in different subcellular locations.

Here, we use postembedding immunogold electron microscopy to study the organization of these three AMPAR subunits in axospinous synapses within CA1 stratum radiatum of the rodent hippocampus. We find that GluA1 distributes uniformly along the PSD, extending into extrasynaptic membrane, while GluA3 lies more centrally within the PSD. These findings point to a hitherto-unrecognized organizational complexity tangentially along the synaptic apposition. They raise the possibility that GluA3-containing AMPARs may play a specific role within the center of the synapse, and support previous suggestions that GluA1/2 traffics into and out

of the synapse via lateral diffusion, while GluA2/3 receptors traffic from postsynaptic cytoplasm directly into the PSD.

2.2 Experimental procedures

Tissue Preparation

All procedures related to the care and treatment of animals were conducted according to institutional and NIH guidelines. For this study, we used six male Sprague-Dawley rats, ages 2 - 4.5 months old; to assess whether synaptic organization might differ in the juvenile, we also sacrificed one 40 day-old rat (Charles River Laboratories; Raleigh, NC, USA). To control for antibody specificity and to examine effects of subunit deletion on the location of AMPARs within the synapse, we used two GluA1 KO mice (seven weeks old), two GluA2 KO mice (eight weeks old), and one C57BL/6 WT mouse (one month old). GluA1 KO and Glu2 KO mice were generated as previously described (Zamanillo et al., 1999, Jia et al., 1996) and were initially maintained on a C57BL/6 background. After anesthetizing rats with sodium pentobarbital (60 mg/kg), and mice with a mixture of ketamine (100 mg/kg) and xylazine (10 mg/kg), animals were intracardially perfused with saline, followed by ~ 500 ml (for rats) and ~50 ml (for mice) of a mixture of 2% paraformaldehyde and 2% glutaraldehyde in phosphate buffer (PB). Brains were removed and postfixed 12-48 hours in the same fixative at 4℃. Coronal sections were cut on a Vibratome at 200-250 μm and collected in cold PB.

Sections pretreated with 0.1% $CaCl_2$ in sodium acetate were cryoprotected in 30% glycerol overnight. Small blocks CA1 stratum radiatum were cut from sections and frozen in isopentane chilled with dry ice. Frozen blocks were immersed in 1.5% uranyl acetate in methanol at -90℃ for 48 hours wit hin a freeze-substitution

instrument (AFS, Leica). Blocks were gradually warmed to -45℃, then infiltrated with Lowicryl (HM-20, Electron Microscopy Science) and polymerized under UV light.

Antibodies

Primary antibodies included affinity-purified rabbit polyclonal antibodies against AMPA receptor subunit 1(GluA1; 0.8 – 2.0 μg/ ml; Chemicon, Temecula, CA; AB1504) and AMPA receptor subunits 2 and 3 (GluA2-3; 0.4 - 0.8 μg/ ml; Chemicon; AB1506), and a mouse monoclonal antibody raised against AMPA receptor subunit 3 (GluA3; 0.5 – 1.0 μg/ ml; Chemicon; MAB5416).

The GluA1 antibody was raised against a peptide (SHSSGNPLGATGL) corresponding to the carboxyl terminus of human GluA1, conjugated to keyhole limpet hemocyanin. In Western blot on homogenized cells that were transfected with GluA1 cDNA, the GluA1 antibody recognized a single band at ~108 kDa corresponding to GluA1, while antibodies against GluA2, GluA3,or GluA4 produced no staining (Wenthold et al., 1992).The GluA2-3 antibody was raised against a peptide (EGYNVYGIESVKI) corresponding to the carboxyl terminus of rat GluR2, conjugated to BSA. On immunoblots of protein extract from heterologous expression systems, it recognizes both GluA2 and GluA3 (whose C-terminal is nearly identical to GluA2) with equal efficacy, but does not recognize GluA1 (Wenthold et al., 1992). The GluA3 antibody was raised against a fusion protein containing amino acids 245-451 of GluA3. The specificity of the GluA3 antibody was demonstrated in Western blots of HEK cell lysates transfected with various AMPAR cDNAs; the antibody reacted with lysate containing GluA3, but not lysate from cells expressing GluA1, GluA2, or GluA4 (Moga et al. 2003).

Postembedding Electron Microscopy

For postembedding immunogold labeling, 60 nm sections were cut from the polymerized tissue blocks and collected on nickel grids. For serial section electron microscopy, 50 nm sections were collected on Formvar-coated nickel slot grids to preserve cutting order.

Grids were pretreated with 4% *p*-phenylenediamine in TRIS-buffered saline with 0.005% Tergitol NP-10 (TBSN), pH 7.6 before treatment with 1% bovine serum albumin in TBSN, pH 7.6, followed by overnight treatment with the primary antibody. Grids were subsequently treated with 1% normal goat serum in TBSN pH 8.2, after which a gold-conjugated secondary was applied (10 nm, Jackson ImmunoResearch). The sections were post-stained using uranyl acetate and Sato's lead salts. Grids were examined on a Philips Tecnai electron microscope at 80 kV; images were collected with a Gatan 12 bit 1024 X 1024 cooled CCD camera.

Image Processing

Figures were composed, and contrast and brightness adjusted, with Adobe Photoshop CS (v 9.0.2, Adobe Systems, Mountain View, CA USA). All processing procedures were applied uniformly across the entire image.

Analysis of Synaptic Immunogold Labeling

To determine the percentage of synapses immunopositive for GluA1, GluA2-3 and GluA3, synapses within random fields in grids from CA1 stratum radiatum were counted. Synapses containing at least one gold particle within 100 nm of the PSD were counted as positive; all other synapses were negative. To assure synapses were chosen at random, the first 100 synapses encountered in a grid square were

counted. We examined 500 synapses for each antibody on WT, GluA1 KO, and GluA2 KO tissue. These data were used to calculate the fraction of synapses immunopositive for each antibody. When calculating the fraction of immunopositive synapse for each antibody, each grid square was taken as a single sample

To determine AMPAR position within the PSD, we collected electron micrographs of randomly-selected synapses from CA1 stratum radiatum that contained gold particles within 100 nm of the PSD and that had a clearly-defined postsynaptic membrane. Using ImageJ, we measured "axo-dendritic" position, the distance from the center of each gold particle to the postsynaptic plasma membrane, and “lateral" position, the distance (measured tangentially along the plasma membrane) from the particle to each edge of the postsynaptic density (Fig. 1). From the lateral position data, we calculated a “normalized lateral" (NL) position using the following formula:

$$NL\ position = \frac{Distance\ of\ gold\ particle\ from\ PSD\ center}{Distance\ from\ PSD\ edge\ to\ center}$$

such that an NL position of 0 corresponds to a particle lying at the middle of the synapse, and an NL position of 1.0 to a particle lying at its lateral edge. For further details, see Kharazia et al (1997); Valtschanoff et al (2001).

We compared axo dendritic and NL position from the 40 day old animal (weight 125g) against data from the six other rats. Data from the 40 day old rat was not significantly different from the rest of the data, thus we grouped all data together.

For axo-dendritic position, the postsynaptic direction was denoted by positive numbers; negative numbers denoted the presynaptic direction. When assessing axo-dendritic position, we limited our analysis to gold particles whose NL position

was less than 1.5 and did not lie more than 60 nm away from the edge of the PSD, to limit consideration to gold particles associated with the synapse. Likewise, when calculating the mean axo-dendritic position, our goal was to estimate positions of receptors inserted into the plasma membrane. Therefore, for this computation we considered only particles lying in the range from -50 to 50 nm in the axo-dendritic axis. When graphing axo-dendritic position, we divided the data into 5 nm bins, smoothing with a three-point weighted running average:

$$y_{j(smoothed)} = \frac{\left[y_{(j-1)} + 2y_j + y_{(j+1)} \right]}{4}$$

Data analysis was performed in Excel (Microsoft); graphs were prepared with KaleidaGraph (Synergy Software, Reading, Pa, USA). Values are reported as means and standard errors. These were calculated either by treating each gold particle as a sample (to provide an optimal estimate of the population mean, in the face of random measurement noise), or by calculating averages for each animal and treating these average values as single samples (to permit robust testing of possible differences between data sets, using 2-sided paired t tests.

Serial Section Analysis

In our hands, immunoreaction is impaired when serial sections are used (at least in part because only one side of the thin section is exposed to antibody). To assess whether this might have led us to misleading conclusions, we performed a pilot serial section analysis, collecting several series of electron micrographs of the same area from grids containing ~ 50 nm thick serial sections, stained against either GluA1 or GluA3. We chose areas containing landmarks that would simplify tracking the same synapse. For analysis, stained synapses were examined across multiple

sections until no longer visible; PSD length and gold particle position(s) were measured.

2.3 Results

Immunolabeling for AMPAR subunits in rat hippocampus

Tissue processed by freeze substitution exhibited satisfactory ultrastructural preservation, while retaining immunoreactivity against all three AMPAR antibodies. Immunogold label for all three antibodies showed a clear association with asymmetric synapses, concentrating in the vicinity of the postsynaptic membrane (Fig. 2). Labeling for GluA2-3 seemed most abundant, whereas labeling for GluA3 seemed noisier with less prominent synaptic label. Our visual impression was that labeling for GluA1 often lay near the lateral edge of synapses, GluA2-3 seemed more uniformly spread over synapses, and GluA3 generally seemed to lie closer to the center of synapses.

Immunolabeling in knockout material.

To assess antibody specificity, we performed immunogold staining in GluA1 KO and GluA2 KO mice, focusing on CA1 stratum radiatum. In grids prepared from a WT mouse, the GluA1 antibody labeled 47 ± 3% of synapses, but only 6.4 ± 0.2% of synapses were labeled in the GluA1 KO, implying that at least 85% ((1 - 6.4/47) x 100%) of label in the WT mouse reflected authentic GluA1 (Table 1). Likewise, the GluA2-3 antibody (expected to recognize both GluA2 and GluA3) labeled 54 ± 2% of WT synapses versus 11 ± 2%of GluA2 KO synapses. This five-fold reduction in labeling also supports the specificity of the immunogold signal, especially considering that much of the signal remaining in the GluA2 KO likely reflects GluA3. Because of the limited sensitivity of postembedding methods and the fact that these

data were from single sections, the observed fraction of immunopositive synapses in the WT may underestimate their true frequency. The 44% reduction in GluA1-positive synapses in the GluA2 KO presumably reflects the predominance of GluA1/GluA2 heteromeric receptors in the intact animal (c.f. Petralia et al., 2004), and the synaptic GluA3 remaining in the GluA2 KO animal might reflect aberrant presence of GluA1/GluA3 receptors after deletion of GluA2 (Table 1). However, the 37% reduction of synaptic GluA3 in the GluA1 KO mouse raises the possibility that GluA1/GluA3 receptors are present in the hippocampus even in the normal animal.

We were unable to obtain GluA3 KO mice; to assess specificity of the GluA3 antibody, we instead compared immunogold labeling for GluA2-3 and GluA3 in cerebellar cortex, whose layers (which are easily recognized at the electron microscope) express message for different AMPAR subunits at markedly different levels. Thus, *in situ* hybridization indicates high levels of gene expression for both GluA2 and GluA3 in the molecular layer; in contrast, GluA3 expression is substantially reduced in the granule cell layer, while message for GluA2 remains high (Lein et al., 2007). Therefore, one would predict that a greater fraction of synapses would label for GluA3 in the molecular layer than in the granule cell layer, while comparable fractions would label for GluA2 in both layers. Consistent with this expectation, 53 ± 2% of synapses labeled for GluA3 in the molecular layer, whereas only 22 ± 2% of synapses labeled for GluA3 in the granule cell layer. In contrast, there was no difference in GluA2-3 labeling between the molecular and the granule cell layers.

In summary, these data, along with the extensive previous work using these antibodies, lead us to conclude with high confidence that the observed labeling identifies authentic subunit protein.

Position of AMPAR subunits within the synapse

Using quantitative immunogold labeling on grids prepared from rat CA1, we measured the “axo-dendritic” position of gold particles coding for GluA1, GluA2-3, and GluA3 subunits in synapses within stratum radiatum (Fig. 3). When determining average axo-dendritic position, we limited our data set to particles between -50 to 50 nm from the postsynaptic membrane to get the average axo-dendritic position of AMPAR closely associated with the postsynaptic membrane. Mean positions for both GluA1 and GluA2-3 were postsynaptic; GluA1 and GluA2-3 averaged 4.2 ± 0.6 nm and 3.3 ± 0.6 nm inside the postsynaptic membrane, respectively. Both antibodies displayed similar axo-dendritic distributions. The distribution of GluA3 also had a similar shape, but its mean value was within the synaptic cleft, -4.3 ± 0.8 nm from the postsynaptic membrane. The shapes of all three curves resembled Gaussian curves with standard deviation of ~15 nm, and each had a tail extending into the postsynaptic cytoplasm (Fig. 3). The GluA3 distribution was statistically different from both GluA1 and GluA2-3, as verified by comparing average values on a per-animal basis ($p < 0.001$, 2-sided t-test; $N = 7$ animals), whereas GluA1 was not significantly different from GluA2-3. The different axo-dendritic positions likely reflect the different location of the epitopes recognized by the three antibodies: the GluA1 and GluA2-3 antibodies were raised against peptides corresponding to the C terminals (which should lie within the postsynaptic cytoplasm when the receptor is

inserted into the plasma membrane), while the GluA3 antibody was raised against a peptide corresponding to an extracellular region near the N terminal (see Methods). These results suggest that the large majority of immunogold-detected AMPARs lying within 50 nm of the postsynaptic plasma membrane are embedded within the plasma membrane.

Next, we examined the organization of different AMPAR subunits tangentially along the synapse. Because our interest was specifically in AMPARs inserted into the postsynaptic plasma membrane, we restricted the data set accordingly: For GluA1 and GluA2-3 antibodies (both targeted against the cytoplasmic C terminus) we considered only particles in a 50 nm window lying between -20 nm and 30 nm from the postsynaptic membrane (i.e., within ~25 nm of the likely position of the relevant epitope). Likewise, for the GluA3 antibody (targeted against an extracellular N-terminal region), we considered only particles lying between -30 nm and 20 nm. To compare lateral position across PSDs of different lengths, we calculated normalized lateral (NL) position, such that a value of 0 corresponds to a particle centered in the synapse, and a value of 1.0 corresponds to a particle at the PSD edge (See Methods and Figure 1). GluA1 had a mean NL position of 0.64 ± 0.01, while GluA3 concentrated closer to the PSD center, with a mean NL position of 0.51 ± 0.03; GluA2/3 lay between GluA1 and GluA3, with an average NL position of 0.59 ± 0.02. We also measured NL position of the AMPAR subunits in KO animals. For the GluA2 KO, the average NL position of GluA1, GluA2-3 and GluA3 were 0.62 ± 0.02, 0.55 ± 0.02, and 0.52 ± 0.02 respectively (close to the values for WT animals). In contrast, in the GluA1 KO animal, the NL position of GluA2-3 was 0.47 ± 0.01 and

of GluA3 was 0.46 ± 0.02 (Table 3). Thus, labeling for GluA3 and especially for GluA2-3 was more centrally localized than in WT animals, suggesting that the presence of GluA1 protein allows AMPA receptors to spread out tangentially along the synapse.

The GluA2-3 antibody can bind to AMPARs containing either GluA1/2 or GluA2/3 subunits. Since the GluA1 antibody is expected to label GluA1/2 receptors, but not GluA2/3 receptors, while the GluA3 antibody should label GluA2/3 receptors, but not GluA1/2 receptors, we restricted our attention to these two antibodies. Quantitative analysis showed that labeling for GluA1 was rather uniformly distributed tangentially along the synapse, extending beyond the limits of the PSD; in contrast, labeling for GluA3 concentrated at the center of the synapse, with very little labeling beyond its lateral edge (Fig. 4A). Labeling for GluA2-3 was intermediate between GluA1 and GluA3 (data not shown). This difference was significant, as demonstrated by examining data from N = 7 animals (mean NL position for GluA1, 0.64 ± 0.01; mean position for GluA3, 0.51 ± 0.03; $p < 0.05$).

To quantify the difference in normalized position, we calculated the ratio of the number of gold particles that were greater than a NL position of 0.5 over the number of gold particles that were less than a NL position of 0.5 for GluA1 and GluA3. The ratio for GluA1 displayed an approximately twofold increase over the ratio for GluA3, indicating that GluA1 localizes closer to the PSD edge than GluA3 (Fig. 4). We used normalized lateral positions to facilitate comparisons among synapses of different sizes. However, it is conceivable that at least part of the observed effect might represent an artifact arising from a systematic difference in size between synapses

immunopositive for GluA1 and those positive for GluA3.To exclude such possibilities, we directly compared the number of immunogold particles lying just beyond the edge of the synapse with the number in the center of the PSD, for both antigens. Accordingly, we computed the ratio of the total number of particles lying 0-25 nm beyond each side of the synaptic border with the number of particles lying within a 50 nm strip at the very center of the PSD. As with the NL position ratio, there was an approximately twofold increase in ratio in GluA1 compared with GluA3, confirming that more GluA1 lies beyond the edge of the synapse (Fig 4C).

The relative levels of expression of GluA1/2 and GluA2/3 receptors in adult hippocampal synapses remain somewhat controversial (Wenthold et al., 1996; Lu et al., 2009). Our data on the lateral distribution of subunits provides a novel way to estimate the proportion of synaptic AMPARs that contain GluA1/2 versus GluA2/3. Assuming that AMPAR in the postsynaptic membrane of CA1 pyramidal cells are either GluA1/2 or GluA2/3 heteromers, the antibody against GluA1 would label only GluA1/2 receptors, while the antibody against GluA3 would label only GluA2/3 receptors; thus, the NL position for GluA1 (0.64) should provide an unbiased estimate of the mean position of GluA1/2 receptors in the synapse, whereas the NL position of GluA3 (0.51) estimates the mean position of GluA2/3 receptors. The NL position of the GluA2-3 antibody (0.59) includes information from both GluA1/2 and GluA2/3 receptors. Combining these data, we can estimate what percentage of synaptic AMPARs is GluA1/2 versus GluA2/3.

The GluA2-3 antibody recognizes a C-terminal epitope shared by GluA2 and GluA3, and would therefore be expected to bind to each with comparable efficiency.

However, considering AMPA receptor stoichiometry ((2*GluA1 + 2*GluA2), or (2*GluA2 + 2*GluA3 (Wenthold et al., 1996), one would expect twice as many gold particles coding for the GluA2-3 antibody to bind to GluA2/3 receptors as to GluA1/2 receptors. Thus,

$$\mathrm{NLP}_{GluA2-3} = \frac{(\mathrm{NLP}_{GluA1} + 2 * \mathrm{NLP}_{GluA3})}{(\text{fraction of AMPARs containing GluA1}) + 2 * (\text{fraction of AMPARs containing GluA3})}$$

Using this method, we estimate that 74% of AMPARs contain GluA1, while 26% are GluA2/3.

AMPAR subunit lateral position and PSD size.

Serial-section electron microscopy reveals variability within the seemingly homogeneous population of axospinous synapses in stratum radiatum of CA1 in the adult rat (Harris et al., 1989). The surface area of the synaptic contact varies by more than an order of magnitude; this variation is closely correlated both with other anatomical features (e.g. spine volume) and with parameters of direct functional significance, including the number of AMPARs (Kharazia et al., 1999, Takumi et al., 1999. Moreover, accumulating recent evidence suggests that large spines (which receive large synaptic contacts) are highly stable, whereas small spines (with small synapses) may be quite plastic (Kasai et al., 2010). For these reasons, we wondered whether the organization of AMPARs might vary with the size of the synapse, as estimated by PSD length. To address this question, we compared the lateral position of AMPAR subunits in large synapses with those in small synapses, examining gold particles coding for GluA1 and GluA3. To simplify data analysis, we bifurcated the

data for each receptor into equal halves, comparing positions of gold particles from “short PSD” and “long PSD” data sets.

Viewed from this binary perspective, we found that PSD size had little or no effect on AMPAR lateral distribution for GluA3, but had a marked effect on GluA1 lateral position. GluA1 in short PSDs (ranging from 75 to 237 nm) spread over the PSD, with a considerable number of extrasynaptic particles, whereas GluA1 in long PSDs (ranging from 237 to 501 nm) exhibited a distribution more like that of GluA3, concentrating in the PSD center, with few extrasynaptic particles (Fig 5). Thus, GluA1 lateral position varies with PSD size, while GluA3 remains centrally localized regardless of PSD size.

For technical reasons, we find postembedding immunogold label is optimal when sections are collected on fine mesh grids, but it is unfeasible to study serial sections on mesh grids. However, when examining single thin sections, it is impossible to know whether short PSD profiles represent slices from PSDs with small areas, or instead slices near the edges of larger PSDs. To explore whether this error might have affected our conclusions, we performed serial section electron (Fig 6). We found that the distribution of normalized lateral position is quite similar to that from EM of single sections: GluA1 lateral position extends to the PSD edge, while GluA3 concentrates in the center of the PSD (Fig. 7). When performing analysis on serial sections, edge sections are the first and last sections identified before the PSD is no longer visible. To assess whether data taken at the PSD edge significantly affects lateral position, we calculated average NL position for the complete data set, and compared this to the average NL position calculated after excluding data from

micrographs of thin sections collected at the edge of the synapse. The NL position of GluA1 and GluA3 for all data closely resembled that computed only from data without the edge (Table 3). In summary, we conclude that possible errors introduced by analysis of single sections had no significant impact on our results.

2.4 Discussion

Here, we used immunogold electron microscopy to study the organization of AMPAR subunits in synapses of CA1 stratum radiatum. Although unsuitable for studying the dynamic properties of receptors, this technique provides an unbiased view of protein at a high spatial resolution in adult tissue. Labeling for all AMPAR subunits examined concentrated at the postsynaptic membrane of asymmetric synapses. On average, GluA1 was closer to the lateral edge of the PSD than GluA3 (especially in small synapses), suggesting a differential synaptic organization of GluA1/2 and GluA2/3 receptors.

Previous studies have reported higher immunogold labeling for AMPARs towards the edge of the PSD in multiple brain regions, including organ of Corti, neostriatum, cerebral cortex, and olfactory bulb (Matsubara et al., 1996; Bernard et al., 1997; Kharazia et al., 1997; Ottersen et al., 1998; Sassoe-Poenetto et al., 2000). This result was confirmed using electron tomography (Chen et al., 2005). While our results are generally consistent with these studies, we find that GluA3 is more centrally localized. The significance of the position of GluA3- containing receptors in the synapse center is unclear, though N-methyl-D-aspartate receptors (NMDARs) also concentrates in the synapse center (Kharazia et al., 1997), raising the possibility of a local interaction between NMDARs and GluA2/3receptors.

Computational studies predict that precise alignment between presynaptic sites of glutamate release and postsynaptic receptors increases synaptic efficiency (Xie et al., 1997; Raghavachari et al., 2002; Franks et al., 2003). Immediately after its

release from a presynaptic vesicle, glutamate concentration within the synaptic cleft is thought to reach a peak concentration of ~1-3 mM, decaying within 100-200 μs. Since AMPAR have a rather low affinity for glutamate, the precise alignment between presynaptic release sites and postsynaptic receptors is likely to modulate efficacy of neurotransmission (Clements et al., 1992; Clements et al, 1996). Intriguingly, overexpression of the presynaptic cell adhesion protein neurexin and its postsynaptic partner neuroligin decreases the surface diffusion of AMPAR, apparently through the interaction of neuroligin with PSD-95 (Mondin et al., 2001), pointing to a mechanism by which presynaptic release machinery could be coupled to postsynaptic receptors. Such coupling has been supported by (very limited) previous ultrastructural evidence (Kharazia et al., 1999)

Several mechanisms have been proposed to control the lateral distribution of AMPARs. Protein-protein interactions between AMPARs and synaptic scaffolds can limit AMPAR diffusion (MacGillavry et al., 2011). PSD-95 and SAP97 are both strong candidates to serve this role. PSD-95, which distributes fairly uniformly across the PSD (Valtschanoff et al., 2001; Sassoe-Pognetto et al., 2003), overexpression increases and knockdown decreases AMPAR synaptic expression (El-Husseini et al., 2000; Elias et al., 2006;Ehrlich et al., 2007). However, there is no evidence of PSD-95 increasing in response to LTP. SAP97, the only protein known to interact with the PDZ domain of GluA1, distributes over the PSD, concentrating at its edge, similar to our finding for GluA1 (Valtschanoff et al., 2000; DeGiorgis et al., 2006). While the function of SAP97 remains unclear, neurons with increased levels of

SAP97 through development have enhanced AMPAR currents (Howard et al., 2010).

The organization of different AMPAR subunits may suggest possible differences in trafficking of GluA1/2 and GluA2/3. GluA1/2 receptor insertion is activity-dependent while GluA2/3 receptor trafficking is constitutive, but it remains unknown if GluA1/2 and GluA2/3 receptor insertion follows the same route into the synapse. Multiple studies suggest that AMPAR insertion mainly occurs outside of the PSD (Kopec et al., 2006; Park et al., 2006; Yudowski et al., 2007; Yang et al., 2008; Makino et al., 2009;Kennedy et al., 2010), and then diffuses laterally through the postsynaptic membrane to enter the PSD (Borgdorff et al., 2002; Choquet et al., 2003). However, components of the exocyst, a collection of proteins important for membrane insertion, have been found associated with the PSD, suggesting that AMPARs might also be directly inserted into the PSD (Gerges et al., 2006). We find that GluA1- containing receptors are closer to the PSD periphery while GluA3-containing receptors are in the PSD center. This difference in lateral position suggests that to GluA1-containing receptors entering the sides of the PSD, while GluA3-containg receptors enter in the center.

We established a link between AMPAR organization and size, finding that GluA1 distributes over the PSD in short PSD, whereas GluA1 concentrates near the center in longer PSD. Differences in subunit position due to PSD length were not displayed by GluA2/3 and GluA3. The reason for this PSD-size variation in GluA1 position is unclear, but we speculate that short PSDs, which are likely to represent smaller

PSDs, are more likely to be in the process of undergoing LTP and thus have more GluA1/2 receptors moving into them at any given time.

2.5 Tables and Figures

Table 1. Genetic deletion of GluA1 or GluA2 and labeling with AMPAR antibodies.

Antibody	WT	GluA1KO	GluA2KO
GluA1	47.2 ± 3.2%	6.4 ± 0.2% (-86%)	26 ± 1.7% (-44%)
GluA2-3	54.0 ± 2.2%	45.0 ± 1.9% (-17%)	11.4 ± 1.8% (-79%)
GluA3	42.4 ± 1.2%	26.8 ± 2.2% (-37%)	22.6 ± 2.7% (-47%)

Percentage of immunopositive synapses ± SEM (500 synapses, where equal 100 is assume to be a single sample). Percent reduction is in parentheses.

Table 2. Normalized lateral positions (means ± SEM) for three antibodies

Antibody	Rats (WT)	GluA1KO	GluA2KO
GluA1	0.64 ± 0.01 (N = 866)	---	0.62 ± 0.02 (314)
GluA2-3	0.59 ± 0.01 (N = 822)	0.47 ± 0.01 (488)	0.55 ± 0.02 (200)
GluA3	0.50 ± 0.01 (N = 510)	0.46 ± 0.02 (336)	0.52 ± 0.02 (190)

Numbers in parenthesis are number of particles used to calculate each average value. For rats, particles were divided by animal (N=7) and the average value was calculated from the average value for each animal. Few knockout mice were available, thus we calculated average values by pooling all particles.

Table 3: Normalized Lateral Position for Serial Sections with and without edge data removed

Antibody used	Sections included	NL position
GluA1	All	0.61 ± 0.04 (137)
	No Edge	0.59 ± 0.04 (81)
GluA3	All	0.46 ± 0.04 (89)
	No Edge	0.44 ± 0.04 (54)

NL position calculated for all sections, and after excluding sections at the PSD edge. The number of particles measured is listed

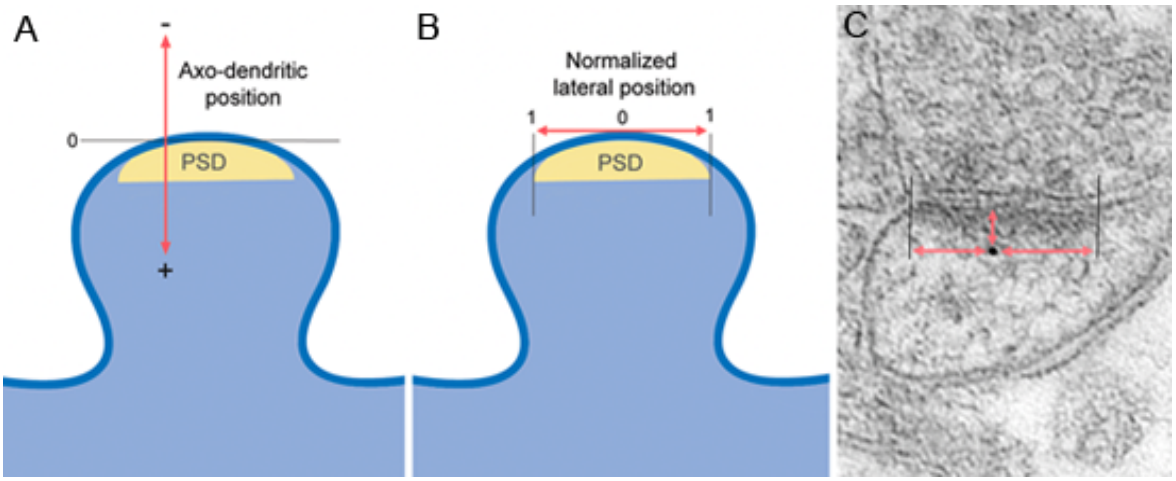

Fig. 1. Diagram illustrates measurements for positions of gold particles.

(A) Schematic red arrow illustrates the axis, zero-point, and sign for measurements of "axo-dendritic" position. (B) Schematic red arrow illustrates the axis for measurement of "lateral" position; 0 and 1 define corresponding normalized lateral positions. C. Red arrows on micrograph illustrate the measurements made for a single gold particle on a real micrograph.

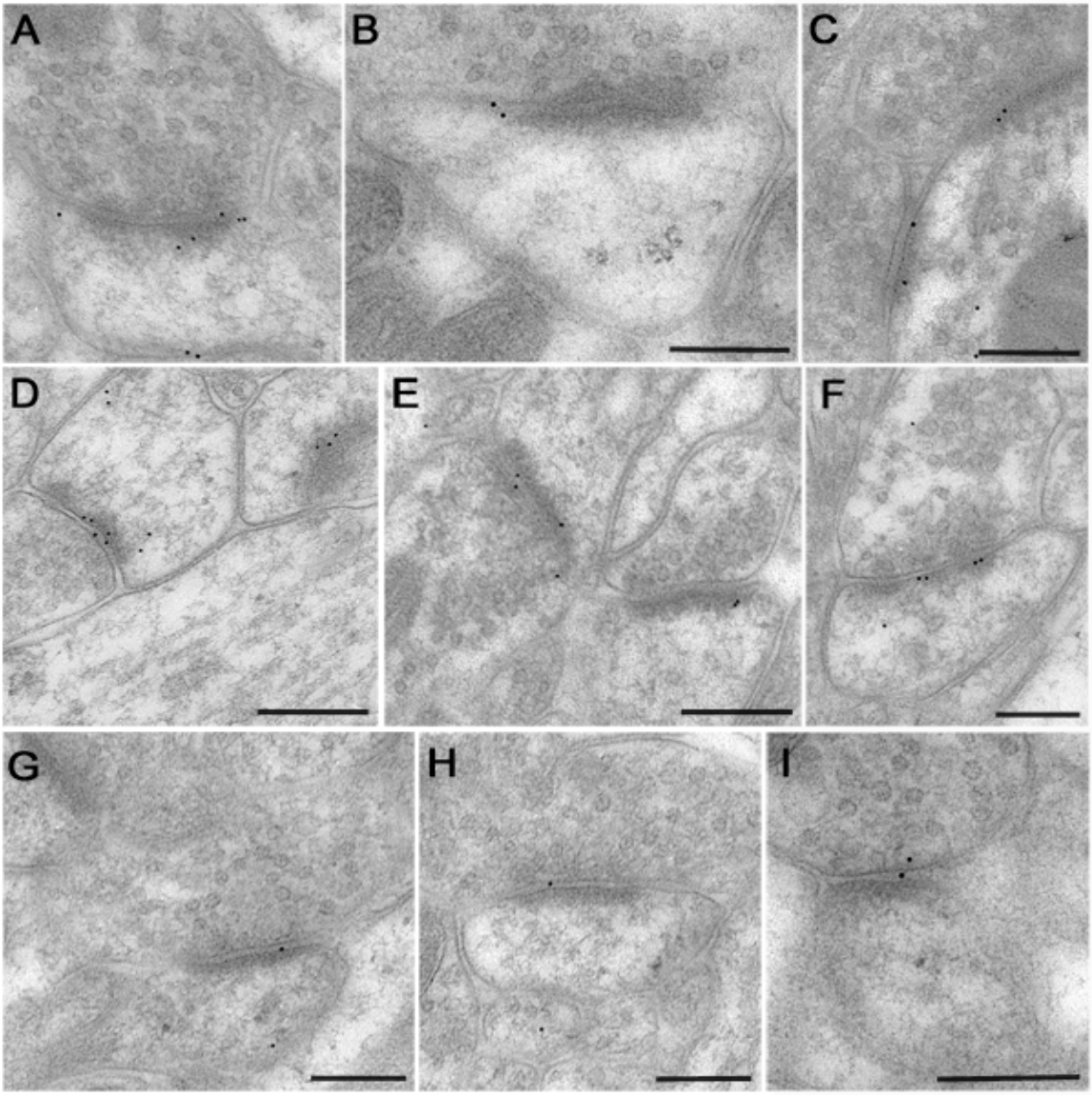

Fig. 2. Postembedding immunogold.

Micrographs illustrate the material used in this study. All images are from stratum radiatum of CA1 hippocampus, from adult rat. Gold particles (black dots) are 10 nm in diameter. Material in top panel was reacted with an antibody to GluA1 (A-C); middle panel, with antibody to GluA2-3 (D-F); and bottom panel, with antibody to GluA3 (G-I; see Methods for details). Most of the labeling is clearly associated with asymmetric synapses. (A) Axospinous synapse strongly labeled for GluA1 (presynaptic terminal at top). (B) Large axospinous synapse; labeling lies near the edge of the synaptic specialization. (C) A small dendritic shaft (identified by microtubules (cut *en face*) and by mitochondrial profile at bottom right of image) receives two immunopositive synaptic contacts. We excluded such synapses from analysis, focusing exclusively on axospinous synapses. (D, E): Each panel shows two axospinous synapses, both immunopositive for GluA2-3. (F) Axospinous

synapse cut in favorable section to allow clear visualization of the entire plasma membrane of the spine. While gold particles clearly associate with the postsynaptic specialization, a few particles are also visible within the spine cytoplasm. Synapses in F and at bottom left in D exhibit incomplete perforation; we excluded synapses with complete perforation from analysis of "lateral" position. (G-I) labeling for GluA3 is typically weaker than for the other antibodies. Note that synaptic labeling often lies outside the spine. Scale bars = 200 nm

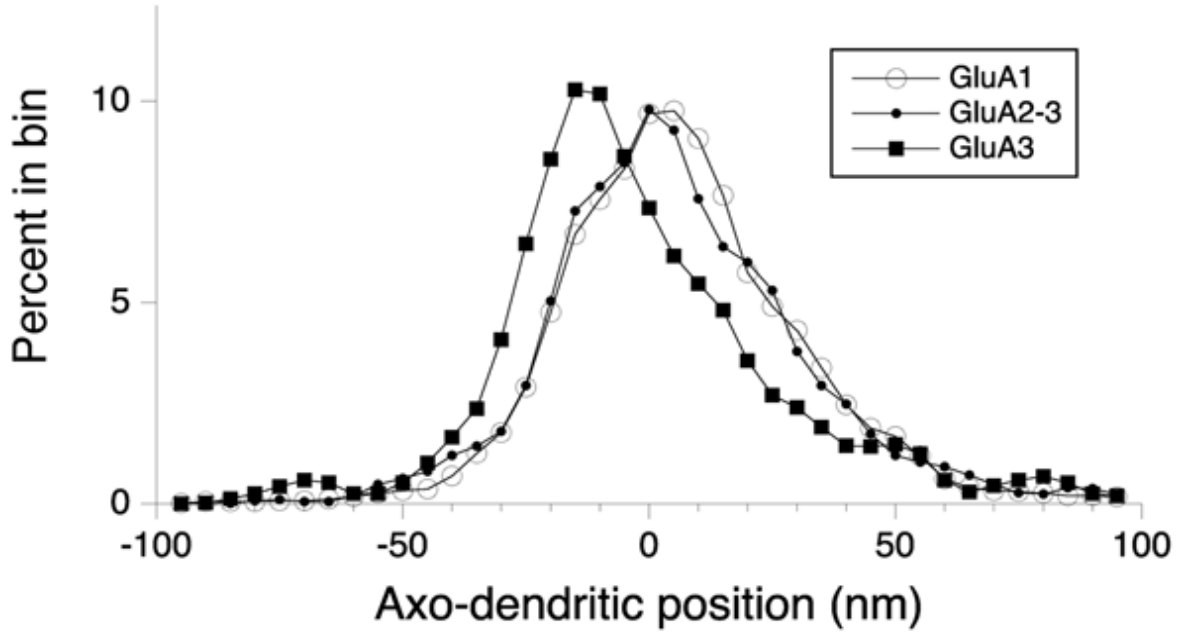

Fig. 3: Axo-dendritic distribution of labeling for three AMPAR antibodies.

0 on the x-axis corresponds to the postsynaptic membrane; positive numbers are in the postsynaptic direction; negative numbers are in the presynaptic direction (see Fig. 1 for details). To reduce noise, the curve is smoothed with a three-point weighted moving average (see Methods for details). Labeling for both GluA1 and GluA2-3 is predominantly postsynaptic (4.1 ± 1.1 nm and 2.9 ± 1.0 nm, respectively), while GluA3 label concentrates in the synaptic cleft (-3.9 ± 1.3 nm from the postsynaptic membrane, n=7 animals). The mean axo-dendritic position of GluA3 was significantly different from that of both GluA1 and GluA2-3 ($p < 0.001$).

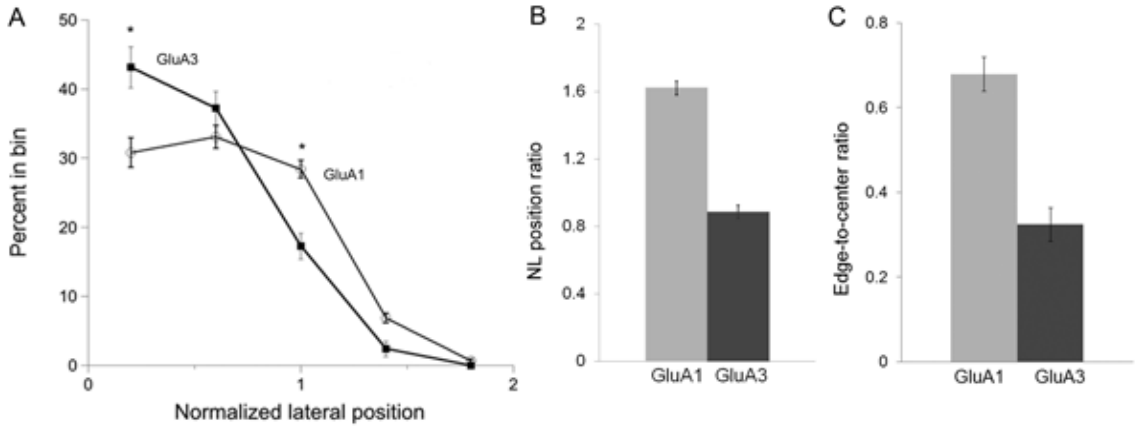

Fig. 4: Lateral position of GluA1 and GluA3 at the synapse.

(A) Graph of normalized lateral position (computed for five bins). 0 corresponds to the center of the PSD, and 1 corresponds to its edge. Labeling for GluA1 remains at high levels all along the PSD, extending beyond the edge of the PSD, whereas GluA3 concentrates at the center of the synapse. The fraction of synapses labeled for GluA3 was significantly greater than GluA1 in the 0 to 0.4 bin ($p < 0.01$) and significantly less than GluA1 in the 0.8 to 1.2 bin ($p < 0.001$; N = 7 animals). (B) Bar chart shows the ratio of labeling associated with the postsynaptic membrane extending from a NL position of 0.5, divided by labeling within the central 0.5 NL position of the synapse for GluA1 and GluA3. GluA1 has a twofold increase compared against GluA3. (C) Bar chart showing the ratio of the number of particles 25 nm extrasynaptic over the central 50 nm of the PSD. A much greater proportion of GluA1 than GluA3 lies beyond the edge of the synapse

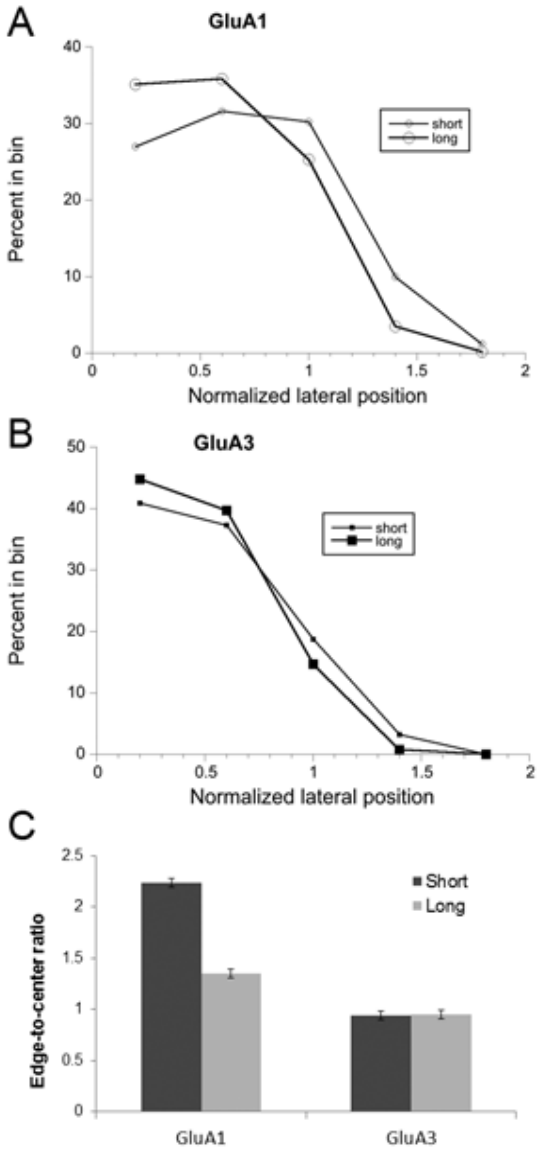

Fig. 5: AMPAR subunit position versus PSD size.

We divided the normalized lateral position data for each antibody in half based on PSD size, creating a short and long PSD data set. (A) The lateral position of GluA1 varies with PSD size: the NL position of shorter PSDs is displaced toward the edge of the synapses, compared to longer PSDs. (B) In contrast, little evidence for a size effect is seen for GluA3. (C) This difference is especially marked for the “edge-to-center” ratio (the raio of the number of gold particles outside the central half of the synapse to the number within the central half).

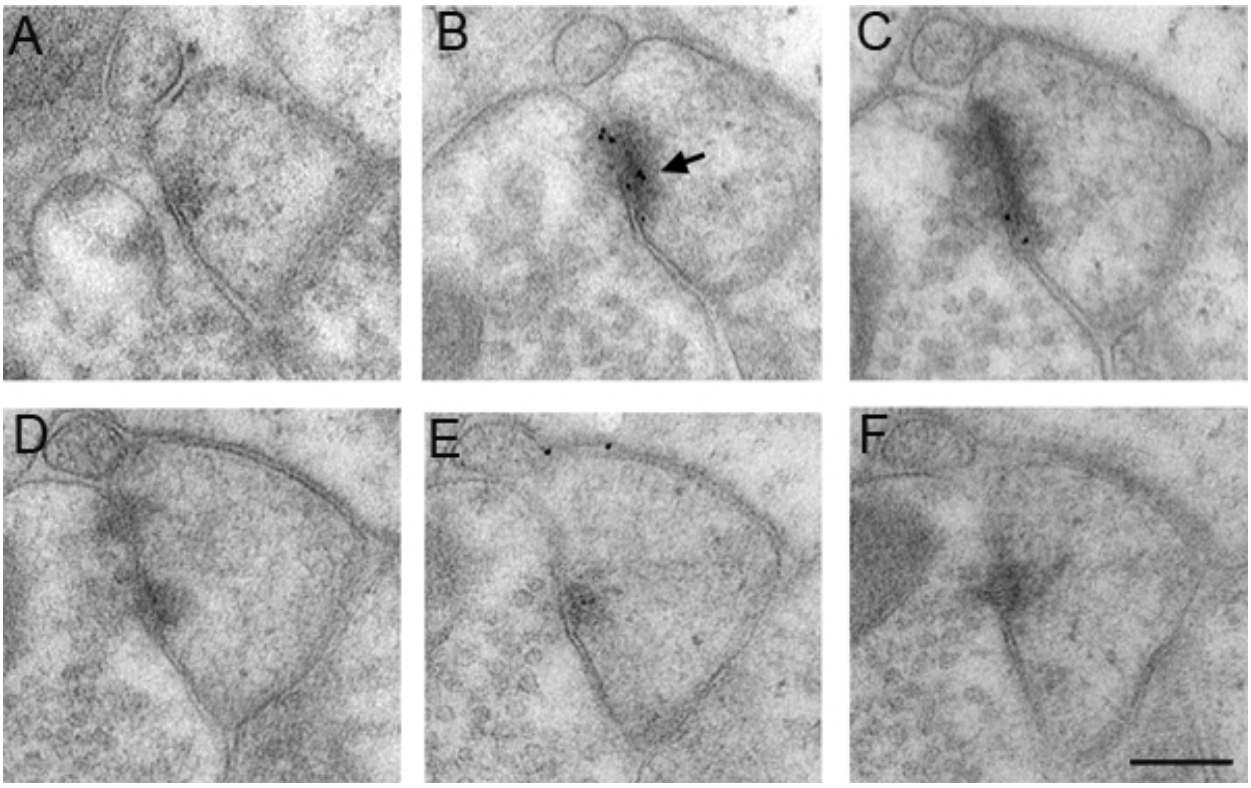

Fig. 6: Serial sections, immunoreacted for GluA1.

In section A, a true synapse is undetectable, though a poorly-defined area of electron density near the postsynaptic membrane is visible, presumably associated with the edge of the PSD. PSDs in sections B and C label for GluA1; note that gold particles in section B seem to lie in the middle of the PSD, but are actually closer to the PSD edge. Scale bar = 200 nm

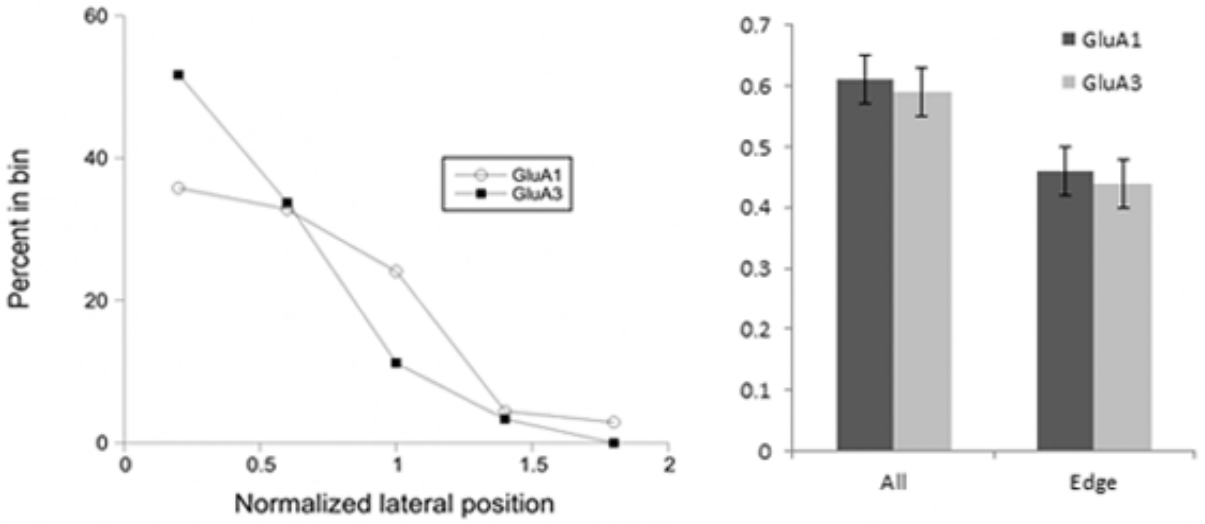

Fig. 7: Normalized lateral position of GluA1 vs.GluA3 in serial sections.

Graph shows normalized lateral distribution of GluA1 and GluA3. These distributions are similar to the distribution of AMPAR subunits we found using single section EM (A). Our data suggest that AMPARs in small PSD have a different organization than longer PSDs. However, in single section EM, it is not possible to know if short PSDs are sections through the center of small PSDs or if they are sections from the edges of larger PSDs. To study this effect, we compared average NL position for the complete data set to the average NL position calculated without data from the PSD edge. These average values were not significantly different.

CHAPTER 3

The organization of amyloid-β protein precursor intracellular domain-associated protein-1 in the rat forebrain.

3.1. Introduction

The intercellular appositions at synapses are specialized sites of communication between neurons. Transmitter receptors concentrate in the postsynaptic density (PSD), a protein-rich zone that acts as a general organizer of signal transduction, including pathways associated with synaptic plasticity (Ziff, 1997; Okabe, 2007; Sheng et al., 2007). Available data suggest that long-term plasticity requires synthesis of new protein to be sustained (Krug et al., 1984; Nguyen et al*.,* 1994; Abraham et al., 2008). While the precise balance between local dendritic versus remote somatic protein translation is a topic of continued study (Schuman et al., 2006; Skup, 2008), nuclear transcription leading to subsequent protein translation is required for sustained expression of several types of long-term synaptic plasticity (Frey et al., 1989; Calixto et al., 2003; Reymann et al*.,* 2007).

β-amyloid, a cleavage product of amyloid-β protein precursor (APP), is a major component of amyloid plaques, a hallmark of the Alzheimer's disease (Duyckaerts et al., 2009). Another cleavage product, APP intracellular domain (AID, or AICD), may play a role in apoptosis, calcium homeostasis, and transcriptional regulation (Hamid et al., 2007; Müller et al., 2008; Slomnicki et al., 2008); however, whether AID plays a role in Alzheimer disease remains controversial. AID-

associated protein-1 (AIDA-1) is a recently discovered protein that binds AID (Ghersi, Noviello et al., 2004; Ghersi, Vito et al., 2004). Proteomic studies suggest that AIDA-1 is a major component of the biochemically-isolated PSD fraction (Jordan et al., 2004; Peng et al., 2004; Yoshimura et al., 2004). Its function remains rather mysterious, but recent evidence suggests that AIDA-1 provides a novel route of communication between synapses and nuclei. In cultured hippocampal neurons, AIDA-1 translocates to the nucleus in an NMDAR-dependent manner, leading to downstream increases in protein translation (Jordan et al., 2007). A recent study confirmed that AIDA-1 contains a nuclear localization signal (Kurabi et al., 2009). Together, this evidence suggests that AIDA-1 might link synaptic activity to a nuclear response.

AIDA-1 has been studied in culture systems, but little is known about its distribution *in vivo*. Here, we use immunocytochemistry to study the organization of AIDA-1 in adult rat brain. Our results show both nuclear and synaptic localization, providing new clues concerning possible functions of AIDA-1 in neurons.

3.2. Experimental procedures

Tissue Preparation

Experiments were carried out on 13 adult male Sprague-Dawley rats ranging from 3 to 10 months old, from Charles River Laboratories (Raleigh, NC, USA). Four were used for DAB staining, 4 were used for confocal microscopy, 2 were used for preembedding electron microscopy, and 3 were used for postembedding electron microscopy. All procedures related to the care and treatment of animals were conducted according to institutional and NIH guidelines. Animals were deeply anesthetized with sodium pentobarbital (60 mg/kg) and intracardially perfused with saline followed by ~ 500 mL of fixative. For light microscopy, fixation was with 4% depolymerized paraformaldehyde (PFA) in 0.1 M phosphate buffer, pH 7.4 (PB); for electron microscopy, fixation was with either a mixture of 2% PFA and 2% glutaraldehyde (GA) in PB or 4% PFA and 0.5% GA in PB. The brains were removed and postfixed for 2 hours in the same fixative at 4℃. Coronal sections containing hippocampus and cerebral cortex were cut on a Vibratome at 40-60 μm (for light and electron microscopy) or 200-250 μm (for freeze substitution electron microscopy) and collected in cold PB.

Antibodies

Primary antibodies used were affinity-purified polyclonal antibodies against AIDA-1 raised in rabbit (2.5 – 6.3 μg/mL, Zymed, San Francisco, CA; 36-7000); against vesicular glutamate transporter 1 in guinea pig (VGLUT1, 0.2 μg/mL, Chemicon, Temecula, CA; AB5905); against glutamate decarboxylase-65 in mouse (GAD-65, 8 μg/mL, Chemicon; AB5082), and a mouse monoclonal antibody raised

against nuclear pore complex proteins (NPC; 1 μg/mL, Covance, Princeton, NJ; MAb414).

To prepare the AIDA-1 antibody, rabbits were injected repeatedly with a peptide conjugate corresponding to the sequence RLHDDPPQKPPRSIT starting at position 172 on AIDA-1d. This antibody recognizes both cleaved and uncleaved AIDA-1. (See Results for further details on antibody characterization.)

The VGLUT1 antibody was raised against a 19-residue peptide sequence (GATHSTVQPPRPPPPVRDY) found at the C terminus of rat VGLUT1. The specificity of this antibody has been confirmed by Western blot; the VGLUT1 antibody recognized a single ~60 kDa band (Melone et al., 2005).

The GAD-65 antibody, raised against human GAD-65 from baculovirus-infected cells, recognized two bands on Western blot. A 65 kDa band corresponded to GAD-65, and a 62kDa corresponding to a protease fragment. Results from this antibody have been reported in numerous publications, and it yields a pattern of staining in many brain regions characteristic of GABAergic innervation (Mi et al., 2002; Swanwick et al., 2006; Belichenko et al., 2009).

The widely-used NPC antibody, raised against a nuclear pore complex mixture and purified via protein-G chromatography, recognizes the conserved domain FXFG repeats in nucleoporins. In Western blot, the antibody recognized a single band at 62 kD. Immunofluorescence staining revealed punctate staining along the nuclear border. Immunoelectron microscopy confirmed this finding (Davis et al., 1986).

Immunocytochemistry for Light Microscopy

All incubations were carried out on a shaker at room temperature. Fixed sections were treated with 3% H_2O_2 in 0.01M phosphate-buffered saline, pH 7.2 (PBS) to suppress endogenous peroxidases, and 10% normal donkey serum (NDS; Jackson ImmunoResearch, West Grove PA, USA) in PBS to mask secondary antibody binding sites. Sections were then incubated overnight with primary antibodies in various combinations. For immunoperoxidase staining, sections were rinsed in PBS and blocked with 2% NDS before treatment with biotin-conjugated donkey anti-rabbit antibody (5 μg/mL; Jackson ImmunoResearch) in PBS. After rinsing in PBS, sections were treated with Extravidin-peroxidase (0.4-0.5 μg/mL ; Sigma, St Louis, MO, USA) and processed with nickel-intensified 3,3'–diaminobenzidine tetrahydrochloride (Ni-DAB). Sections were then mounted on gelatin-coated slides, air-dried, cleared with xylene, and coverslipped with DPX (BDH Laboratory Supplies, Poole, UK). For immunofluorescence, sections were washed in PBS, incubated in a fluorochrome-conjugated secondary antibody (Cy3, FITC, or Cy5, 7.5 μg/mL in PBS; Jackson Immunoresearch), rinsed, mounted on slides, and coverslipped with Vectashield mounting medium (Vector, Burlingame, CA, USA). To counterstain nuclei, 4',6-diamidino-2-phenylindole dihydrochloride (DAPI, 0.5 μg/mL in PBS; Molecular Probes, Eugene, OR) was applied after the secondary antibody. Sections were then mounted on gelatin-coated slides and coverslipped. DAB sections were examined with a Leitz DMR microscope (Lecia, Wetzlar, Germany), and images were collected using a 12-bit cooled charge-coupled device camera(Retiga EX, QImaging, Canada) coupled to a Macintosh computer

(Apple Inc., Cupertino, CA, USA). Confocal images were collected with a Zeiss 510-LSM confocal microscope.

Immunocytochemistry for Electron Microscopy

For pre-embedding electron microscopy, sections were treated sequentially for 30 minutes in 1% sodium borohydride in PB, in 3% H_2O_2 in 0.01M PBS, and in 10% NDS, and then incubated overnight with the primary antibody. Following rinses in PBS, sections were either treated with Extravidin-peroxidase (0.4-0.5 μg/mL) followed by Ni-DAB (for immunoperoxidase staining), or incubated in streptavidin coupled to 1.4 nm gold particles (1:100, Nanoprobes Inc., Yaphank, NY, USA) for 2 hrs at room temperature (for immunogold detection). Gold-treated sections were rinsed in 0.1 M sodium acetate (to remove phosphate and chloride ions) and underwent silver enhancement with an Amersham IntenSE^{TM} M kit (GE Healthcare, Buckinghamshire, UK). Immunoreacted sections were postfixed in 0.5-1% osmium tetroxide in 0.1 PB for 45 min, and then stained *en bloc* with 1% uranyl acetate for 45 mins. After dehydration in ascending ethanol series and propylene oxide, sections were infiltrated with Epon/Spurr resin (Electron Microscopy Science, Hatfield, PA, USA) and mounted between sheets of Aclar within glass slides. Sections were cut at ~100 nm, mounted on 200 mesh copper grids, and contrasted with uranyl acetate and Sato's lead.

Postembedding immunogold staining was performed on sections according to a freeze-substitution protocol: sections, some pretreated with 0.1% 0.1 M $CaCl_2$ in sodium acetate, were cryoprotected in 30% glycerol overnight. Areas of interest were removed and frozen in isopentane chilled with dry ice. Frozen tissue blocks

were immersed in 4% uranyl acetate in methanol at -90℃ for 48 hours in a freeze-substitution instrument (AFS, Lecia). Following gradual warming, blocks were infiltrated with Lowicryl (HM-20, Electron Microscopy Science) at -45℃ and polymerized under UV light. Sixty nm sections were cut from the polymerized blocks and collected on nickel grids for post-embedding staining. Grids were treated with 1% bovine serum albumin in TRIS-buffered saline with 0.005% Tergitol NP-10 (TBSN), pH 7.6, followed by overnight treatment with the primary antibody. Section then underwent treatment with 1% normal goat serum in TBSN pH 8.2 before application of gold-conjugated secondary (10 or 18 nm, Jackson ImmunoResearch). The sections were post-stained using uranyl acetate and Sato's lead salts. Grids were examined on a Philips Tecnai electron microscope (Hillsboro, OR) at 80 kV; images were collected with a Gatan 12 bit 1024 X 1024 cooled CCD camera (Pleasanton, CA).

Image Processing

Figures were composed and contrast and brightness were adjusted with Adobe Photoshop CS (v 9.0.2, Adobe Systems, Mountain View, CA USA). Color tools were used to enhance visibility in double-labeling images, and many images were sharpened using the Photoshop "unsharp filter" tool. All processing procedures were applied uniformly across the entire image.

Analysis of AIDA-1 Nuclear and Nuclear Pore Association

Data was taken from confocal images collected using a 63x oil objective (numerical aperture1.4) of material immunostained for both AIDA-1 and NPC. To determine nuclear association, puncta contained entirely within the border of nuclei

were counted and recorded. To determine NPC association, AIDA-1 puncta colocalizing with NPC were counted. Puncta were defined by both size and brightness; in 300 dpi images, “large” puncta contained a minimum of 25 pixels at an intensity of 100 out of 256 and 7 pixels at an intensity of 200 out of 256. Data was taken in Adobe Photoshop CS and analyzed and graphed in Excel (Microsoft, Redmond, WA, USA).

Analysis of Presynaptic Immunogold Labeling

Electron micrographs containing presynaptic vesicle pools were collected from both CA1 stratum radiatum and CA3 stratum lucidum. The area of the presynaptic vesicle pool was measured, and the number of gold particles contained in the vesicle pool was counted in NIH ImageJ (v1.42; see http://rsb.info.nih.gov/ij) permitting us to calculate particle densities in Excel.

Analysis of Synaptic Immunogold Labeling

To determine the percentage of synapses containing AIDA-1, all synapses within randomly observed fields in AIDA-1-stained grids of stratum radiatum in hippocampus, cerebral cortex, and cerebellum were counted. Synapses containing gold particles within 50 nm of the PSD were counted as AIDA-1-positive; all other synapses were negative. Percentage of synapse expression was calculated from this data.

Electron micrographs of randomly-selected fields containing gold particles within 100 nm of the PSD were taken from CA1 stratum radiatum. For clearly-defined synapses, the distance of gold particles from the postsynaptic membrane (“axo-dendritic position”) and tangentially away from the edge of the postsynaptic

density (“lateral position”) were measured. When computing the axo-dendritic position, particles that were >25 nm away from the lateral ends of the PSD were ignored, and when computing lateral position, particles far from the postsynaptic membrane (< -50 or > 75 nm away) were ignored, since these particles were unlikely to be related to the PSD. When graphing axo-dendritic position, the data was smoothed using a three-point weight running average. For all but the end points, $y_{j(smoothed)} = [y_{(j-1)} + 2y_j + y_{(j+1)}]/4$. For the end points, $y_{1(smoothed)} = (2y_1 + y_2)/3$ and $y_{n(smoothed)} = [y_{(n-1)} + 2y_n]/3$.

The lateral position was normalized, to estimate the position of the particles along the PSD. This was computed using the following formula:

$$Normalized\ value = \frac{Gold\ particle\ distance\ from\ PSD\ center}{Distance\ from\ PSD\ edge\ to\ center}$$

Thus, a value of 0 corresponds to a particle centered in the synapse; a value of 1.0 corresponds to a particle at the PSD edge. (For further details, see Kharazia et al, 1997 and Valtschanoff et al, 2001.) Data were collected in an Excel spreadsheet (Microsoft) for further analysis. DataDesk (Data Description, Ithaca, NY) and KaleidaGraph (Synergy Software, Reading, PA, USA) were used to compute statistics. CricketGraph (Computer Associates, Islandia, NY) was used to generate graphs and perform data smoothing.

3.3. Results

AIDA antibody characterization and biochemical distribution

To confirm the specificity of this antibody, 10 μg of nuclear fraction, total lysate, synaptosomes, and postsynaptic densities were isolated from rat brains (Jordan et al., 2007) and subjected to SDS-PAGE (Fig 1A). Western blots showed staining for at least 4 different bands corresponding to different isoforms: AIDA-1d (~60 kDa and ~28 kDa), AIDA-1e (~49 kDa) and EB-1 (~72 kDa). The identities of these bands were confirmed by comparing the immunoreactivity in brain lysates to that observed in extracts from HeLa cells transfected with specific AIDA-1 isoforms. For further confirmation, we generated lentiviruses expressing AIDA-1-specific shRNAs, using the pTRIP vector system as described elsewhere (Janas et al., 2006). We generated 19 basepair shRNAs against sequences starting at bp 138, 207, and 384. Cultured hippocampal neurons (Jordan et al., 2007) infected at DIV 10, incubated for 7 days and then lysed, showed a nearly complete downregulation of most isoforms using shRNAs targeting bp 138 and 207 on AIDA-1d, and all isoforms with shRNAs targeting bp 384 (Fig 1B). The average downregulation observed by shRNA 384 was 74.5% ± 2.6 (Fig 1C). HEK-293T cells transfected with AIDA-1d and stained with the Zymed Ab showed no staining when co-tranfected with AIDA-1 specific siRNAs (Ambion; Austin, Texas; s232460), while HEK-293T cells co-transfected with AIDA-1d and control siRNAs stained prominently (Fig 1D-F). Primary hippocampal neurons infected with AIDA-1 specific shRNA 384 showed a marked reduction in AIDA-1 staining (Fig 1G-I). To confirm method specificity, we performed immunoperoxidase staining on brain sections without including the AIDA-

1 antibody. Sections lacking this antibody showed very weak nonspecific staining (Fig 1J), while sections stained with the AIDA-1 antibody had high levels of staining (Fig 1K).

Light Microscopic Immunohistochemistry

We performed immunoperoxidase staining to assess the general organization of AIDA-1. Immunoreactivity was found throughout the brain, generally concentrating in gray matter and much weaker in white matter. Immunopositive neurons were scattered throughout the brain, standing out from diffusely stained neuropil. Staining was strong in forebrain, including hippocampus, cerebral cortex, and striatum, and in cerebellum; and weaker in brain stem and spinal cord.

The olfactory bulb had moderate overall levels of staining. The external plexiform layer and mitral cell layer had the strongest staining; some mitral cells contained prominently stained nuclei (Fig 2). The internal plexiform layer and the internal granule cell layer had modest staining, while glomeruli were more weakly stained than the matrix.

AIDA-1 staining extended throughout the layers of cerebral cortex, somewhat weaker in layer IV; no obvious differences in staining intensity were detected tangentially along the cortex (Fig 3A). Staining of somata seemed evenly distributed through the cell layers; the weaker staining in layer IV reflected a decrease in neuropil staining. AIDA-1 labeled some nuclei, but not all of them (Fig 3B). Staining often concentrated around the perimeter of nuclei (black arrowhead).

Striatum exhibited strong neuropil staining, which was largely excluded from the fascicles of myelinated fibers. Staining was stronger in caudate-putamen than

globus pallidus. Much of this staining was organized into small puncta, perhaps related to the spines of medium spiny cells in the caudate-putamen (Fig 3C-D).

In the hippocampus, staining for AIDA-1 was strong in areas with high concentrations of cell bodies, especially the pyramidal cell layer of Ammon's horn, with weaker staining throughout the hippocampal formation (Fig 4A-B). Staining was especially prominent in large puncta in stratum lucidum of CA3, likely to correspond to the boutons of mossy fibers (Fig 4C).

Staining was moderate in the thalamus, with little obvious distinction among thalamic nuclei (Fig 5A). Within cerebellum, Purkinje cells stained strongly for AIDA-1, with staining extending into the proximal dendritic arbor. Unlike most brain areas, the large majority of Purkinje cell nuclei were immunonegative (Fig 5B). Granule cells displayed low levels of staining, while moderate diffuse staining was seen in the molecular layer.

Overall, the brain stem stained more weakly than forebrain and cerebellum (Fig. 6). Superior and inferior colliculus, pons, and medulla generally exhibited relatively weak diffuse staining, although some areas stained more strongly. Strongly stained neurons were present in a number of regions. Prominent staining was observed in the red nucleus, pontine nucleus, and the ventral cochlear nucleus (not shown), in motoneurons of the motor trigeminal nucleus (Fig $6A_1$), neurons in the superior olivary complex (Fig 6B), and large neurons in the gigantocellular reticular nucleus (Fig $6C_1$). The nuclei of many, but not all, of the strongly-stained neurons were immunopositive.

The spinal cord displayed generally low levels of staining (Fig 7). Motoneurons in the ventral horn stained for AIDA-1, and many of these contained AIDA-1 positive nuclei. Pronounced diffuse staining was detected in the superficial dorsal horn.

To assess the locus of staining at higher resolution, we performed high-resolution confocal microscopy on AIDA-1-stained sections, focusing on the cerebral cortex and hippocampus. In both cortex and hippocampus, immunofluorescent staining was organized into puncta of different sizes and subcellular locations, presumably representing distinct pools of AIDA-1. The pattern of staining varied with depth, presumably due to variable antibody penetration (Fig 8). At the section surface, the most prominent staining was diffuse or organized into numerous small puncta in the neuropil; this pattern dissipated rapidly with depth. A few μm beneath the surface, staining was largely confined to large puncta associated with cell bodies.

The most prominent staining was in stratum lucidum of CA3, which contained numerous very large puncta. To clarify the nature of these puncta, sections were stained with AIDA-1 and either VGLUT1 (a presynaptic excitatory marker) or GAD-65 (a presynaptic inhibitory marker). AIDA-1 colocalized with VGLUT1 in large puncta, but showed little colocalization with GAD-65 (Fig 9), suggesting that AIDA-1 concentrates in the excitatory terminations of mossy fibers onto the thorny excrescences of CA3 neurons.

Another population of AIDA-1 puncta (best defined 3-5 μm beneath the surface of the section) lay within nuclei of neurons. Z series confocal stacks were

acquired to ensure that staining was within the nucleus, and not restricted to the nuclear border. Nuclei generally were either essentially devoid of AIDA-1 staining, or contained many large puncta throughout each optical section (Fig 10). These were present in both excitatory and inhibitory cells. This staining was usually excluded from nucleoli, although AIDA-1 puncta occasionally lay adjacent to nucleoli.

In both cerebral cortex and hippocampus, nuclei generally contained either ten or more of these large puncta, or none (Fig 10C-D). We therefore dichotomized nuclei into “positive” and “negative” populations, defining immunopositive nuclei as those containing ≥5 large puncta in the nucleus in a given optical section. In cerebral cortex, 55% of nuclei (78/142) were immunopositive. The prevalence of nuclear staining was relatively constant through the layers of cortex; 57% of nuclei (36/63) in layer 2/3 were immunopositive, and 54% (45/82) in layer 4/5. The prevalence of nuclear staining in hippocampus was similar: 61% of nuclei (45/73) in CA1 and 56% in CA3 (37/66) were immunopositive. We conclude that AIDA-1 is expressed at substantial levels in ~ 60% of the nuclei of neurons throughout cerebral cortex and Ammon’s horn. Due to tight packing of cells, we were unable to perform quantitative analysis of nuclei within dentate gyrus, but it was apparent that both positive and negative nuclei were common.

AIDA-1 puncta could also be seen in the cytoplasm, especially near the nuclear border. Confocal microscopic analysis of double staining with AIDA-1 and NPC (a core protein of the nuclear pore complex) showed large AIDA-1 puncta associated with the nuclear membrane, with immunopositive nuclei exhibiting more nuclear envelope-associated puncta (Fig 11). Assessing staining 3-6 μm beneath

the section surface, AIDA-1-positive nuclei in the hippocampus had 2.8 ± 0.2 nuclear envelope-associated puncta (n=82), while nuclei lacking AIDA-1 had 2.0 ± 0.2 puncta (n=55). Cerebral cortex exhibited a similar relationship, with positive nuclei having 1.9 ± 0.2 puncta (n=81) and nuclei lacking AIDA-1 having 1.3 ± 0.2 nuclear envelope-associated puncta (n=64).

Ultrastructural Observations

To gain a clearer understanding of its subcellular organization, we performed immuno-electron microscopy for AIDA-1 in hippocampus. Pre-embedding immunogold staining revealed silver-enhanced gold particles associated with the nuclear envelope and nuclear pores, on both cytoplasmic and nuclear surfaces (Fig 12A-C). Cytoplasmic staining was also observed, often associated with intracellular membranes (Fig 12D).

Pre-embedding immunoperoxidase showed AIDA-1 staining in mossy fiber terminals (Fig 12E); staining concentrated at the center of vesicle pools and was seldom seen close to the plasma membrane. A similar pattern of staining in mossy fibers was seen with immunogold in postembedded material (data not shown). In contrast, presynaptic terminals in CA1 did not share this high level of expression. However, mossy fibers terminals are exceptionally large. To explore whether the difference in size could explain the observed difference in presynaptic label, we computed staining density over vesicle pools in both CA1 and CA3. Staining in CA3 synapses proved to be 4 times denser than in CA1 synapses, confirming our qualitative impression that the difference is not merely an artifact arising from the size of mossy fibers.

We seldom observed labeling associated with the postsynaptic specialization in pre-embedding material, but pre-embedding techniques often fail to detect antigens in the PSD, presumably due to the poor penetration of antibodies into this protein-dense compartment. Therefore, we performed postembedding immunogold labeling on tissue processed with freeze-substitution techniques. As with pre-embedding, staining was prominent along the nuclear envelope and within mossy fiber terminals was prominent, but synaptic staining was especially conspicuous, concentrating at the PSD (Fig 13A-C). Approximately 37% of asymmetric excitatory synapses (174/467) in the CA1 region of the hippocampus and 26% of excitatory synapses within cerebral cortex (40/150) displayed immunogold labeling. In contrast, labeling was uncommon in the molecular layer of cerebellar cortex, where only 6% (15/235) of synapses labeled.

We performed quantitative analysis of postembedding immunogold material in hippocampus, to determine the position of gold particles in relation to the synaptic cleft, and found that AIDA-1 was closely associated with the PSD. To analyze antigen position in relation to the PSD, gold particles more than 25 nm beyond the lateral ends of the PSD were ignored. For this subgroup, particles coding for AIDA-1 lay at a mean distance of 13 ± 2 nm from the postsynaptic plasma membrane (n = 334). Particles clustered into a peak -20 to 50 nm from the membrane, resembling a Gaussian distribution with an added cytoplasmic tail (Fig 13D). In the tangential axis, particles far from the postsynaptic membrane (< -50 or > 75 nm away) were ignored, since these particles were unlikely to be related to the PSD. Labeling distributed fairly uniformly along the PSD, rapidly dropping off at its edge (Fig 13E).

3.4. Discussion

Synaptic activity is linked to transcription via a variety of signals that translocate from the synapse to the nucleus (Deisseroth et al., 2003; West et al., 2002). Ca^{2+} from the synapse can spread into to the nucleus and directly activate the transcription factor DREAM (downstream regulatory element antagonist modulator, Osawa et al., 2001). Alternatively, Ca^{2+} can bind to calmodulin at synapses to trigger nuclear translocation of calmodulin and other downstream signals that activate CREB (cAMP response element binding; Deisseroth et al., 1996; Deisseroth et al., 1998; Dolmetch et al., 2001). Several transcription factors have been shown to travel from the synapse to the nucleus, where they can modulate gene expression (Graef et al., 1999; Kaltcshmidt et al., 1995; Lai et al., 2008). AIDA-1 uses a different strategy: after being cleaved at the PSD, the AIDA-1 fragment containing a nuclear localization sequence translocates to the nucleus (Jordan et al., 2007).

High levels of AIDA-1 have been reported in biochemically-isolated PSD fractions (Yoshimura et al., 2004, Peng et al., 2004, Jordan et al., 2004), but little information is available concerning its anatomical localization. Our study in adult rat brain reveals strong staining in forebrain regions rich in spiny dendrites containing excitatory synapses. Staining difference in striatum are noteworthy; caudate-putamen, which contains many excitatory synaptic connections on spiny neurons, exhibits stronger staining than globus pallidus, which contains inhibitory connections from the caudate-putamen (Gerfen,1988; Difiglia et al., 1988).

Purkinje cells stained prominently for AIDA-1. This was unexpected, since Western blot failed to detect AIDA-1 in biochemically-isolated PSDs from cerebellum (Jordan et al., 2007). Likewise, in the present study we found that synapses in cerebellar cortex were only seldom immunopositive for AIDA-1. Multiple splice variants of AIDA-1 have been identified (Ghersi, Noviello et al., 2004;.Ghersi, Vito, et al., 2004; Xu et al., 2005), and these may exhibit different staining patterns. For example, AIDA-1a, but not AIDA1b, is found in nuclei of transfected HeLa cells (Ghersi, Noviello et al., 2004). Likewise, our biochemical data (Fig. 1) suggest differential subcellular expression patterns for different splice variants. We speculate that different splice variants may play distinct functional roles. Synapses of Purkinje cells were seldom labeled, and their nuclei were seldom immunostained, leading us to suggest that AIDA-1 staining in cerebellum represents some isoform not involved in synapse-to-nucleus signaling.

In hippocampus, AIDA-1 was found in a large fraction of excitatory synapses. Within CA1 synapses, AIDA-1 concentrated centrally within PSDs, the same general location previously reported for both PSD-95 and NR2A/B (Valtschanoff et al., 2001). Co-immunoprecipitation experiments have shown that AIDA-1 binds to PSD-95 and associates with NMDARs (Jordan et al., 2007). The present data suggest that AIDA-1 forms similar signaling complexes *in vivo*. Mossy fiber synapses within CA3 display a strikingly different pattern; AIDA-1 in these synapses associated with vesicle pools. Thus, the pattern of AIDA-1 staining within distinct areas of hippocampus correlates with the locus of LTP expression: AIDA-1 is postsynaptic within synapses that exhibit NMDAR-dependent postsynaptic LTP, and presynaptic

in synapses expressing NMDAR-independent presynaptic LTP (Malenka et al., 1999; Nicoll et al., 2005; McBain et al., 2008). We suggest that AIDA-1 may serve as a link between synapses and nuclei in both these areas, despite the functional difference in LTP induction and expression.

In our study, more than half of nuclei contained large AIDA-1 puncta in cerebral cortex and hippocampus, in contrast to dissociated hippocampal neuron cultures, where only 15%-20% of nuclei were AIDA-1 positive under basal conditions. This quantitative discrepancy may reflect higher levels of neuronal activity *in vivo,* since NMDAR activation greatly increased the fraction of cultured neurons with AIDA-1 positive nuclei. Previous *in vitro* work showed that NMDAR activation caused AIDA-1 to enter the nucleus and stabilize connections between Cajal bodies and nucleoli. This connection may promote mRNA synthesis, leading to increased protein translation (Jordan et al., 2007). In our study, nucleolar AIDA-1 staining was infrequent, but our data do not directly question the hypothesis that AIDA-1 promotes Cajal body/nucleolar interactions; AIDA-1 staining was seen at nucleolar borders in our material. However, the more obvious staining we detected at the nuclear membrane, often in association with the nuclear pore complex (NPC), suggests another mechanism of action. The NPC, a large multimeric assembly of proteins, serves as “gatekeeper” that mediates signals into the nucleus (Schwartz, 2005; D'Angelo et al., 2008). Staining of AIDA-1 at nuclear pores could indicate trafficking of AIDA-1 into the nucleus; however, even in the absence of nuclear AIDA-1 staining, AIDA-1 puncta were found along the nuclear border. We speculate that AIDA-binding at NPC may help to regulate nuclear/cytoplasmic trafficking.

3.5. Figures

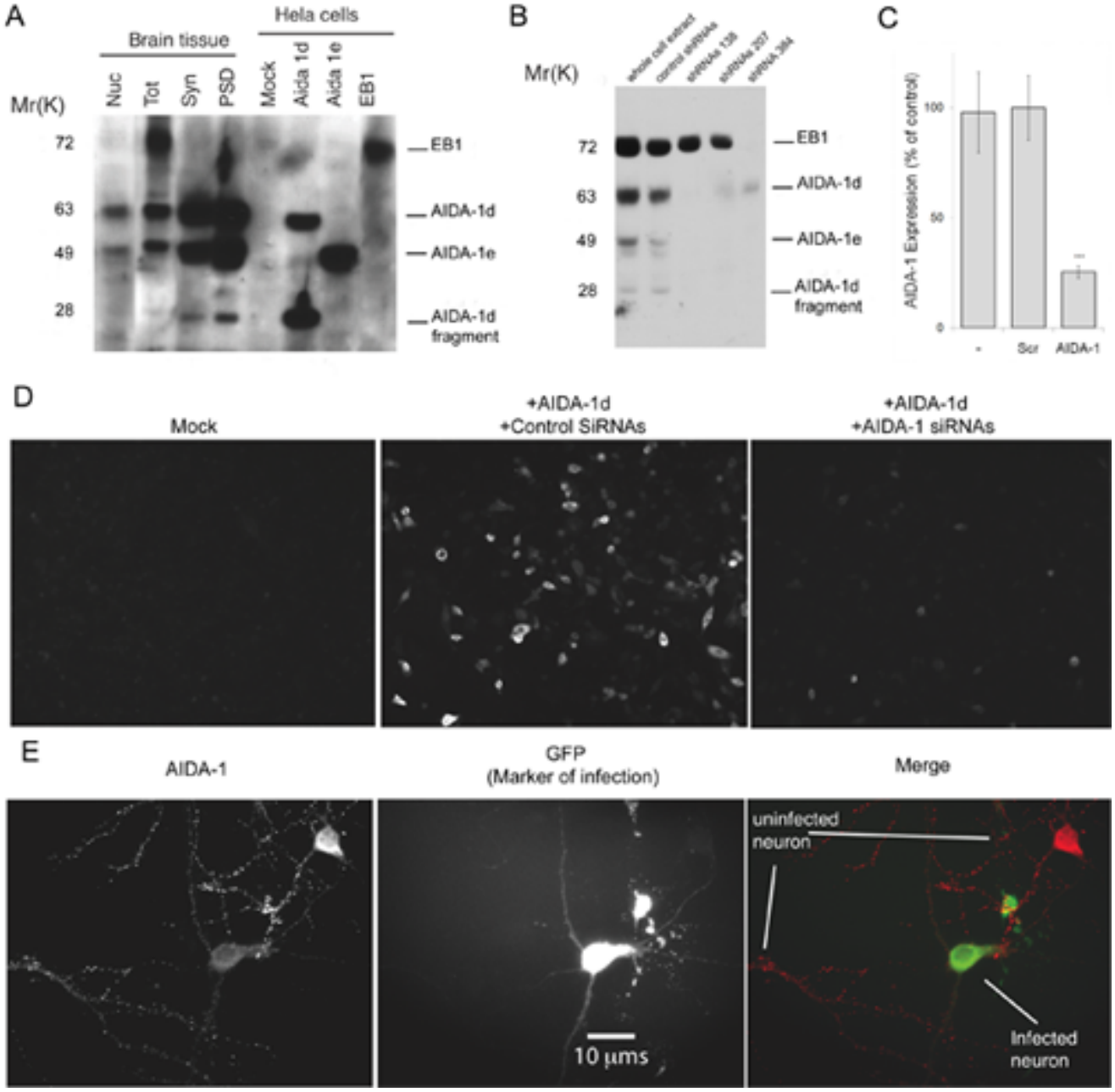

Fig. 1. Characterization of AIDA-1 antibody.

The AIDA-1 antibody (Zymed, Invitrogen) was raised against a peptide conjugate corresponding to the sequence RLHDDPPQKPPRSIT at position 172 on AIDA-1. **A:** Western blot; the AIDA-1 antibody detected for at least 4 different bands corresponding to different AIDA-1 isoforms: 1d (~60 kDa and ~28 kDa), 1e (~49 kDa) and EB-1 (~72 kDa). Nuclei (Nuc) contained prominent bands corresponding to

AIDA-1d and AIDA-1e; total lysate (Tot) contained prominent bands corresponding to EB-1, AIDA-1d, and AIDA-1e; and synaptosomes (Syn) and postsynaptic densities (PSD) contained prominent bands corresponding to AIDA-1d, AIDA-1e, and the AIDA-1d fragment. HeLa cells transfected with specific AIDA-1 isoforms confirmed identities of these bands. **B**: Lentivirus transfection with AIDA-1-specific shRNAs downregulated AIDA expression in cultured hippocampal neurons. ShRNAs targeting bp 138 and 207 on AIDA-1 downregulated 1d and 1e isoforms, while shRNA 384 downregulated all isoforms. **C:** shRNA 384 reduced expression by 74.5% ± 2.6 (AIDA-1) vs nonspecific shRNA (SCR) (densitometry, N =8 gels, *** p-value < 0.0001). No changes were observed for other markers (not shown). **D:** HEK-293T cells transfected with AIDA-1d and stained with the Zymed Ab showed no staining when cotranfected with AIDA-1 specific shRNAs. **E:** Div 14 hippocampal neurons infected with AIDA-1 specific shRNA 384 showed a reduction in AIDA-1 staining. AIDA-1 immunoreactivityin the infected (green) neuron is reduced in both soma and dendrites.

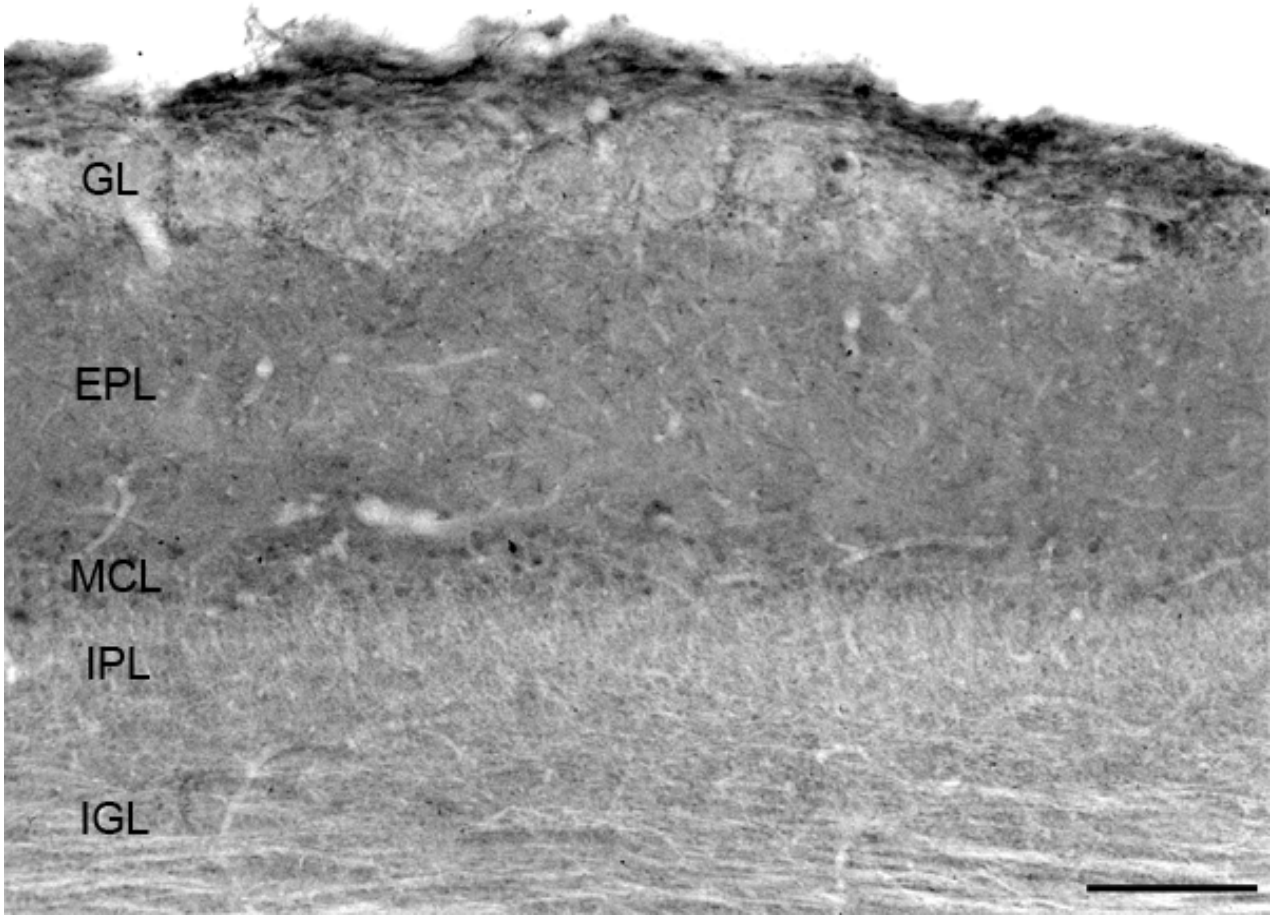

Fig. 2. Immunoperoxidase staining for AIDA-1 in olfactory bulb.

The external plexiform layer (EPL) and mitral cell layer had the strongest staining; some mitral cells contained stained nuclei. Staining was weaker in glomeruli (GL), internal plexiform layer (IPL), and internal granule cell layer (IGL) had modest staining. Scale bar = 250 μm.

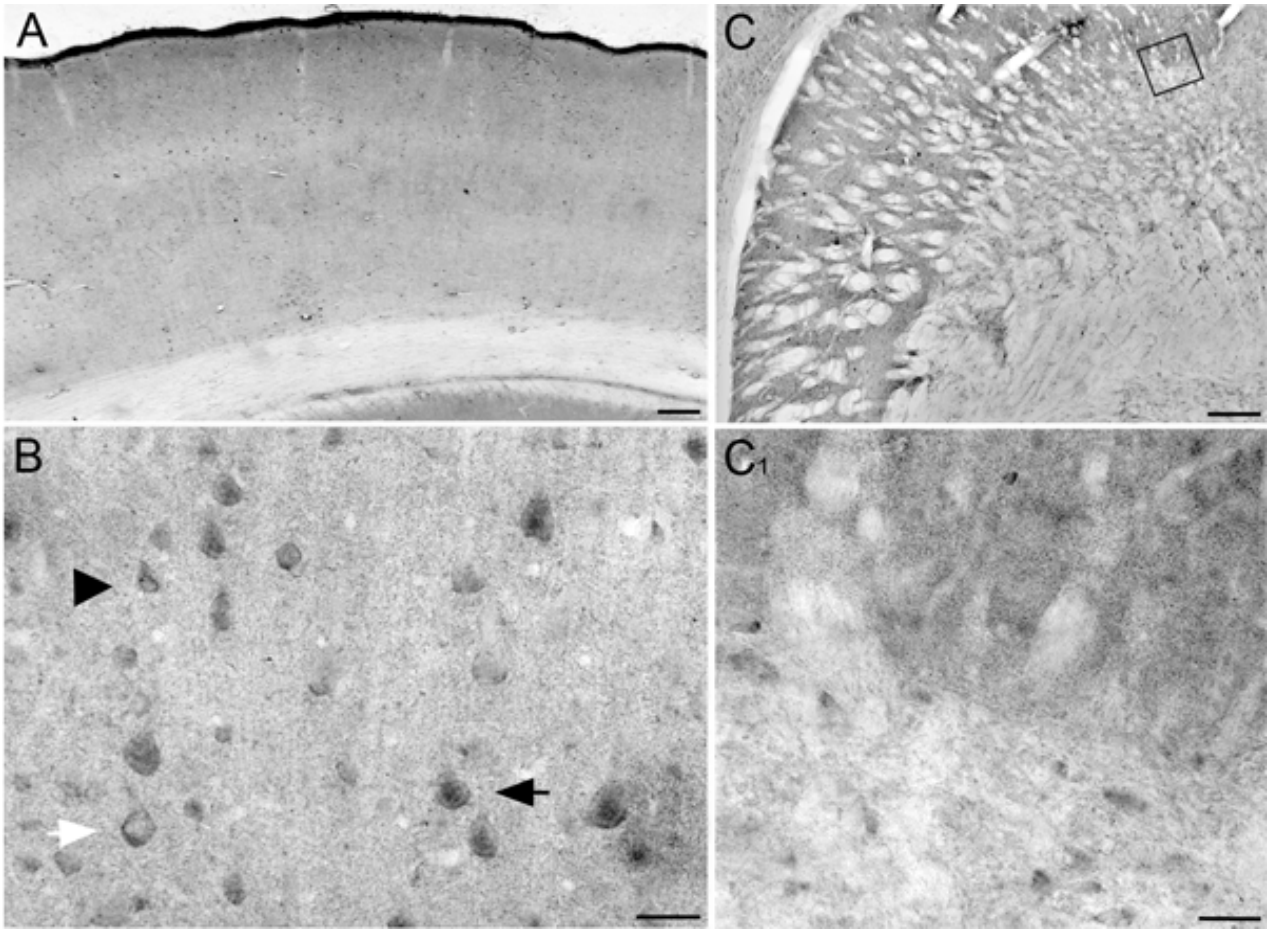

Fig. 3. Immunoperoxidase staining for AIDA-1 in cerebral cortex and striatum.

A: Immunostaining for AIDA-1 in cerebral cortex. Staining is found throughout cortical layers, somewhat weaker in layer IV. No obvious differences in staining were detected tangentially. **B:** Higher magnification micrograph of cortex illustrates various patterns of cellular staining. Some nuclei stain for AIDA-1 (black arrow), while others lack AIDA-1 staining, though cytoplasm is stained (white arrow). In many neurons, staining is especially prominent along the nuclear border (black arrowhead). **C:** In striatum, AIDA-1 is confined to the neuropil between fascicles of myelinated fibers. Staining is stronger in the caudate-putamen (CP) than the globus pallidus (GP) C_1: Higher magnification view of boxed area in $C_{1;}$ staining in neuropil appears punctate Scale bars: A = 250 μm, B = 40 μm, C = 250 μm, C_1 = 40 μm.

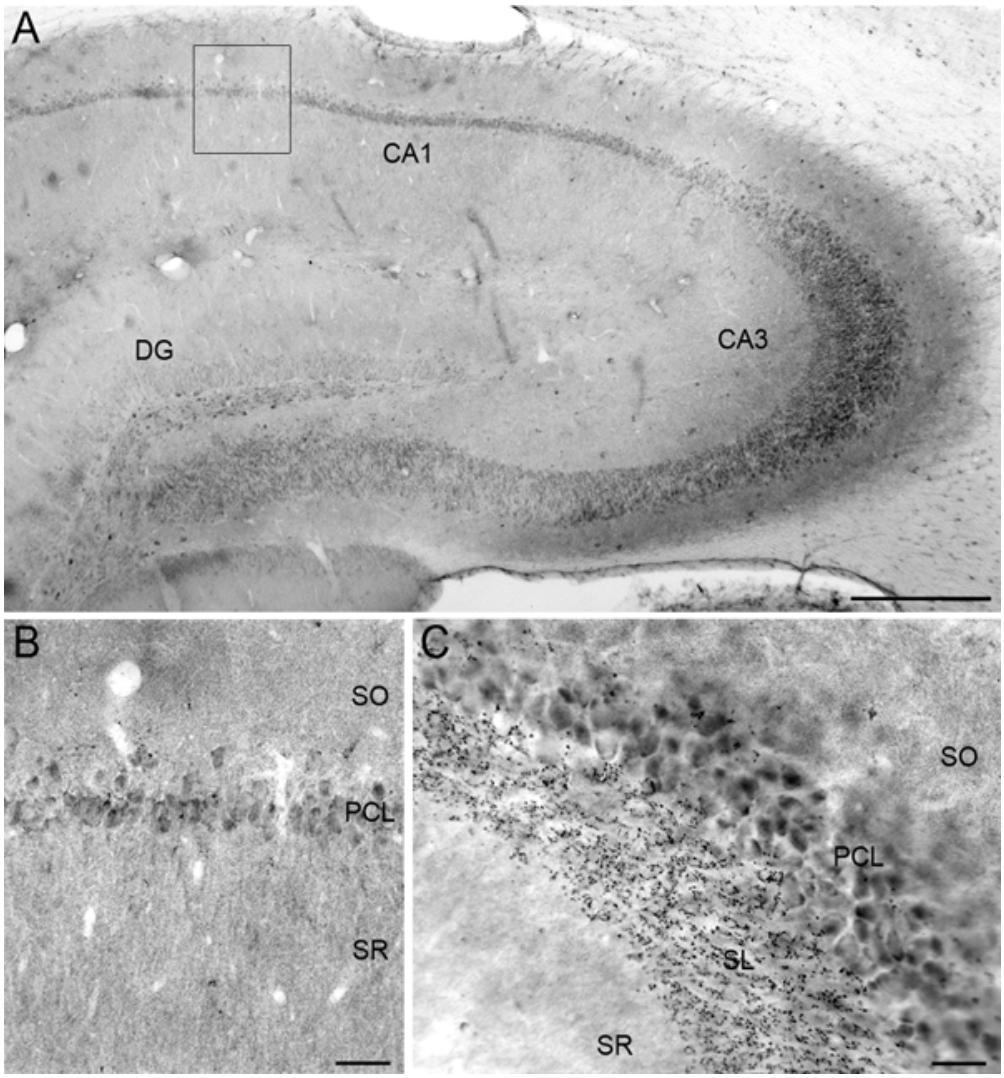

Fig. 4. Immunoperoxidase staining for AIDA-1 in hippocampus.

A: Low magnification view of the hippocampal formation. Pyramidal cells in Ammon's horn stain for AIDA-1. Granule cell in dentate gyrus (DG) stain more weakly than pyramidal cells; note scattered darkly-stained interneurons. **B:** Higher magnification view of the boxed area in CA1 shows that AIDA-1 staining in both stratum oriens (SO) and stratum radiatum (SR) is organized into small puncta; note somatic staining within the pyramidal cell layer (PCL). **C:** Darkly-stained large puncta in stratum lucidum (SL) likely correspond to the mossy fiber connections between dentate gyrus and CA3. In contrast, staining in SO is diffuse, with tiny puncta. Prominent staining is visible in the pyramidal cell layer. Scale bars A = 500 μm; B, C = 50 μm.

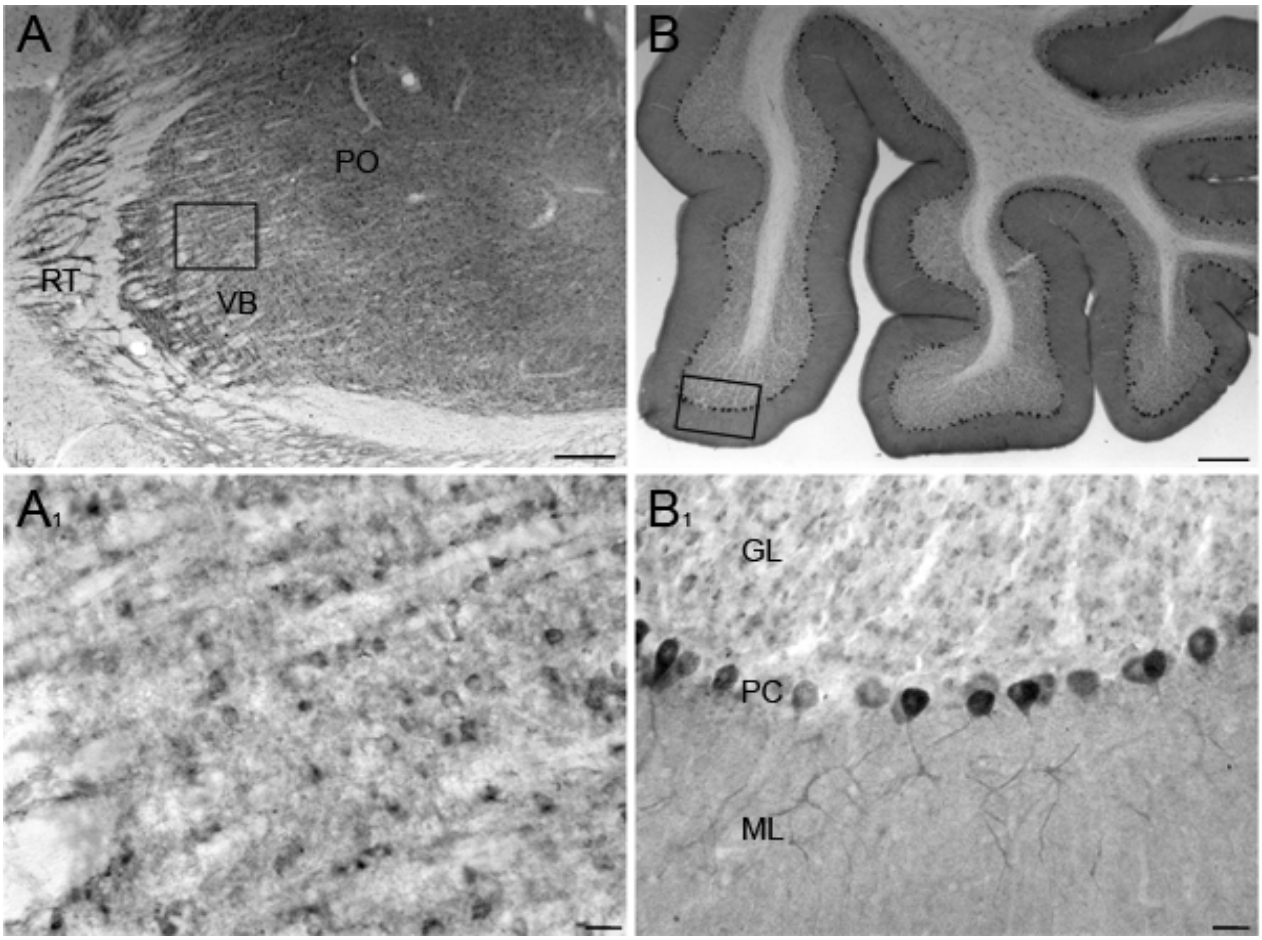

Fig. 5. Immunoperoxidase staining in thalamus and cerebellum

A: Immunostaining within the thalamus. Moderate levels of staining were seen uniformly across most of the thalamus; the reticular thalamic (RT) nucleus and the lateral areas of the ventrobasal nucleus (VB) contained comparable staining levels. Slightly stronger staining is visible in the posterior nuclear complex (PO). A_1: Higher magnification of the VPL revealed strongly stained cell bodies, whose nuclei were mostly devoid of staining. Diffuse staining is also visible. **B:** Immunostaining within cerebellum. Low magnification view of the cerebellum reveals strongly stained Purkinje neurons, a moderately stained molecular layer, and lightly stained granule cells. B_1 At higher magnification, nuclei of Purkinje cells usually lack staining, although staining is visible in a few scattered neurons. Scale bars: A, B = 250 μm; A_1, B_1 = 50 μm.

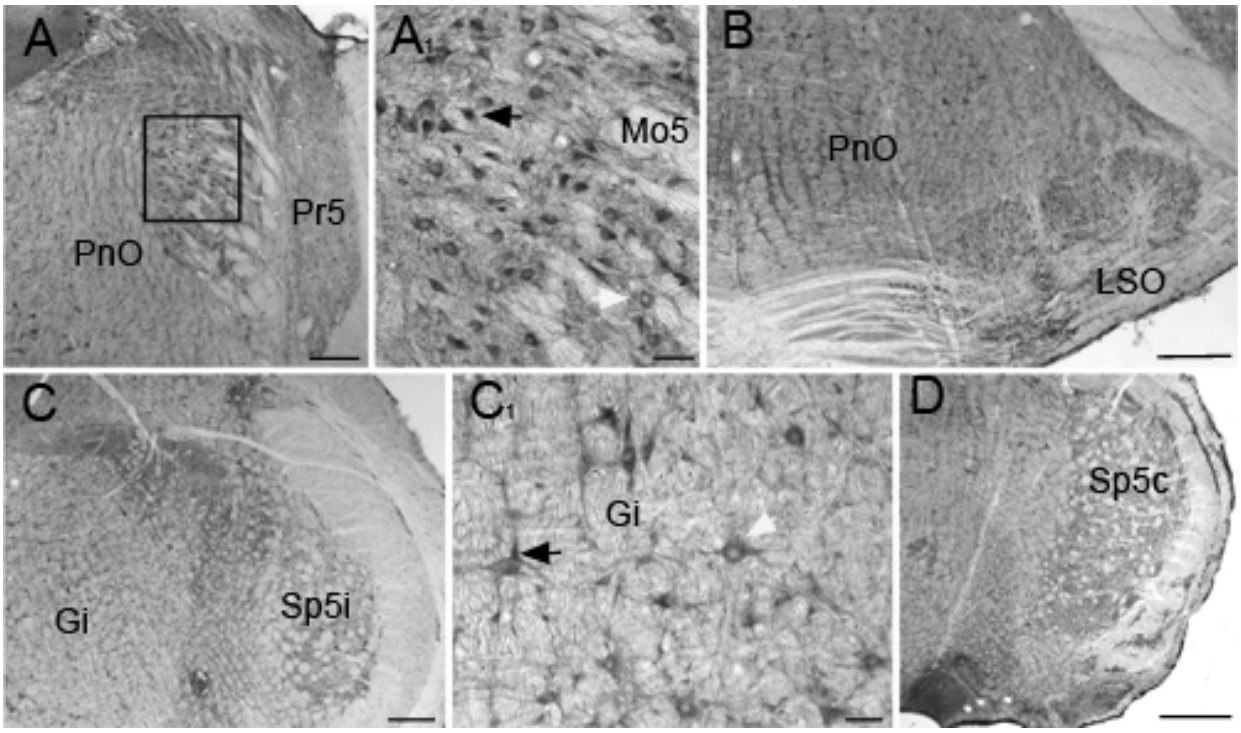

Fig. 6. Staining in brain stem.

Moderate levels of diffuse staining are present throughout brainstem. **A:** Pontine reticular nucleus (PnO) and principle sensory trigeminal nucleus (Pr5) have similar levels of diffuse staining. Neurons throughout these areas display somatic and nuclear staining. A_1 Higher magnification view of motor trigeminal nucleus (Mo5) show well-stained motor neurons, some containing immunopositive nuclei (black arrowhead) whereas other nuclei are negative (white arrowhead). **B:** Field illustrates relatively strong immunostaining within the superior olivary complex (LSO). **C:** Section through rostral medulla. Diffuse staining is generally weak. C_1 Higher magnification view of well-stained gigantocellular neurons (Gi); some containing immunopositive nuclei (black arrowhead) whereas other nuclei are negative (white arrowhead). **D:** Section through caudal medulla; note staining in spinal trigemial nucleus (Sp5c). Scale bars: A, B, C = 250 μm ; A_1, C_1 = 50 μm; D = 500 μm.

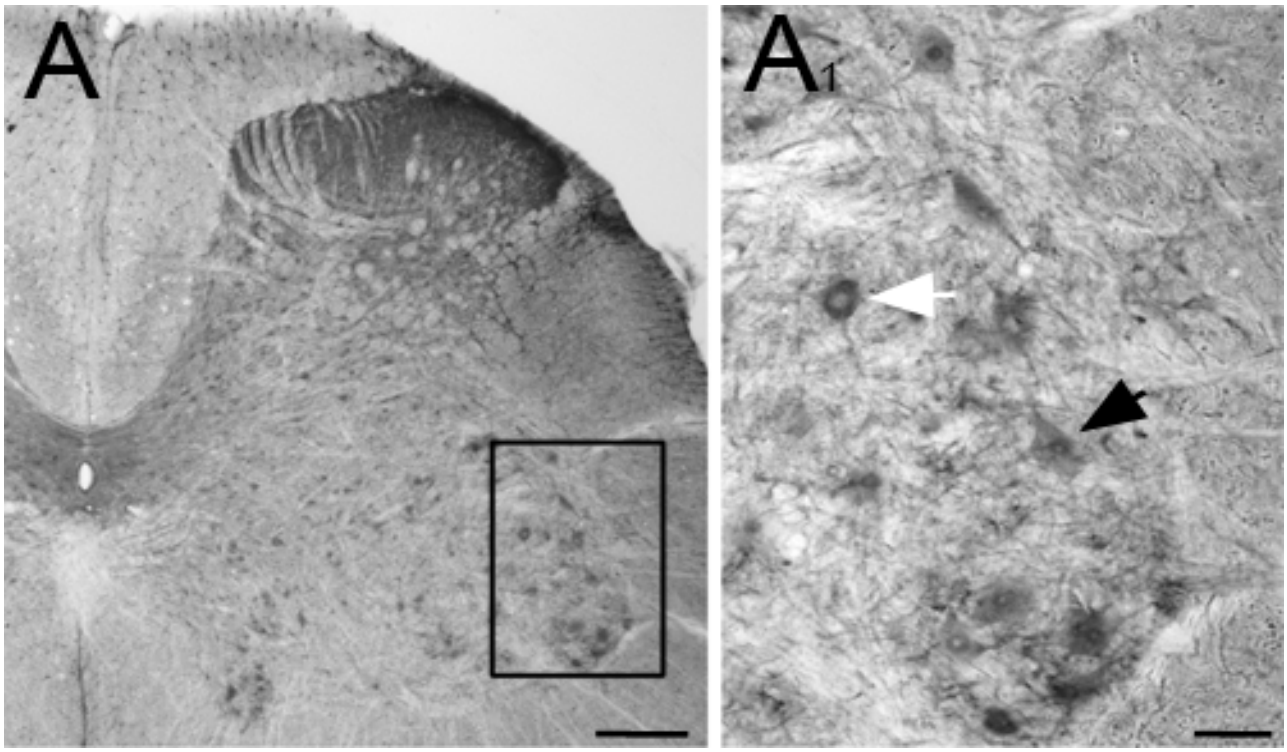

Fig. 7. Immunoperoxidase staining in spinal cord.

A: Low power magnification of the lumbar enlargement of spinal cord (L5). Diffuse staining is visible in the dorsal horn. A_1: A higher magnification view of the ventral horn shows staining in motoneurons. Some contain immunopositive nuclei (black arrowhead) whereas other nuclei are negative (white arrowhead). Scale Bars A= 250 μm; A_1 = 50 μm.

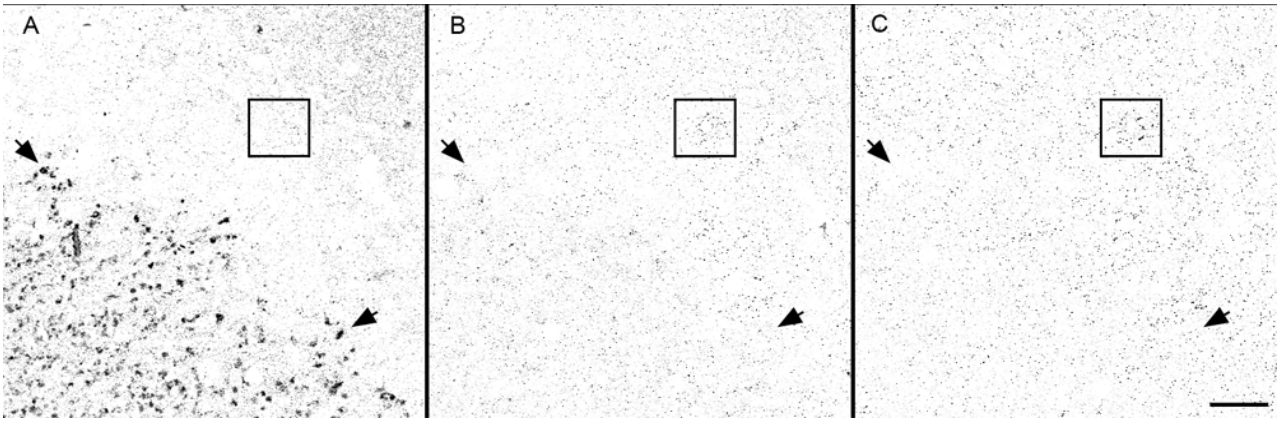

Fig. 8. Confocal images of AIDA-1 immunofluorescence in CA3 hippocampus

Optical sections illustrate how immunolabel varies with depth. Gray scale has been inverted to improve visibility. **A:** At the surface, staining is present in large puncta in stratum lucidum (arrows), while staining in the pyramidal cell layer is very weak. At 2.5 μm (**B**) and 5 μm (**C**) below surface, mossy fiber staining is barely detectable, whereas somatic staining becomes more obvious (open box). Scale bar = 20 μm.

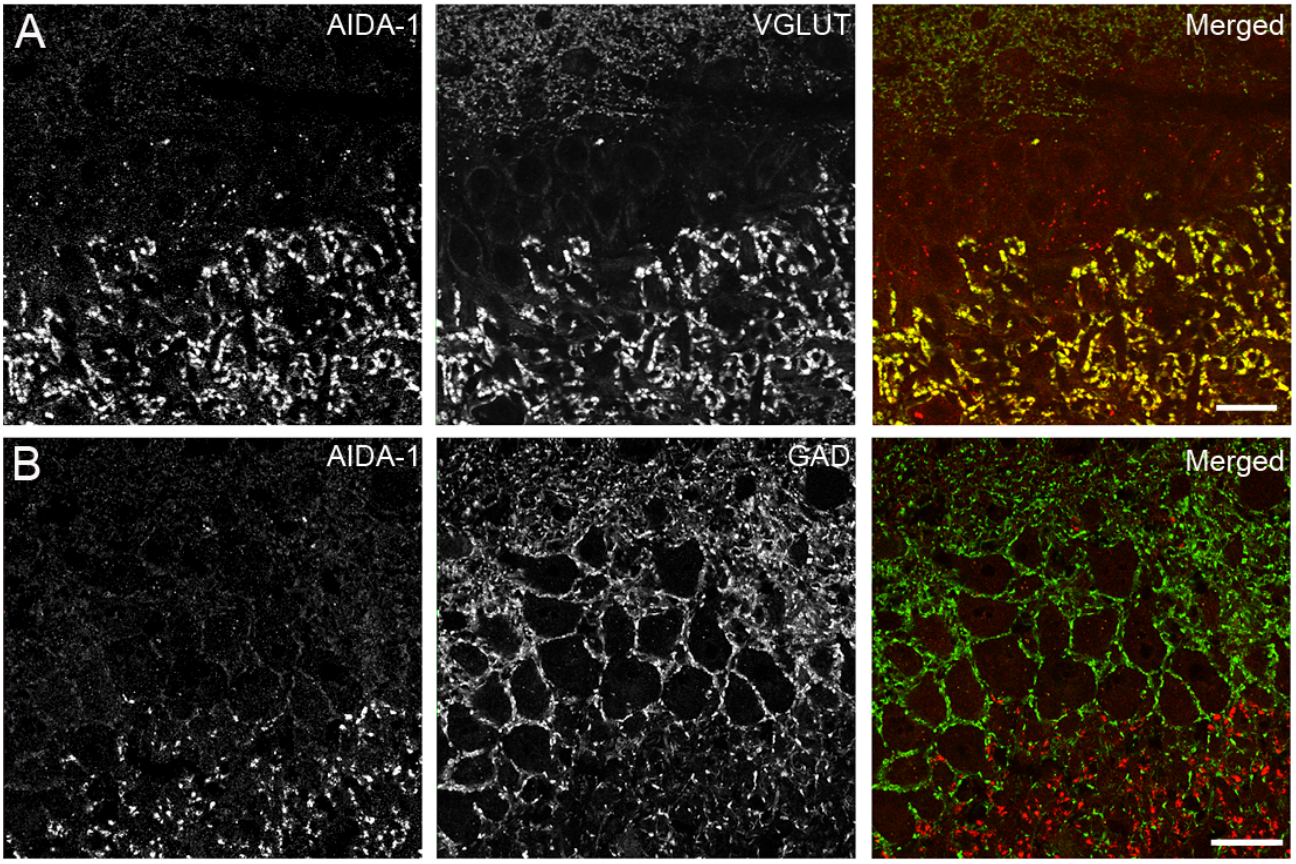

Fig. 9. Double-label immunofluorescence in hippocampal CA3.

A: Double labeling for AIDA-1(left panel) and VGLUT1 (middle panel). The right panel superimposes the AIDA-1 channel (red) and the VGLUT1 channel (green). Colocalization is apparent in large puncta in stratum lucidum. **B:** Double labeling with AIDA-1 (left panel) and GAD-65 (middle panel). Little evidence of colocalization can be seen (right panel). Slight bleedthrough of GAD-65 in the left panel outlines the cell bodies. These images were collected from the section surface: therefore, cytoplasmic/nuclear AIDA-1 is not clearly visible (compare Fig 4). Scale bar = 20 μm.

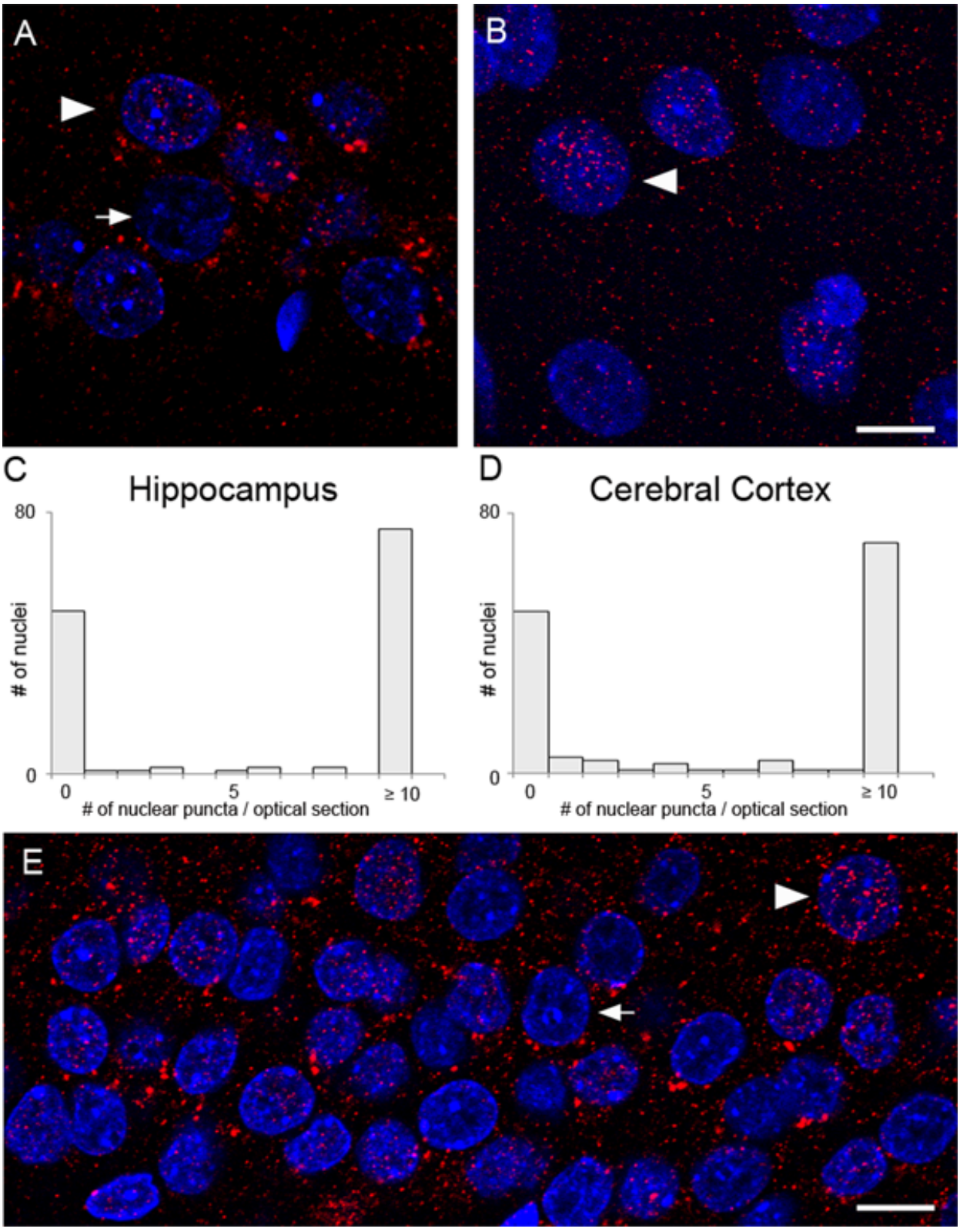
A
B
C
Hippocampus
80
0
# of nuclei
0
5
≥ 10
# of nuclear puncta / optical section
D
Cerebral Cortex
80
0
# of nuclei
0
5
≥ 10
# of nuclear puncta / optical section
E

Fig. 10. Expression of AIDA-1 in the nucleus.

Confocal image of AIDA-1 staining (red) within the pyramidal cell layer of CA1(**A**) and layer 5 of cerebral cortex (**B**); DAPI counterstain (blue) identifies nuclei. In many cells, large AIDA-1 puncta distribute throughout the nucleus, but these are generally absent from nucleoli. White arrowheads indicate nuclei containing prominent AIDA-1 puncta; white arrow points to nucleus containing little AIDA-1. Large AIDA-1 puncta outside nuclei are likely to lie within somatic cytoplasm. Smaller AIDA-1 puncta seen throughout the section may represent synaptic staining. Scale bar = 10 μm. **C,D:** Graphs showing the number of large puncta in nuclei in hippocampus (left) and cerebral cortex (right). Staining is bimodal; nuclei generally contain either very few or many large puncta. **E:** Confocal image of AIDA-1 staining (red) and granule cell nuclei (blue) in dentate gyrus. Tight packing of cells did not allow for further analysis, but both AIDA-1 positive (white arrowhead) and negative (white arrow) nuclei are visible.

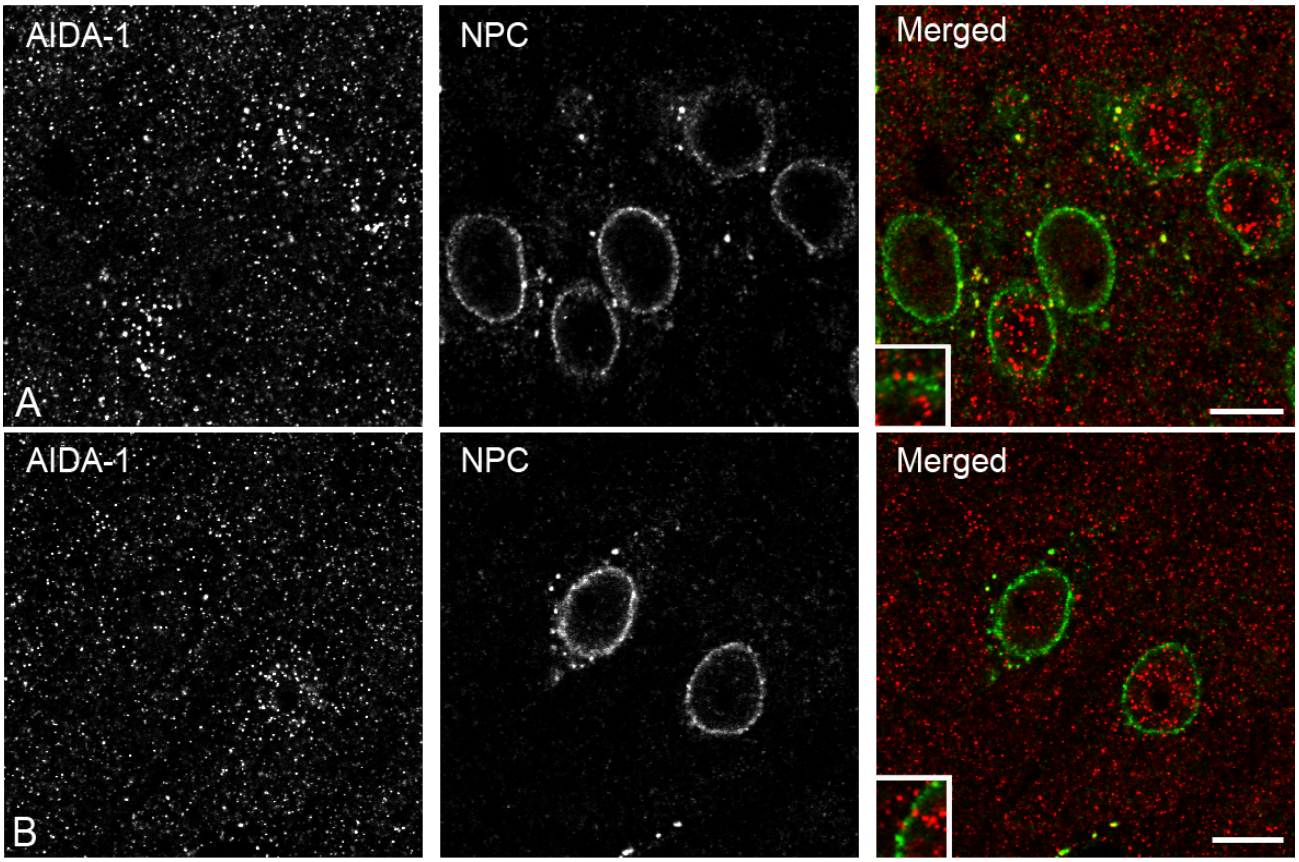

Fig. 11. Expression of AIDA-1 at the nuclear membrane.

Confocal images of material double-stained for AIDA-1 (left panels) and the nuclear pore complex (NPC, middle panels). The right panels merge the AIDA-1 channel (red) and the NPC channel (green). Some AIDA-1 puncta lie adjacent to the nuclear membrane in hippocampus (**A**) and cerebral cortex (**B**). Note that AIDA-1-positive nuclei generally exhibit more NPC-associated puncta. Small boxes in the right panels are enlargements, illustrating AIDA-1 puncta close to the nuclear membrane. Scale bar = 10 μm.

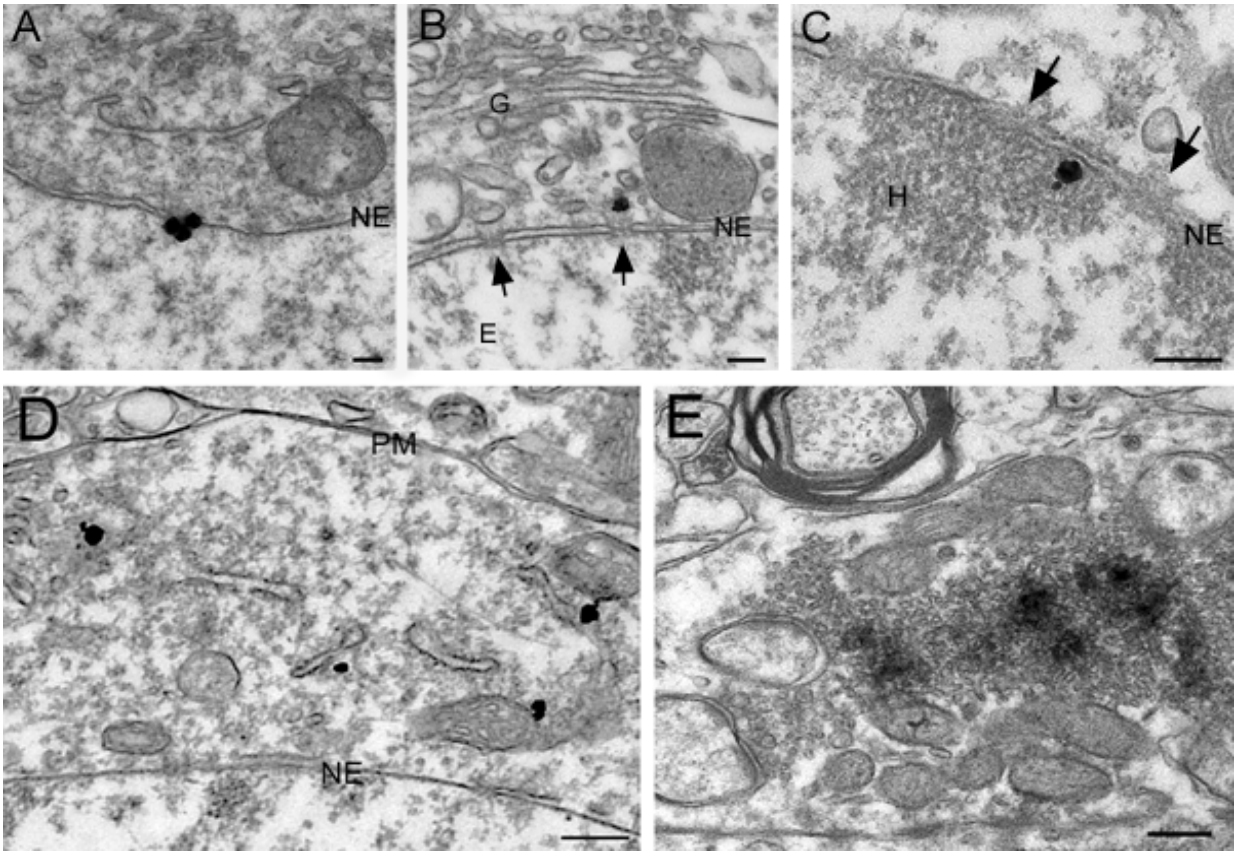

Fig. 12. Pre-embedding immunostaining for AIDA-1.

A-C: AIDA-1 associated with nuclear pores and the nuclear membrane. Silver-enhanced gold particles coding for AIDA-1 are at tne nuclear membrane (A); some lie directly outside (B) and inside (C) nuclear pores (arrows) . **D:** Immunogold particles in the cytoplasm, often associated with endomembranes. **E:** Electron-dense DAB reaction product shows staining of AIDA-1 in mossy fiber terminals. Staining typically concentrates in the middle of vesicle pools. Abbreviations: G, Golgi apparatus; NE, nuclear envelope; E, euchromatin; H, heterochromatin; PM, plasma membrane. Scale bars: A-C = 100 nm; D,E = 250 nm.

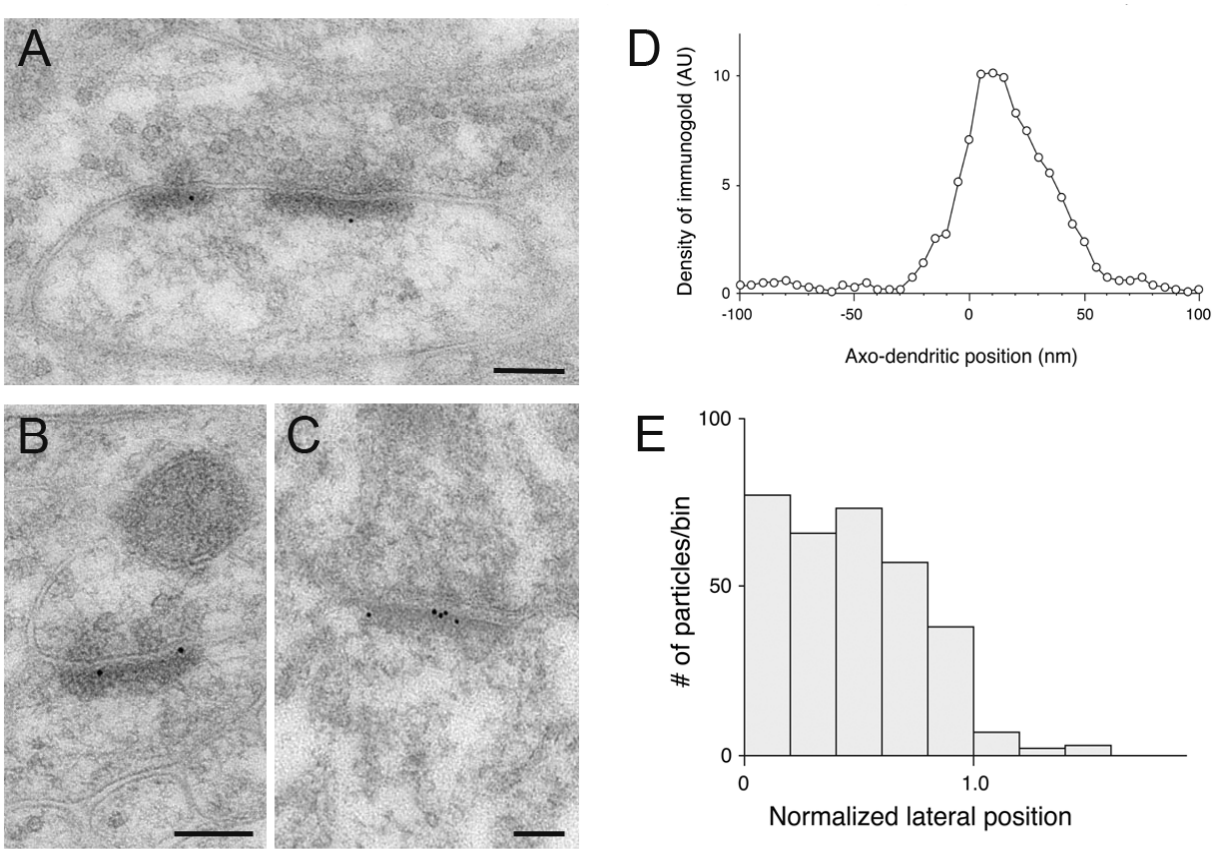

Fig. 13. Postembedding immunogold staining for AIDA-1.

A-C: Electron micrographs show immunogold labeling for AIDA-1; note association of particles with the PSD. Scale bars = 100 nm. **D:** Graph showing the "axo-dendritic" position of AIDA-1 labeling. Only particles within the width of the PSD were counted (see Methods for details). AIDA-1 concentrates postsynaptically, centered over the external part of the PSD. **E:** Graph showing the "lateral" distribution of AIDA-1. Only particles between -50 to +75 nm from the postsynaptic membrane were counted. To pool data, position was normalized: 0 corresponds to the PSD edge and 1 corresponds to the PSD center (see methods for details). AIDA-1 distributes fairly uniformly along the PSD, decreasing rapidly at its edge. Very little labeling is associated with the spine plasma membrane away from the synaptic specialization.

CHAPTER 4

Implications and Future Directions

4.1. Summary of Results

In this dissertation, I studied the basal organization of two proteins found within the PSD implicated in NMDAR-LTP: AMPAR and AIDA-1. For AMPAR, I studied the distribution of different AMPAR subunits within the PSD. When looking at axo-dendritic position within the PSD, I found that antibodies against GluA1 and GluA2/3 concentrated on the cytoplasmic side of the postsynaptic membrane, whereas GluA3 concentrated in the synaptic cleft. This difference reflects the different regions that the AMPAR subunits target; GluA1 and Glu2/3 antibody target the C terminal of AMPAR subunits, while GluA3 targets the N terminal. For lateral distribution, AMPARs have a subunit-dependent organization within the PSD; GluA1 distributes uniformly over the PSD, with its average normalized lateral position lying closer to the PSD edge than GluA3. KO of GluA1 causes the average normalized lateral position of particles coding for GluA2/3 and GluA3 to move closer to the center of the PSD, while KO of GluA2 did not modify GluA1, GluA2/3, or GluA3 subunit position. I also explored the relationship between lateral position and PSD size, finding GluA1 distributes over the PSD in small synapses, but near the center in longer PSD. Differences in subunit position due to PSD length were not displayed by GluA2/3 and GluA3. Serial section electron microscopy confirmed this result.

For AIDA-1, I studied the organization of AIDA-1 throughout the rat nervous system. A high level of AIDA-1 was seen in forebrain, including hippocampus, cerebral cortex, and striatum, and in cerebellum; moderate levels of AIDA-1 were found in olfactory bulb; and low level of staining in brain stem and in spinal cord. I investigated its subcellular distribution in hippocampus and in cerebral cortex, finding that AIDA-1 was organized into puncta throughout neurons. I next focused on staining in nuclei and synapses. In nuclei, AIDA-1 staining was variable; nuclei either stained heavily for AIDA-1(with 10 or more puncta) or lacked staining. To gain a detailed view of AIDA-1 interaction with nuclei, I used pre-embedding immunogold and detected AIDA-1 label at the nuclear pore complex, the entry way to the nucleus. AIDA-1 co-localize with a marker of excitatory, but not inhibitory synapses. Immunogold labeling against AIDA-1 in PSDs distributed fairly uniformly along the PSD, rapidly dropping off at its edge.

4.2. Relationship to Prior Studies and Discussion

A. AMPARs

Organization of AMPARs within the PSD has been suggested to play an important role in synaptic efficiency. After release in the synaptic cleft, glutamate concentration rapidly peaks and then quickly disperses. AMPARs have a low affinity for glutamate, so alignment between presynaptic sites of release and postsynaptic receptors could have a strong effect on synapse function (Clements et al., 1992; Clements, 1996). The mechanisms that coordinate of presynaptic and postsynaptic organization remain unknown. However, LTP is accompanied by clustering of the presynaptic protein synaptophysin, which interacts with postsynaptic GluA1

(Antonova et al., 2001), and a recent study demonstrated that presynaptic cell adhesion protein neurexin and its postsynaptic partner neuroligin can limit surface diffusion of AMPARs (Mondin et al., 2001), providing a potential mechanism that may links presynaptic and postsynaptic protein organization.

Using electron microscopy to evaluate the lateral distribution of AMPARs within the PSD, multiple studies have determined that AMPARs display higher immunogold labeling towards PSD edge in multiple brain regions (Matsubara et al., 1996; Bernard et al., 1997; Kharazia et al., 1997; Ottersen et al., 1998; Sassoe-Poenetto et al., 2000). These studies were performed using a GluA1 and/or GluA2/3 antibody; no previous study has examined the distribution of GluA3 within the PSD. Since GluA1 should exclusively label GluA1/2 receptors and GluA3 should exclusively label GluA2/3, ours is the first study to investigate possible differences in organization of GluA1/2 and GluA2/3 receptors.

The electrophysiological response of GluA1/2 and GluA2/3 receptors to glutamate is similar (Traynelis et al., 2010.), suggesting that the main differences between the functions of GluA1/2 and GluA2/3 receptors from differences in protein binding and trafficking of GluA1/2 and GluA2/3 receptors. GluA1 has many unique phosphorylation and binding sites that may be involved in activity-dependent insertion (Palmer et al., 2005). GluA2 and GluA3 share many of the same phosphorylation and binding sites; however, GluA2 interactions with other proteins, such as NSF and AP-2, are thought to play an important role in removal of synaptic receptors. A distinct function for GluA3 remains unknown.

We are only beginning to understand what interactions underlie AMPAR lateral position. Two general factors have been proposed to organize AMPARs within the PSD: protein-protein interactions and diffusion trapping. In protein-protein interactions, AMPARs are positioned within the PSD by binding to scaffolding proteins. PSD-95 is a plausible candidate for this role (MacGillavry et al., 2011; Opazo et al., 2011). The distribution of PSD-95 over the PSD is similar to GluA1; however, unlike GluA1, PSD-95 does not concentrate at the PSD edge, indicating that lateral organization of GluA1 is not entirely explained by its interactions with PSD-95. The distribution of PSD-95 differs greatly from GluA3. However, NMDAR, which like GluA3 are found to the center of PSDs, bind and are thought to be organized by PSD-95 (Valtschanoff et al., 2001). This suggests that although PSD-95 and GluA3 have different distribution across the PSD, PSD-95 may help localized GluA3 to the synapse center. SAP97 is a strong candidate to organize GluA1-containing receptors within the PSD. Overexpression of SAP97 increases AMPAR currents, suggesting that it has the ability to collect AMPAR within the PSD (Howard et al., 2011), and EM studies have determined that SAP97 has a lateral distribution over the PSD similar to GluA1 (DeGiorgis et al., 2000; Valtschanoff et al., 2000). Diffusional trapping of AMPARs makes use of protein barriers, which prevent unrestricted lateral diffusion of AMPAR without binding them directly. Although computational studies have predicted that receptor movement in PSD is limited by obstacles, the protein(s) involved remains unknown (Holcman et al., 2006).

Here, we suggest a dynamic mechanism to organize AMPARs in the PSD. Current work suggests that GluA1/2 and GluA2/3 receptors may take different routes

into the synapse; however no direct evidence has shown that different types of receptors are inserted into different locations. Our finding that GluA1/2 and GluA2/3 receptors have different lateral distributions across the PSD could indicate that GluA1/2 and GluA2/3 receptors have different sites of AMPAR insertion. Multiple studies have shown that AMPARs are inserted outside the PSD and undergo lateral diffusion into the synapse (Kopec et al., 2006; Park et al., 2006; Yudowski et al., 2007; Yang et al., 2008; Makino et al., 2009; Kennedy et al., 2010). However, these studies were all performed using tracking of GluA1 or GluA2, so no previous study has exclusively tracked GluA2/3 receptors. Evidence suggests that can be directly inserted into the PSD; components of the exocyst, a collection of proteins important for membrane insertion, have been found associated with the PSD (Gerges et al., 2006). Our finding suggests that GluA1/2 receptors, which distribute uniformly over the PSD, may enter synapses through lateral diffusion, whereas GluA2/3 receptors, which are found in the PSD center, may be directly inserted into the PSD.

B. AIDA-1

In contrast to AMPARs, few studies have investigated AIDA-1, and its functions remain mysterious. Within different areas of the brain that prominently stained for AIDA-1, subcellular distribution varied; within hippocampus and cerebral cortex, AIDA-1 was found in both nuclei and synapses, while in cerebellum, AIDA-1 was predominantly located in Purkinje cells and was not found to localize in cerebellar synapse. Work in cultured hippocampal cells found that AIDA-1 might serve as a synapse-to-nucleus signaling mechanism. However, the lack of synaptic

staining in cerebellum suggests that AIDA-1 may serve another function in this region.

Within pyramidal cells in CA1 and cerebral cortex, approximately half of nuclei contain 10 or more AIDA-1 puncta; the other half lack staining. In nuclei, AIDA-1 promotes interactions between Cajal bodies and nucleoli, which lead to increased downstream protein translation. We found that AIDA-1 often associates with the nuclear pore complex (NPC), a collection of proteins found at nuclear pores. Although labeling at NPC could be against AIDA-1 in the process of undergoing transport into the nucleus, labeling could also indicate that AIDA-1 interacts with NPC and plays some sort of function in nuclear transport.

AIDA-1 was highly concentrated the PSD, and concentrated in excitatory, but not inhibitory synapses. Within CA1 SR synapses, AIDA-1 distributes fairly uniformly over the PSD. This distribution is likely due to its interaction with PSD-95; co-immunoprecipitation experiments have shown that AIDA-1 binds to PSD-95, and PSD-95 distributes uniformly across the PSD (Valtschanoff et al., 2001; Jordan et al., 2007). Interestingly, NMDAR-induced AIDA-1 cleavage and subsequent translocation do not require Ca^{2+} rises. Since Ca^{2+} is a diffusible signal, this suggests that AIDA-1 may require physical contact with NMDARs to activate. Within CA3 mossy fibre synapses, AIDA-1 showed a different in organization, colocalizing with both pre- and postsynaptic markers. Unlike NMDAR-dependent LTP, LTP in mossy fibers leads to increased presynaptic release probability (Nicoll et al., 2005; McBain, 2008), suggesting that AIDA-1 may play a role in the presynaptic expression of LTP.

One of the most intriguing features of AIDA-1 is its method of translocation to the nucleus. NMDAR activation induces cleavage of AIDA-1; one fragment undergoes translocation to the nucleus, while the other AIDA-1 fragment remains bound to the PSD (Jordan et al., 2007). No other proposed signal that translocates from synapses to nuclei leaves a portion of itself behind in the PSD (Deisseroth et al., 2003; Ch'ng et al., 2011). This provides the intriguing suggesting that AIDA-1 might serve as a "synaptic tag", indicating previously potentiated synapses and playing some role in the capture of plasticity related particles (Reymann et al., 2007).

4.3. Potential future dirrections

Here, I briefly pose a few questions that follow from my work on AMPARs and AIDA-1, and propose methods to experimentally address these issues. Unlike AMPARs, the function of AIDA-1 is just beginning to be understood, and extensive work will be required to elucidate its function. I therefore limit my focus to issues that elaborate the role of AIDA-1 in synaptic plasticity or directly follow from my findings in Jacob et al., 2010.

A. AMPAR studies

I. Do AMPAR subunits colocalize with other proteins within the PSD?

My work established that AMPAR subunits organize in different regions of the PSD: on average, GluA1 is found close to the PSD edge, while GluA3 is found in the PSD center. However, studying multiple proteins within the same sample is daunting in electron microscopy; double labeling of EM samples is difficult. Recent advances in light microscopy have increased resolution, allowing PSD organization

to be visualized (Dani et al., 2009). In the previous section, I suggested PSD-95 and SAP97 may serve as protein binding partners underlying AMPAR lateral position within PSDs. To determine if protein interactions between AMPARs and either PSD-95 and/or SAP97 underlie AMPAR organization, I propose using, STORM (stochastic optical reconstruction microscopy), a superresolution light microscopy technique, to study the potential interaction of AMPAR subunits and several scaffolding proteins that are likely candidates to organize AMPAR within the PSD.

In addition, I propose studying how AMPAR lateral distribution alters in response to changes (overexpression, knock down, or knock out) in these scaffold proteins. For PSD-95, a knockout mouse is available, so I propose performing STORM microscopy to determine if lateral distribution of AMPAR subunits, particularly GluA1 and GluA3, is altered. KO of SAP97 is lethal, so a different strategy for determining the role of SAP97in AMPAR lateral distribution must be used. For these experiments, I suggest studying AMPAR lateral distribution in cultured neurons where SAP97 is knocked down using siRNA and in cultured neurons where SAP97 is overexpressed. These studies may be complicated by redundancy of MAGUK proteins. PSD-93 has been shown to take over many of the functions of PSD-95 in PSD-95 mice, and in neurons with both PSD-93 and PSD-95 knocked out, SAP102, another MAGUK, is up-regulated.

II. How is AMPAR subunits organized in live tissue?

For my current work using electron microscopy, I studied the organization of AMPAR within the PSD within fixed tissue. However, AMPAR are highly dynamic, thus studying AMPAR in living cell is essential to understanding their organization

within the PSD. The Blanpied lab has studied AMPAR within PSD of cultured hippocampal neurons using confocal microscopy (Kerr et al., 2012). Although the resolution of this technique is limited, I propose imagining dissociated neuronal cultures to see if differences in GluA1 and GluA3 organization can be detected.

III. How do GluA3 containing AMPARs traffic into the synapse?

Little information is known about the trafficking of GluA3-containing receptors. Daniel Choquet and colleagues have tagged single AMPAR and tracked them as they move along the postsynaptic membrane and into synapse (Borgdorff et al., 2002; Groc et al., 2007). However, these studies have tracked either GluA1 or GluA2, thus no definitive trafficking of GluA3 containing AMPAR has occurred. I propose using single particle trafficking to study the dynamics of GluA3 containing AMPAR within both the synaptic membrane and PSD.

IV. Does LTP alter AMPAR organization?

Upregulation of AMPARs serves as the expression mechanism of NMDAR-LTP. However, it remains unknown if lateral organization of AMPAR subunits alters in response to NMDAR-LTP. Several experiments could be used to address this issue. Using confocal microscopy on cultured neurons, chemical LTP could be applied and the synapse organization could be monitored to see if changes occur between. However, AMPAR trafficking within dissociated neurons might operate differently than *in vivo*. Thus, I suggest performing EM on tissue that had undergone LTP, using methods similar to my past experiments to determine AMPAR subunit distribution. To induce LTP, I propose performing chemLTP on slice cultures, since a

high percentage of synapses in this model system will undergo LTP. Another potential method is to induce LTP through behavioral methods

V. How does KO of different AMPAR subunits change AMPAR organization?

I think one of my most intriguing finding was that lateral distribution of AMPAR differs in GluA1 animals. Within GluA1 KO animals, GluA2 and GluA3 position became more centrally localized, suggesting that GluA1 interactions may account for ability of AMPAR to spread over the PSD. To study this effect, I propose a full scale EM study analogue to the one carried out in chapter 2. In addition, both STORM microscopy on fixed tissue, where I could evaluate multiple proteins at the same time, and confocal microscopy on living cultures, where I could perturb the system in multiple ways, could be used to study AMPAR organization in Kos.

B. AIDA-1 studies

I. Does AIDA-1 play a role in late phase LTP?

Although NMDAR activation leads to AIDA-1 translocation to the nucleus, leading to increase in protein translation (Jordan et al., 2007), it remains unknown if AIDA-1 plays a role late phase LTP. Here I suggest several experiments to determine the role(s) that AIDA-1 plays in NMDAR-LTP.

One strategy would be to perform slice electrophysiology to measure if perfuse the cleaved (thus the active) form of AIDA-1 postsynaptically to see if increased l-LTP results. If increasing AIDA-1 does not increase l-LTP, thus does not indicate AIDA-1 plays no role in l-LTP; AIDA-1 addition might not be sufficient to induce increased l-LTP. By inhibiting AIDA-1 cleavage, l-LTP in slice

electrophysiology may be perturbed. Another strategy would be to create an AIDA-1 knockout, or conditional KO, mouse, and perform slice electrophysiology on it to see if late phase LTP is perturbed. If a KO mouse is lethal, molecular biology could potentially be used to alter AIDA-1 so it could no longer be cleaved; however, this assumes that translocation of the AIDA-1 portion to the nucleus is what would account of the role of AIDA-1 in l-LTP. In addition, I suggest that AIDA-1 subcellular organization be evaluated in slice cultures that undergone chemical LTP to see whether its distribution alters in response to LTP.

II. How does AIDA-1 in organize in cerebellum?

The organization of AIDA-1 within cerebellum displayed a striking difference from that seen in hippocampus and cerebral cortex; AIDA-1 is absent from synapses and was restricted mainly to the Purkinje cells. However, details of this organization remain unknown. To aid in understanding the function of AIDA-1 in cerebellum, I propose a study of cerebellar distribution to gain a better understanding of the sites where AIDA-1 may function. For this study, I would focus on the subcellular distribution of AIDA-1 within Purkinje cells, performing electron microscopy to identify subcellular components that AIDA-1 binds. Organization of AIDA-1 may differ between forebrain and cerebellum because different isoforms of AIDA-1 are expressed in these areas. Some isoform specific antibodies are available, and I would propose using those in addition to the pan-AIDA-1 antibody.

REFERENCES

Abraham WC, Williams JM. 2008. LTP maintenance and its protein synthesis-dependence. Neurobiol Learn Mem. 89:260-268.

Adams JP, Dudek SM. 2005. Late-phase long-term potentiation: getting to the nucleus. Nat Rev Neurosci. 6:737-43.

Adesnik H, Nicoll RA. 2007. Conservation of glutamate receptor 2-containing AMPA receptors during long-term potentiation. J Neurosci. 27:4598-602.

Aicardi G, Argilli E, Cappello S, Santi S, Riccio M, Thoenen H, Canossa M. 2004. Induction of long-term potentiation and depression is reflected by corresponding changes in secretion of endogenous brain-derived neurotrophic factor. Proc Natl Acad Sci USA 101:15788-92.

Antonova I, Arancio O, Trillat AC, Wang HG, Zablow L, Udo H, Kandel ER, Hawkins RD.2001. Rapid increase in clusters of presynaptic proteins at onset of long-lasting potentiation. Science 294:1547-50.

Anwyl R. 1999. Metabotropic glutamate receptors: electrophysiological properties and role in plasticity. Brain Res Brain Res Rev. 29:83-120.

Appleby VJ, Corrêa SA, Duckworth JK, Nash JE, Noël J, Fitzjohn SM, Collingridge GL, Molnár E. 2011. LTP in hippocampal neurons is associated with a CaMKII-mediated increase in GluA1 surface expression. J Neurochem. 116:530-43

Araki Y, Lin DT, Huganir RL. 2010. Plasma membrane insertion of the AMPA receptor GluA2 subunit is regulated by NSF binding and Q/R editing of the ion pore. Proc Natl Acad Sci USA 107:11080-5.

Ayalon G, Stern-Bach Y. 2001. Functional assembly of AMPA and kainate receptors is mediated by several discrete protein-protein interactions. Neuron 31:103-13.

Barria A, Derkach V, Soderling T. 1997. Identification of the Ca2+/calmodulin-dependent protein kinase II regulatory phosphorylation site in the alpha-amino-3-hydroxyl-5-methyl-4-isoxazole-propionate-type glutamate receptor. J Biol Chem. 272:32727-30.

Bats C, Groc L, Choquet D. 2007. The interaction between Stargazin and PSD-95 regulates AMPA receptor surface trafficking. Neuron. 53:719-34.

Baude A, Nusser Z, Molnár E, McIlhinney RA, Somogyi P. 1995. High-resolution immunogold localization of AMPA type glutamate receptor subunits at synaptic and non-synaptic sites in rat hippocampus. Neuroscience 69:1031-55.

Baude A, Nusser Z, Roberts JD, Mulvihill E, McIlhinney RA, Somogyi P. 1993. The metabotropic glutamate receptor (mGluR1 alpha) is concentrated at perisynaptic membrane of neuronal subpopulations as detected by immunogold reaction. Neuron 11:771-87.

Béïque JC, Lin DT, Kang MG, Aizawa H, Takamiya K, Huganir RL. 2006. Synapse-specific regulation of AMPA receptor function by PSD-95.Proc Natl Acad Sci USA 103:19535-40.

Belichenko PV, Kleschevnikov AM, Masliah E, Wu C, Takimoto-Kimura R, Salehi A, Mobley WC. 2009. Excitatory-inhibitory relationship in the fascia dentata in the Ts65Dn mouse model of Down syndrome. J Comp Neurol. 512:453-66.

Bernard V, Somogyi P, Bolam JP. 1997. Cellular, subcellular, and subsynaptic distribution of AMPA-type glutamate receptor subunits in the neostriatum of the rat. J Neurosci. 17:819-33.

Bliss TV, Collingridge GL 1993. A synaptic model of memory: long-term potentiation in the hippocampus. Nature 361: 31–39.

Borgdorff AJ, Choquet D. 2002. Regulation of AMPA receptor lateral movement. Nature 417:649-653.

Bourne JN, Harris KM. 2008. Balancing structure and function at hippocampal dendritic spines. Annu Rev Neurosci. 31:47-67.

Burnashev N, Khodorova A, Jonas P, Helm PJ, Wisden W, Monyer H, Seeburg PH, Sakmann B. 1992. Calcium-permeable AMPA-kainate receptors in fusiform cerebellar glial cells. Science 256:1566-70.

Calixto E, Thiels E, Klann E, Barrionuevo G. 2003. Early maintenance of hippocampal mossy fiber--long-term potentiation depends on protein and RNA synthesis and presynaptic granule cell integrity. J Neurosci. 23:4842-4849.

Ch'ng TH, Martin KC. 2011. Synapse-to-nucleus signaling. Curr Opin Neurobiol. 21:345-52.

Chang MC, Park JM, Pelkey KA, Grabenstatter HL, Xu D, Linden DJ, Sutula TP, McBain CJ, Worley PF. 2010. Narp regulates homeostatic scaling of excitatory synapses on parvalbumin-expressing interneurons.Nat Neurosci. 13:1090-7.

Chen HJ, Rojas-Soto M, Oguni A, Kennedy MB. 1998. A synaptic Ras-GTPase activating protein (p135 SynGAP) inhibited by CaM kinase II. Neuron 20:895-904.

Chen X, Vinade L, Leapman RD, Petersen JD, Nakagawa T, Phillips TM, Sheng M, Reese TS. 2005. Mass of the postsynaptic density and enumeration of three key molecules. Proc Natl Acad Sci USA 102:11551-6

Chicurel ME, Harris KM. 1992. Three-dimensional analysis of the structure and composition of CA3 branched dendritic spines and their synaptic relationships with mossy fiber boutons in the rat hippocampus. J Comp Neurol. 325:169-82.

Choquet D. 2010. Fast AMPAR trafficking for a high-frequency synaptic transmission. Eur J Neurosci. 32:250-60.

Choquet D, Triller A. 2003. The role of receptor diffusion in the organization of the postsynaptic membrane. Nat Rev Neurosci. 4:251-265.

Chowdhury S, Shepherd JD, Okuno H, Lyford G, Petralia RS, Plath N, Kuhl D, Huganir RL, Worley PF. 2006. Arc/Arg3.1 interacts with the endocytic machinery to regulate AMPA receptor trafficking. Neuron 52:445-59.

Citri A, Bhattacharyya S, Ma C, Morishita W, Fang S, Rizo J, Malenka RC. 2010. Calcium binding to PICK1 is essential for the intracellular retention of AMPA receptors underlying long-term depression. J Neurosci. 30:16437-52.

Clements JD. 1996. Transmitter timecourse in the synaptic cleft: its role in central synaptic function. Trends Neurosci. 19:163-71.

Clements JD, Lester RA, Tong G, Jahr CE, Westbrook GL. 1992. The time course of glutamate in the synaptic cleft. Science 258:1498-501.

Correia SS, Bassani S, Brown TC, Lisé MF, Backos DS, El-Husseini A, Passafaro M, Esteban JA. 2008. Motor protein-dependent transport of AMPA receptors into spines during long-term potentiation. Nat Neurosci.11:457-66.

Cuadra AE, Kuo SH, Kawasaki Y, Bredt DS, Chetkovich DM. 2004. AMPA receptor synaptic targeting regulated by stargazin interactions with the Golgi-resident PDZ protein nPIST.J Neurosci. 24:7491-502.

D'Angelo MA, Hetzer MW. 2008. Structure, dynamics and function of nuclear pore complexes. Trends Cell Biol.18:456-466.

Dani A, Huang B, Bergan J, Dulac C, Zhuang X. 2010. Superresolution imaging of chemical synapses in the brain. Neuron 68:843-56.

Davis LI, Blobel G.1986. Identification and characterization of nuclear pore complex protein. Cell 45:699-709.

DeGiorgis JA, Galbraith JA, Dosemeci A, Chen X, Reese TS. 2006. Distribution of the scaffolding proteins PSD-95, PSD-93, and SAP97 in isolated PSDs. Brain Cell Biol. 35:239-50.

Deisseroth K, Bito H, Tsien RW. 1996. Signaling from synapse to nucleus: postsynaptic CREB phosphorylation during multiple forms of hippocampal synaptic plasticity. Neuron 16:89-101.

Deisseroth K, Heist EK, Tsien RW. 1998.Translocation of calmodulin to the nucleus supports CREB phosphorylation in hippocampal neurons. Nature 392:198-202.

Deisseroth K, Mermelstein PG, Xia H, Tsien RW. 2003. Signaling from synapse to nucleus: the logic behind the mechanisms. Curr Opin Neurobiol. 13:354-65.

Derkach V, Barria A, Soderling TR. 1999. Ca2+/calmodulin-kinase II enhances channel conductance of alpha-amino-3-hydroxy-5-methyl-4-isoxazolepropionate type glutamate receptors. Proc Natl Acad Sci USA 96:3269-74.

Difiglia M, Pasik P, Pasik T. 1982. A Golgi and ultrastructural study of the monkey globus pallidus. J Comp Neurol 212:53-75.

Dingledine R, Borges K, Bowie D, Traynelis SF.1999. The glutamate receptor ion channels. Pharmacol Rev. 51:7-61.

Dolmetsch RE, Pajvani U, Fife K, Spotts JM, Greenberg ME. 2001. Signaling to the nucleus by an L-type calcium channel-calmodulin complex through the MAP kinase pathway. Science 294:333-9.

Dudek SM, Fields RD. 2002. Somatic action potentials are sufficient for late-phase LTP-related cell signaling. Proc Natl Acad Sci USA 99:3962-7.

Duyckaerts C, Delatour B, Potier MC. 2009. Classification and basic pathology of Alzheimer disease. Acta Neuropathol. 118:5-36.

Franks KM, Stevens CF, Sejnowski TJ. 2002. Independent sources of quantal variability at single glutamatergic synapses. J Neurosci. 23:3186-95.

Frey U, Frey S, Schollmeier F, Krug M. 1996. Influence of actinomycin D, a RNA synthesis inhibitor, on long-term potentiation in rat hippocampal neurons in vivo and in vitro. J Physiol. 490:703-11.

Frey U, Krug M, Brodemann R, Reymann K, Matthies H. 1989. Long-term potentiation induced in dendrites separated from rat's CA1 pyramidal somata does not establish a late phase. Neuroscience Letters 97:135-39.

Geinisman Y, deToledo-Morrell L, Morrell F. 1991. Induction of long-term potentiation is associated with an increase in the number of axospinous synapses with segmented postsynaptic densitites. Brain Res. 1-2:77-88

Gerges NZ, Backos DS, Rupasinghe CN, Spaller MR, Esteban JA. 2006. Dual role of the exocyst in AMPA receptor targeting and insertion into the postsynaptic membrane. EMBO 25:1623-34.

Gerfen CR. 1988. Synaptic organization of the striatum. J Electron Microsc Tech 10:265-281.

Ghersi E, Noviello C, D'Adamio L. 2004. Amyloid-beta protein precursor (A□PP) intracellular domain-associated protein-1 proteins bind to AbetaPP and modulate its processing in an isoform-specific manner. J Biol Chem. 279:49105-49112.

Ghersi E, Vito P, Lopez P, Abdallah M, D'Adamio L. 2004. The intracellular localization of amyloid beta protein precursor (A□PP) intracellular domain associated protein-1 (AIDA-1) is regulated by AbetaPP and alternative splicing. J Alzheimers Dis 6:67-78.

Gill MB, Kato AS, Roberts MF, Yu H, Wang H, Tomita S, Bredt DS. 2011. Cornichon-2 modulates AMPA receptor-transmembrane AMPA receptor regulatory protein assembly to dictate gating and pharmacology. J Neurosci.31:6928-38.

Graef IA, Mermelstein PG, Stankunas K, Neilson JR, Deisseroth K, Tsien RW, Crabtree GR. 1999. L-type calcium channels and GSK-3 regulate the activity of NF-ATc4 in hippocampal neurons. Nature 401:703-8.

Gray EG. 1959. Electron microscopy of synaptic contacts on dendrite spines of the cerebral cortex. Nature. 183:1592-3.

Gray EG. 1961. The granule cells, mossy synapses and Purkinje spine synapses of the cerebellum: light and electron microscope observations. J Anat. 95:345-56.

Greger IH, Esteban JA. 2007a. AMPA receptor biogenesis and trafficking. Curr Opin Neurobiol. 17:289-97.

Greger IH, Khatri L, Ziff EB. 2002. RNA editing at arg607 controls AMPA receptor exit from the endoplasmic reticulum. Neuron 34:759-72.

Greger IH, Khatri L, Kong X, Ziff EB. 2003. AMPA receptor tetramerization is mediated by Q/R editing. Neuron. 40:763-74.

Greger IH, Ziff EB, Penn AC. 2007b. Molecular determinants of AMPA receptor subunit assembly. Trends Neurosci. 30:407-16

Groc L, Lafourcade M, Heine M, Renner M, Racine V, Sibarita JB, Lounis B, Choquet D, Cognet L 2007. Surface trafficking of neurotransmitter receptor: comparison between single-molecule/quantum dot strategies. J. Neurosci. 27, 12433–12437.

Hamid R, Kilger E, Willem M, Vassallo N, Kostka M, Bornhövd C, Reichert AS, Kretzschmar HA, Haass C, Herms J. 2007. Amyloid precursor protein intracellular domain modulates cellular calcium homeostasis and ATP content. J Neurochem. 102:1264-1267.

Harris KM, Stevens JK. 1988. Dendritic spines of rat cerebellar Purkinje cells: serial electron microscopy with reference to their biophysical characteristics. J Neurosci. 8:4455-69

Harris KM, Stevens JK. 1989. Dendritic spines of CA 1 pyramidal cells in the rat hippocampus: serial electron microscopy with reference to their biophysical characteristics. J Neurosci. 9:2982-97.

Hayashi Y, Shi SH, Esteban JA, Piccini A, Ponzer JC, Malinow R. 2000. Driving AMPA receptors into synapses by LTP and CAMKII: requirement for GluR1 and PDZ domain interation. Science 287:2262-7

He K, Song L, Cummings LW, Goldman J, Huganir RL, Lee HK. 2009. Stabilization of Ca2+-permeable AMPA receptors at perisynaptic sites by GluR1-S845 phosphorylation. Proc Natl Acad Sci U S A. 106:20033-8.

Holcman D, Triller A. 2006. Modeling synaptic dynamics driven by receptor lateral diffusion. Biophys J. 91:2405-15.

Hollmann M, Hartley M, Heinemann S. 1991. Ca2+ permeability of KA-AMPA—gated glutamate receptor channels depends on subunit composition. Science 1991 May 10;252(5007):851-3.

Hollmann M, Heinemann S. 1994. Cloned glutamate receptors. Annu Rev Neurosci. 17:31-108.

Howard MA, Elias GM, Elias LA, Swat W, Nicoll RA. 2010. The role of SAP97 in synaptic glutamate receptor dynamics. Proc Natl Acad Sci U S A. 107:3805-10.

Huettner JE. 2003. Kainate receptors and synaptic transmission. Prog Neurobiol. 70:387-407.

Isaac JT, Ashby MC, McBain CJ. 2007. The role of the GluR2 subunit in AMPA receptor function and synaptic plasticity. Neuron 54:859-71.

Janas J, Skowronski J, Van Aelst L. 2006. Lentiviral delivery of RNAi in hippocampal neurons. Methods Enzymol. 406:593-605.

Jia Z, Agopyan N, Miu P, Xiong Z, Henderson J, Gerlai R, Taverna FA, Velumian A, MacDonald J, Carlen P, Abramow-Newerly W, Roder J. 1996. Enhanced LTP in mice deficient in the AMPA receptor GluR2. Neuron17:945-56.

Jordan BA, Fernholz BD, Boussac M, Xu C, Grigorean G, Ziff EB, Neubert TA. 2004. Identification and verification of novel rodent postsynaptic density proteins. Mol Cell Proteomics 3:857-871.

Jordan BA, Fernholz BD, Khatri L, Ziff EB. 2007. Activity-dependent AIDA-1 nuclear signaling regulates nucleolar numbers and protein synthesis in neurons. Nat Neurosci. 10:427-35.

Kaltschmidt C, Kaltschmidt B, Baeuerle PA. 1995. Stimulation of ionotrophic glutamate receptors activate transcription factor NF-kappa B in primary neurons. Proc Natl Acad Sci U S A 10:9618-9622.

Kato AS, Gill MB, Ho MT, Yu H, Tu Y, Siuda ER, Wang H, Qian YW, Nisenbaum ES, Tomita S, Bredt DS. 2010. Hippocampal AMPA receptor gating controlled by both TARP and cornichon proteins. Neuron 68:1082-96

Kauer JA, Malenka RC, Nicoll RA. 1988. A persistent postsynaptic modification mediates long-term potentiation in the hippocampus. Neuron 1:911-7.

Kennedy MJ, Davison IG, Robinson CG, Ehlers MD. 2010. Syntaxin-4 defines a domain for activity-dependent exocytosis in dendritic spines. Cell 141:524-35.

Kerr JM, Blanpied TA. 2012. Subsynaptic AMPA receptor distribution is acutely regulated by actin-driven reorganization of the postsynaptic density. J Neurosci. 32:658-73.

Kharazia VN, Weinberg RJ. 1997. Tangential synaptic distribution of NMDA and AMPA receptors in rat neocortex. Neurosci Lett. 238:41-44.

Kim JH, Liao D, Lau LF, Huganir RL. 1998. SynGAP: a synaptic RasGAP that associates with the PSD-95/SAP90 protein family. Neuron 20:683-91.

Kirkwood A, Bear MF. 1995. Elementary forms of synaptic plasticity in the visual cortex. Biol Res. 28:73-80.

Klöcker N, Bunn RC, Schnell E, Caruana G, Bernstein A, Nicoll RA, Bredt DS. 2002. Synaptic glutamate receptor clustering in mice lacking the SH3 and GK domains of SAP97.Eur J Neurosci. 16:1517-22.

Knobloch M, Mansuy IM. 2008. Dendritic spine loss and synaptic alterations in Alzheimer's disease. Mol Neurobiol. 37:73-82.

Komiyama NH, Watabe AM, Carlisle HJ, Porter K, Charlesworth P, Monti J, Strathdee DJ, O'Carroll CM, Martin SJ, Morris RG, O'Dell TJ, Grant SG. 2002. SynGAP regulates ERK/MAPK signaling, synaptic plasticity, and learning in the complex with postsynaptic density 95 and NMDA receptor.J Neurosci. 22:9721-32.

Kopec CD, Li B, Wei W, Boehm J, Malinow R. 2006. Glutamate receptor exocytosis and spine enlargement during chemically induced long-term potentiation. J Neurosci. 26:2000–2009

Kreienkamp HJ. 2008. Scaffolding proteins at the postsynaptic density: shank as the architectural framework. Handb Exp Pharmacol. 186:365-80.

Krug M, Lössner B, Ott T. 1984. Anisomycin blocks the late phase of long-term potentiation in the dentate gyrus of freely moving rats. Brain Res Bull. 13:39-42.

Kurabi A, Brener S, Mobil M, Kwan JJ, Donaldson LW. 2009. A nuclear localization signal at the SAM-SAM domain interface of AIDA-1 suggests a requirement for domain uncoupling prior to nuclear transport. J Mol Biol. 392:1168-77.

Lai KO, Zhao Y, Ch'ng TH, Martin KC. 2008. Importin-mediated retrograde transport of CREB2 from distal processes to the nucleus in neurons. Proc Natl Acad Sci U S A 105:17175-17180.

Lein ES, Hawrylycz MJ, Ao N, Ayres M, Bensinger A, Bernard A, Boe AF, Boguski MS, Brockway KS, Byrnes EJ, Chen L, Chen L, Chen TM, Chin MC, Chong J, Crook BE, Czaplinska A, Dang CN, Datta S, Dee NR, Desaki AL, Desta T, Diep E, Dolbeare TA, Donelan MJ, Dong HW, Dougherty JG, Duncan BJ, Ebbert AJ, Eichele G, Estin LK, Faber C, Facer BA, Fields R, Fischer SR, Fliss TP, Frensley C, Gates SN, Glattfelder KJ, Halverson KR, Hart MR, Hohmann JG, Howell MP, Jeung DP, Johnson RA, Karr PT, Kawal R, Kidney JM, Knapik RH, Kuan CL, Lake JH, Laramee AR, Larsen KD, Lau C, Lemon TA, Liang AJ, Liu Y, Luong LT, Michaels J, Morgan JJ, Morgan RJ, Mortrud MT, Mosqueda NF, Ng LL, Ng R, Orta GJ, Overly CC, Pak TH, Parry SE, Pathak SD, Pearson OC, Puchalski RB, Riley ZL, Rockett HR, Rowland SA, Royall JJ, Ruiz MJ, Sarno NR, Schaffnit K, Shapovalova NV, Sivisay T, Slaughterbeck CR, Smith SC, Smith KA, Smith BI, Sodt AJ, Stewart NN, Stumpf KR, Sunkin SM, Sutram M, Tam A, Teemer CD, Thaller C, Thompson CL, Varnam LR, Visel A, Whitlock RM, Wohnoutka PE, Wolkey CK, Wong VY, Wood M, Yaylaoglu MB, Young RC, Youngstrom BL, Yuan XF, Zhang B, Zwingman TA, Jones AR. 2007. Genome-wide atlas of gene expression in the adult mouse brain. Nature 445:168-76.

Lin DT, Makino Y, Sharma K, Hayashi T, Neve R, Takamiya K, Huganir RL. 2009. Regulation of AMPA receptor extrasynaptic insertion by 4.1N, phosphorylation and palmitoylation. Nat Neurosci. 12:879-87.

Ling DS, Benardo LS, Serrano PA, Blace N, Kelly MT, Crary JF, Sacktor TC. 2002. Protein kinase Mzeta is necessary and sufficient for LTP maintenance. Nat Neurosci. 5:295-6.

Lisé MF, Wong TP, Trinh A, Hines RM, Liu L, Kang R, Hines DJ, Lu J, Goldenring JR, Wang YT, El-Husseini A. 2005. Involvement of myosin Vb in glutamate receptor trafficking.J Biol Chem. 281:3669-78.

Lisman J, Schulman H, Cline H. 2002. The molecular basis of CaMKII function in synaptic and behavioural memory. Nat Rev Neurosci. 3:175-90.

Lu J, Helton TD, Blanpied TA, Rácz B, Newpher TM, Weinberg RJ, Ehlers MD. 2007. Postsynaptic positioning of endocytic zones and AMPA receptor cycling by physical coupling of dynamin-3 to Homer. Neuron. 55:874-89.

Lu W, Shi Y, Jackson AC, Bjorgan K, During MJ, Sprengel R, Seeburg PH, Nicoll RA. 2009. Subunit composition of synaptic AMPA receptors revealed by a single-cell genetic approach. Neuron 62:254-68.

Lu Y, Christian K, Lu B. 2008. BDNF: a key regulator for protein synthesis-dependent LTP and long-term memory? Neurobiol Learn Mem 89: 312–323.

Lujan R, Nusser Z, Roberts JD, Shigemoto R, Somogyi P. 1996. Perisynaptic location of metabotropic glutamate receptors mGluR1 and mGluR5 on dendrites and dendritic spines in the rat hippocampus.Eur J Neurosci. 8:1488-500.

Makino H, Malinow R. 2009. AMPA receptor incorporation into synapses during LTP: the role of lateral movement and exocytosis. Neuron 64:381-90.

Malenka RC, Nicoll RA. 1999. Long-Term potentiation – a decade of progress? Science 285: 1870-74.

Malenka RC, Bear MF. 2004. LTP and LTD: an embarrassment of riches. Neuron 44:5-21.

Malinow R, Malenka RC. 2002. AMPA receptor trafficking and synaptic plasticity. Annu Rev Neurosci. 25:103-26.

Malinow R. 2003. AMPA receptor trafficking and long-term potentiation. Philos Trans R Soc Lond B Biol Sci 358:704-14.

Mammen AL, Kameyama K, Roche KW, Huganir RL. 1997. Phosphorylation of the alpha-amino-3-hydroxy-5-methylisoxazole4-propionic acid receptor GluR1 subunit by calcium/calmodulin-dependent kinase II.J Biol Chem. 272:32528-33.

Mansour M, Nagarajan N, Nehring RB, Clements JD, Rosenmund C. 2001. Heteromeric AMPA receptors assemble with a preferred subunit stoichiometry and spatial arrangement. Neuron 32:841-5.

Mannaioni G, Marino MJ, Valenti O, Traynelis SF, Conn PJ. 2001. Metabotropic glutamate receptors 1 and 5 differentially regulate CA1 pyramidal cell function. J Neurosci. 21:5925-34.

Mao L, Takamiya K, Thomas G, Lin DT, Huganir RL. 2010. GRIP1 and 2 regulate activity-dependent AMPA receptor recycling via exocyst complex interactions. Proc Natl Acad Sci USA 107:19038-43.

Masugi-Tokita M, Tarusawa E, Watanabe M, Molnár E, Fujimoto K, Shigemoto R. 2007. Number and density of AMPA receptors in individual synapses in the rat cerebellum as revealed by SDS-digested freeze-fracture replica labeling. J Neurosci. 27:2135-44.

Matsubara A, Laake JH, Davanger S Usami S, Ottersen OP. 1996. Organization of AMPA receptor subunits at a glutamate synapse: a quantitative immunogold analysis of hair cell synapses in the rat organ of Corti. J Neurosci 16:4457-67.

Mayford M, Barzilai A, Keller F, Schacher S, Kandel ER. 1992. Modulation of an NCAM-related adhesion molecule with long-term synaptic plasticity in Aplysia. Science 256:638-44.

McBain CJ. 2008. Differential mechanisms of transmission and plasticity at mossy fiber synapses. Prog Brain Res 169:225-240.

Melone M, Burette A, Weinberg RJ. 2005. Light microscopic identification and immunocytochemical characterization of glutamatergic synapses in brain sections. J Comp Neurol 492:495-509.

Mi R, Tang X, Sutter R, Xu D, Worley P, O'Brian RJ. 2002. Differing mechanisms for glutamate receptor aggregation on dendritic spines and shafts in cultured hippocampal Neurons. J Neurosci 22:7606-16.

Migues PV, Hardt O, Wu DC, Gamache K, Sacktor TC, et al. 2010. PKMzeta maintains memories by regulating GluR2-dependent AMPA receptor trafficking. Nat Neurosci. 13: 630–634

Moga DE, Janssen WG, Vissavajjhala P, Czelusniak SM, Moran TM, Hof PR, Morrison JH. 2003. Glutamate receptor subunit 3 (GluR3) immunoreactivity

delineates a subpopulation of parvalbumin-containing interneurons in the rat hippocampus. J Comp Neurol. 462:15-28.

Muller D, Joly M, Lynch G. 1988. Contributions of quisqualate and NMDA receptors to the induction and expression of LTP. Science 242:1694-7.

Muller D, Toni N, Buchs PA. 2000. Spine changes associated with long-term potentiation. Hippocampus10:596-604.

Müller T, Meyer HE, Egensperger R, Marcus K. 2008. The amyloid precursor protein intracellular domain (AICD) as modulator of gene expression, apoptosis, and cytoskeletal dynamics-relevance for Alzheimer's disease. Prog Neurobiol 85: 393-406.

Nicoll RA, Schmitz D. 2005. Synaptic plasticity at hippocampal mossy fibre synapses. Nat Rev Neurosci. 6:863-876.

Nishimune A, Isaac JT, Molnar E, Noel J, Nash SR, Tagaya M, Collingridge GL, Nakanishi S, Henley JM. 1998. NSF binding to GluR2 regulates synaptic transmission. Neuron 21(1):87-97.

Nguyen PV, Abel T, Kandel ER. 1994. Requirement of a critical period of transcription for induction of late phase LTP. Science 265:1104-1107.

Noel J, Ralph GS, Pickard L, Williams J, Molnar E, Uney JB, Collingridge GL, Henley JM. 1999. Surface expression of AMPA receptors in hippocampal neurons is regulated by an NSF-dependent mechanism. Neuron 23:365-76.

Nusser Z, Mulvihill E, Streit P, Somogyi P. 1994. Subsynaptic segregation of metabotropic and ionotropic glutamate receptors as revealed by immunogold localization. Neuroscience 3:421-7.

O'Brien RJ, Xu D, Petralia RS, Steward O, Huganir RL, Worley P. 1999. Synaptic clustering of AMPA receptors by the extracellular immediate-early gene product Narp. Neuron 23:309-23.

Okabe S. 2007. Molecular anatomy of the postsynaptic density. Mol Cell Neurosci. 34:503-518.

Opazo P, Labrecque S, Tigaret CM, Frouin A, Wiseman PW, De Koninck P, Choquet D. 2010. CaMKII triggers the diffusional trapping of surface AMPARs through phosphorylation of stargazin. Neuron 67:239-52.

Opazo P, Sainlos M, Choquet D. 2011. Regulation of AMPA receptor surface diffusion by PSD-95 slots. Curr Opin Neurobiol.

Osawa M, Tong KI, Lilliehook C, Wasco W, Buxbaum JD, Cheng HY, Penniger JM, Ikura M, Ames JB. 2001. Calcium-regulated DNA binding and oligomerization of the neuronal calcium-sensing protein, calsenilin/DREAM/KChIP3. J Biol Chem. 276:41005-41013.

Ottersen OP, Takumi Y, Matsubara A, Landsend AS, Laake JH, Usami S. 1998. Molecular organization of a type of peripheral glutamate synapse: the afferent synapses of hair cells in the inner ear. Prog Neurobiol. 54:127-48.

Palmer CL, Cotton L, Henley JM. 2005. The molecular pharmacology and cell biology of alpha-amino-3-hydroxy-5-methyl-4-isoxazolepropionic acid receptors. Pharmacol Rev. 57:253-77.

Park M, Salgado JM, Ostroff L, Helton TD, Robinson CG, Harris KM, Ehlers MD. 2006. Plasticity-induced growth of dendritic spines by exocytic trafficking from recycling endosomes. Neuron 52:817–830.

Passafaro M, Piëch V, Sheng M. 2001. Subunit-specific temporal and spatial patterns of AMPA receptor exocytosis in hippocampal neurons. Nat Neurosci. 4:917-26.

Patterson MA, Szatmari EM, Yasuda R. 2010. AMPA receptors are exocytosed in stimulated spines and adjacent dendrites in a Ras-ERK-dependent manner during long-term potentiation. Proc Natl Acad Sci USA 107:15951-6.

Payne HL. 2008. The role of transmembrane AMPA receptor regulatory proteins (TARPs) in neurotransmission and receptor trafficking. Mol Membr Biol. 25:353-62.

Peng J, Kim MJ, Cheng D, Duong DM, Gygi SP, Sheng M. 2004. Semi-quantitative proteomic analysis of rat forebrain postsynaptic density fractions by mass spectrometry. J Biol Chem 279:21003-21011.

Penke Z, Chagneau C, Laroche S. 2011. Contribution of Egr1/zif268 to Activity-Dependent Arc/Arg3.1 Transcription in the Dentate Gyrus and Area CA1 of the Hippocampus. Front Behav Neurosci. 5:48.

Perez JL, Khatri L, Chang C, Srivastava S, Osten P, Ziff EB. 2001. PICK1 targets activated protein kinase Calpha to AMPA receptor clusters in spines of hippocampal neurons and reduces surface levels of the AMPA-type glutamate receptor subunit 2. J Neurosci. 21:5417-28.

Petralia RS, Wenthold RJ. 1992. Light and electron immunocytochemical localization of AMPA-selective glutamate receptors in the rat brain. J Comp Neurol. 318:329-54.

Pfeiffer BE, Huber KM. 2009. The state of synapses in fragile X syndrome. Neuroscientist. 15:549-67.

Pinheiro P, Mulle C. 2006. Kainate receptors. Cell Tissue Res. 326:457-82.

Plant K, Pelkey KA, Bortolotto ZA, Morita D, Terashima A, McBain CJ, Collingridge GL, Isaac JT. 2006. Transient incorporation of native GluR2-lacking AMPA receptors during hippocampal long-term potentiation. Nat Neurosci. 9:602-4.

Poglia L, Muller D, Nikonenko I. 2010. Ultrastructural modifications of spine and synapse morphology by SAP97. Hippocampus 21:990-8.

Proepper C, Johannsen S, Liebau S, Dahl J, Vaida B, Bockmann J, Kreutz MR, Gundelfinger ED, Boeckers TM. 2007. Abelson interacting protein 1 (Abi-1) is essential for dendrite morphogenesis and synapse formation. EMBO 26:1397-409.

Racca C, Stephenson FA, Streit P, Roberts JD, Somogyi P. 2000. NMDA receptor content of synapses in stratum radiatum of the hippocampal CA1 area. J Neurosci. 20:2512-22.

Raghavachari S, Lisman JE. 2002. Properties of quantal transmission at CA1 synapses. J Neurophysiol. 92:2456-67.

Reimers JM, Milovanovic M, Wolf ME. 2011. Quantitative analysis of AMPA receptor subunit composition in addiction-related brain regions.Brain Res. 1367:223-33.

Reymann KG, Frey J. 2007. The late maintenance of hippocampal LTP: requirements, phases, 'synaptic tagging', 'late-associativity' and implications. Neuropharmacology 52:24-40.

Roche KW, O'Brien RJ, Mammen AL, Bernhardt J, Huganir RL. 1996. Characterization of multiple phosphorylation sites on the AMPA receptor GluR1 subunit. Neuron 16:1179-88.

Rosenmund C, Stern-Bach Y, Stevens CF. 1998. The tetrameric structure of a glutamate receptor channel. Science 280:1596-9.

Rothman JE. 1994. Intracellular membrane fusion. Adv Second Messenger Phosphoprotein Res. 29:81-96.

Sacktor TC. 2011. How does PKMzeta maintain long-term memory? Nat Rev Neurosci 12: 9–15

Sajikumar S, Navakkode S, Sacktor TC, Frey JU. 2005. Synaptic tagging and cross-tagging: the role of protein kinase Mzeta in maintaining long-term potentiation but not long-term depression. J Neurosci. 25:5750-6.

Sala C, Futai K, Yamamoto K, Worley PF, Hayashi Y, Sheng M. 2003. Inhibition of dendritic spine morphogenesis and synaptic transmission by activity-inducible protein Homer1a. J Neurosci. 23:6327-37.

Salter MW. 1998. Src, N-methyl-D-aspartate (NMDA) receptors, and synaptic plasticity.Biochem Pharmacol. 56:789-98.

Sanderson JL, Dell'Acqua ML. 2011. AKAP signaling complexes in regulation of excitatory synaptic plasticity.Neuroscientist 17:321-36

Sans N, Racca C, Petralia RS, Wang YX, McCallum J, Wenthold RJ. 2001. Synapse-associated protein 97 selectively associates with a subset of AMPA receptors early in their biosynthetic pathway. J Neurosci. 21:7506-16.

Sans N, Vissel B, Petralia RS, Wang YX, Chang K, Royle GA, Wang CY, O'Gorman S, Heinemann SF, Wenthold RJ. 2003. Aberrant formation of glutamate receptor complexes in hippocampal neurons of mice lacking the GluR2 AMPA receptor subunit. J Neurosci. 23:9367-73.

Sassoè-Pognetto M, Ottersen OP. 2000. Organization of ionotropic glutamate receptors at dendrodendritic synapses in the rat olfactory bulb. J Neurosci. 20:2192-201.

Schuman EM, Dynes JL, Steward O. 2006. Synaptic regulation of translation of dendritic mRNAs. J Neurosci. 26:7143-7146.

Schütt J, Falley K, Richter D, Kreienkamp HJ, Kindler S. 2009. Fragile X mental retardation protein regulates the levels of scaffold proteins and glutamate receptors in postsynaptic densities. J Biol Chem. 284:25479-87.

Schwartz TU. 2005. Modularity within the architecture of the nuclear pore complex. Curr Opin Struct Bio.l 15:221-226.

Schwenk J, Harmel N, Zolles G, Bildl W, Kulik A, Heimrich B, Chisaka O, Jonas P, Schulte U, Fakler B, Klöcker N. 2009. Functional proteomics identify cornichon proteins as auxiliary subunits of AMPA receptors. Science 323:1313-9.

Selkoe DJ. 2002. Alzheimer's disease is a synaptic failure. Science. 298:789-91.

Serrano P, Yao Y, Sacktor TC. 2005. Persistent phosphorylation by protein kinase Mzeta maintains late-phase long-term potentiation. J Neurosci. 25:1979-84.

Setou M, Seog DH, Tanaka Y, Kanai Y, Takei Y, Kawagishi M, Hirokawa N. 2002. Glutamate-receptor-interacting protein GRIP1 directly steers kinesin to dendrites. Nature 417:83-7.

Shen L, Liang F, Walensky LD, Huganir RL. 2000. Regulation of AMPA receptor GluR1 subunit surface expression by a 4.1N-linked actin cytoskeletal association. J Neurosci. 20:7932-40.

Sheng M, Kim MJ. 2002. Postsynaptic signaling and plasticity mechanisms. Science 298:776-80.

Sheng M, Hoogenraad CC. 2007. The postsynaptic architecture of excitatory synapses: a more quantitative view. Annu Rev Biochem. 76:823-847.

Shepherd JD, Bear MF. 2011. New views of Arc, a master regulator of synaptic plasticity.Nat Neurosci. 14:279-84.

Shepherd JD, Huganir RL. 2007. The cell biology of synaptic plasticity: AMPA receptor trafficking. Annu Rev Cell Dev Biol. 23:613-43.

Shi SH, Hayashi Y, Petralia RS, Zaman SH, Wenthold RJ, Svoboda K, Malinow R. 1999. Rapid spine delivery and redistribution of AMPA receptors after synaptic NMDA receptor activation. Science 284:1811-6.

Shi S, Hayashi Y, Esteban JA, Malinow R.2001. Subunit-specific rules governing AMPA receptor trafficking to synapses in hippocampal pyramidal neurons. Cell.105:331-43.

Shinohara Y. 2011. Quantification of postsynaptic density proteins: Glutamate receptor subunits and scaffolding proteins. Hippocampus. doi: 10.1002/hipo.20950

Skup M. 2008. Dendrites as separate compartment - local protein synthesis. Acta Neurobiol Exp 68:305-321.

Slomnicki LP, Lesniak W. 2008. A putative role of the amyloid precursor protein intracellular domain (AICD) in transcription. Acta Neurobiol Exp (Wars) 68:219-228.

Sommer B, Keinänen K, Verdoorn TA, Wisden W, Burnashev N, Herb A, Köhler M, Takagi T, Sakmann B, Seeburg PH.1990. Flip and flop: a cell-specific functional switch in glutamate-operated channels of the CNS. Science 249:1580–1585

Sommer B, Köhler M, Sprengel R, Seeburg PH. 1991. RNA editing in brain controls a determinant of ion flow in glutamate-gated channels. Cell 67:11-9.

Spacek J, Harris KM. 1998. Three-dimensional organization of cell adhesion junctions at synapses and dendritic spines in area CA1 of the rat hippocampus. J Comp Neurol. 393:58-68.

Stein V, House DR, Bredt DS, Nicoll RA. 2003. Postsynaptic density-95 mimics and occludes hippocampal long-term potentiation and enhances long-term depression. J Neurosci. 23:5503-6.

Stephan KE, Baldeweg T, Friston KJ. 2006. Synaptic plasticity and dysconnection in schizophrenia. Biol Psychiatry 59:929-39.

Südhof TC. 2008. Neuroligins and neurexins link synaptic function to cognitive disease. Nature 455:903-11.

Sumioka A, Brown TE, Kato AS, Bredt DS, Kauer JA, Tomita S. 2011. PDZ binding of TARPγ-8 controls synaptic transmission but not synaptic plasticity.Nat Neurosci.14:1410-2

Sutton MA, Schuman EM. 2005. Local translational control in dendrites and its role in long-term synaptic plasticity. J Neurobiol. 64:116-31.

Sutton MA, Schuman EM. 2006. Dendritic protein synthesis, synaptic plasticity, and memory. Cell 127:49-58.

Swanwick CC, Murthy NR, Mtchedlishvili Z, Sieghart W, Kapur J. 2006. Development of g-aminobutyric acidergic synapses in cultured hippocampal neurons. J Comp Neurol 495:497-510.

Takumi Y, Ramírez-León V, Laake P, Rinvik E, Ottersen OP. 1995. Different modes of expression of AMPA and NMDA receptors in hippocampal synapses. Nat Neurosci. 2:618-24.

Tao-Cheng JH, Crocker VT, Winters CA, Azzam R, Chludzinski J, Reese TS. 2011. Trafficking of AMPA receptors at plasma membranes of hippocampal neurons. J Neurosci. 31:4834-43.

Tarusawa E, Matsui K, Budisantoso T, Molnár E, Watanabe M, Matsui M, Fukazawa Y, Shigemoto R. 2009. Input-specific intrasynaptic arrangements of ionotropic glutamate receptors and their impact on postsynaptic responses. J Neurosci. 29:12896-908.

Tomita S, Chen L, Kawasaki Y, Petralia RS, Wenthold RJ, Nicoll RA, Bredt DS. 2003. Functional studies and distribution define a family of transmembrane AMPA receptor regulatory proteins. J Cell Biol. 161:805-16.

Tomita S, Sekiguchi M, Wada K, Nicoll RA, Bredt DS. 2006. Stargazin controls the pharmacology of AMPA receptor potentiators. Proc Natl Acad Sci USA 103:10064-7.

Toni N, Buchs PA, Nikonenko I, Povilaitite P, Parisi L, Muller D. 2001. Remodeling of synaptic membranes after induction of long-term potentiation. J Neurosci. 21:6245-51.

Traynelis SF, Wollmuth LP, McBain CJ, Menniti FS, Vance KM, Ogden KK, Hansen KB, Yuan H, Myers SJ, Dingledine R. 2010. Glutamate receptor ion channels: structure, regulation, and function. Pharmacol Rev. 62:405-96.

Urakubo T, Ogura A, Tominaga-Yoshino K. 2006. Ultrastructural features of hippocampal CA1 synapses with respect to synaptic enhancement following repeated PKA activation. Neurosci Lett. 407:1-5.

Valtschanoff JG, Weinberg RJ. 2001. Laminar organization of the NMDA receptor complex within the postsynaptic density. J Neurosci. 21:1211-1217.

van Spronsen M, Hoogenraad CC. 2010. Synapse pathology in psychiatric and neurologic disease. Curr Neurol Neurosci Rep.10:207-14.

Vandenberghe W, Nicoll RA, Bredt DS. 2005. Interaction with the unfolded protein response reveals a role for stargazin in biosynthetic AMPA receptor transport. J Neurosci. 25:1095-102.

Verdoorn TA, Burnashev N, Monyer H, Seeburg PH, Sakmann B.1991. Structural determinants of ion flow through recombinant glutamate receptor channels. Science 252:1715-8.

Wan Y, Feng G, Calakos N. 2011. Sapap3 Deletion Causes mGluR5-Dependent Silencing of AMPAR Synapses. J Neurosci. 31:16685-91.

Wang X, McCoy PA, Rodriguiz RM, Pan Y, Je HS, Roberts AC, Kim CJ, Berrios J, Colvin JS, Bousquet-Moore D, Lorenzo I, Wu G, Weinberg RJ, Ehlers MD, Philpot BD, Beaudet AL, Wetsel WC, Jiang YH. 2011. Synaptic dysfunction and abnormal behaviors in mice lacking major isoforms of Shank3. Hum Mol Genet. 20:3093-108.

Weisenhaus M, Allen ML, Yang L, Lu Y, Nichols CB, Su T, Hell JW, McKnight GS. 2010. Mutations in AKAP5 disrupt dendritic signaling complexes and lead to electrophysiological and behavioral phenotypes in mice. PLoS One. 5:e10325

Wenthold RJ, Petralia RS, Blahos J II, Niedzielski AS. 1996. Evidence for multiple AMPA receptor complexes in hippocampal CA1/CA2 neurons. J Neurosci. 16:1982-9.

West AE, Griffith EC, Greenberg ME. 2002. Regulation of transcription factors by neuronal activity. Nat Rev Neurosci. 3:921-931.

Xie X, Liaw JS, Baudry M, Berger TW. 1997. Novel expression mechanism for synaptic potentiation: alignment of presynaptic release site and postsynaptic receptor. Proc Natl Acad Sci USA 94:6983-8.

Xu H, Hebert MD. 2005. A novel EB-1/AIDA-1 isoform, AIDA-1c, interacts with the Cajal body protein coilin. BMC Cell Biology 6:23.

Yang Y, Wang XB, Frerking M, Zhou Q. 2008. Delivery of AMPA receptors to perisynaptic sites precedes the full expression of long-term potentiation. Proc Natl Acad Sci USA 105:11388-93.

Yao Y, Kelly MT, Sajikumar S, Serrano P, Tian D, Bergold PJ, Frey JU, Sacktor TC. 2008. PKM zeta maintains late long-term potentiation by N-ethylmaleimide-sensitive factor/GluR2-dependent trafficking of postsynaptic AMPA receptors. J Neurosci. 28:7820-7.

Yoshimura Y, Yamauchi Y, Shinkawa T, Taoka M, Donai H, Takahashi N, Isobe T, Yamauchi T. 2004. Molecular constituents of the postsynaptic density fraction revealed by proteomic analysis using multidimensional liquid chromatography-tandem mass spectrometery. J Neurochem. 88: 759-768.

Yudowski GA, Puthenveedu MA, Leonoudakis D, Panicker S, Thorn KS, Beattie EC, von Zastrow M. 2007. Real-time imaging of discrete exocytic events mediating surface delivery of AMPA receptors. J Neurosci. 27:11112-21.

Zamanillo D, Sprengel R, Hvalby O, Jensen V, Burnashev N, Rozov A, Kaiser KM, Köster HJ, Borchardt T, Worley P, Lübke J, Frotscher M, Kelly PH, Sommer B, Andersen P, Seeburg PH, Sakmann B 1999. Importance of AMPA receptors for hippocampal synaptic plasticity but not for spatial learning. Science 284:1805-11

Zhu JJ, Qin Y, Zhao M, Van Aelst L, Malinow R. 2002. Ras and Rap control AMPA receptor trafficking during synaptic plasticity. Cell 110:443-55.

Ziff EB. 1997. Enlightening the postsynaptic density. Neuron 19:1163-1174.